VALIDATION

JET FIRE

DATE: December 2023

This document describes the validation of the JFSH and radiation (RADS) models which are implemented in PHAST/SAFETI against a range of field data. The models are described separately in the companion theory document.

The validation tests used hydrocarbons and some other materials such as hydrogen and also some mixtures of interest, for instance hydrogen/methane blends and syngas. Hole sizes cover a wide range and release conditions also vary, producing anything from relatively slow jets to supersonic turbulent jets. Release orientation includes vertical, horizontal and angled releases. Weather conditions vary and the wind may be blowing at an angle to the release direction which can be significant for the direction of the jet flame.

Reference to part of this report which may lead to misinterpretation is not permissible.

No.	Date	Reason for Issue	Prepared by	Verified by
1	October 2021	Create separate document apart from the theory and add new Miller model validation	David Worthington	Yongfu Xu, Ade Oke, Jan Stene
2	December 2021	Add a new section on 2 phase hydrogen tests	David Worthington	Jan Stene

Date: December 2023

Prepared by: Digital Solutions at DNV

ABSTRACT

This validation document compares predictions of the JFSH and radiation (RADS) models against field data. The companion JFSH theory document describes the theory of the single and two-phase Jet Fire (JFSH) models which are implemented in PHAST and SAFETI. Two types of jet fire models are described: cone-shaped flame models and a line source emitter flame model.

In cone-shaped flame models, the jet flame is modelled as a conical frustum, emitting radiation as a solid body with uniform surface emissive power. The models predict the flame and frustum lengths, frustum base and tip widths, angle between the frustum and release axes, lift-off distance of the frustum from the release plane, fraction of heat radiated from the flame's surface, and maximum surface emissive power of the flame.

Three conical frustum jet flame models are presented. These are: JFSH-Chamberlain, based on the Shell pure-vapour model by Chamberlain; JFSH-Cook, based on the modified jet flame correlations proposed by Cook et al. (1990) to account for vapour and especially liquid and two-phase releases and JFSH-Johnson, which is an improvement to the JFSH-Chamberlain model to account for horizontal/near horizontal vapour phase releases. The dimensions of the conical frustum, and its orientation in space, as employed in the JFSH-Chamberlain and JFSH-Johnson model, were correlated semi-empirically from results of laboratory and field studies. The Chamberlain, Cook and Johnson models account for the influence of wind speed, air entrainment rate and crosswind effects on flame characteristics.

The multi-point source emitter flame model, Miller model, is based on AP flame (Miller, 2017). The Miller model is an extension of the Chamberlain model, particularly to low luminosity gases, such as hydrogen (Miller, 2017). The jet fire is modelled as a distribution of individual point sources along the flame centreline. The Miller model predicts flame characteristics as in the Chamberlain model except, frustum base and tip widths, and maximum surface emissive power. Radiation emitted along the flame centreline is modelled in terms of a weighting factor representing the proportion of combustion energy multiplied by a fixed fraction of heat radiated at different positions along the flame length.

The JFSH-Cook, JFSH-Chamberlain, JFSH-Johnson and Miller multi-point source (M-MPS) models have been validated by comparing their predictions with appropriate field data reported by Chamberlain, Bennett et al., Miller, Selby and Burgan. Within limits of uncertainty, predictions from the JFSH-Cook and JFSH-Chamberlain models for pure vapour jet flames resulting from vertical releases show good agreement with field data with a maximum absolute deviation and mean deviation of 12.5% and 5.0% respectively when compared with predictions from the Chamberlain model. Based on available field data for horizontal liquid/two-phase releases, the JFSH-Cook liquid/two-phase jet fire model generally predicts flame lengths to within ±30% of measurements, while average estimates of flame SEP lies within -30% of measured data. For horizontal vapour phase releases, the JFSH-Johnson model predicts flame lengths to within ±10% of available field data.

The simulation of received radiation by objects at a distance from a jet flame, using the RADS model, has been validated against field data gathered by Chamberlain and Bennett et al for vertical and horizontal jet flames respectively. Simulated results were based on flame characteristics predicted by the JFSH-Cook, JFSH-Chamberlain and JFSH-Johnson models. The predicted incident radiation over a wide range of observer locations and orientations compare well with field data and generally lie within ±40% of measurements.

Two-phase hydrogen tests at Spadeadam have been compared with predictions made by JFSH. The horizontal fire is predicted with a similar resolution as seen in the other two-phase validation. The downward impinged test is better predicted by an equivalent pool fire rather than JFSH.

The comparison of each model including the data set used by Miller to develop his model is explained in the companion validation document. The results have enabled some advice as to which model to use for different types of release;

- The Cook model for non-vapour releases
- The Miller model for low luminosity gases (e.g. hydrogen and syngas)
- The Chamberlain model for all other releases except horizontal vapour releases where the Johnson model is recommended.

Table of contents

Table of figures

List of tables

1 INTRODUCTION

This document discusses the validation and verification of the JFSH jet fire models in conjunction with the DNV radiation model (RADS). The original validation compared predictions from the model using Chamberlain, Cook and Johnson options against field measurements reported by Chamberlain[1], Johnson et al[2] and Bennett et al[3]. The validation of the radiation model (RADS) (based on the JFSH simulated flame characteristics) were conducted by comparing its predicted incident radiant flux at specified observer locations and orientations with measured data.

For the verification exercise, the predictions from the JFSH-Cook and JFSH-Chamberlain models were compared with simulated data for 7 test cases reported by Chamberlain.

All the earlier work was based on hydrocarbon tests. More recently the validation of the Miller[4] model has been included and this has introduced further data sets including hydrogen, hydrogen/methane blends and different syngas compositions.

2 VERIFICATION AND VALIDATION OF THE VAPOUR PHASE MODEL

2.1 Verification and validation of the JFSH-RADS models against data reported by Chamberlain, 1987

The following presents and discusses the results of the verification and validation of the JFSH-Cook, JFSH-Chamberlain and RADS models against field data and simulated results reported by Chamberlain[3]. JFSH predictions for surface emissive power using the modified Cook et al. correlation (a.k.a. JFSH-Cook) and the Chamberlain correlation (a.k.a. JFSH-Chamberlain) for frustum base widths are compared.

The JFSH code requires the specification of the fuel's post-expansion thermodynamic (temperature or liquid fraction) and dynamic (expanded radius or velocity) states as input data. Values for these release properties were not directly reported by Chamberlain. However, through back calculations using secondary data and recommended discharge equations[1] the post-expansion temperature and velocity for each test case were estimated. The back calculated post-expansion temperature and velocity were employed as input to the JFSH code. The procedures for these back calculations are described in Appendix A. Calculation of post-expansion JFSH input data

		Molar composition (Mole %)	
Label	**Molecular Weight (g/mol)**	**Methane**	**Ethane**
Natural-Gas-Mixture-1	16.9	93.87	6.13
Natural-Gas-Mixture-2	20.8	66.07	33.93
Natural-Gas-Mixture-3	22.3	55.38	44.62

Table 1 Approximate composition of natural gas mixtures employed in jet fire field tests

Field Trial-3	**Test-3A**	**Test-3B**	**Test-3C**	**Test-3D**
Flowrate [kg/s]	21.1	29	36.6	55.6
Molecular Weight [kg/kmol]	20.8	20.8	20.8	22.3
Mach number [-]	0.07	0.1	0.13	0.19
Air Temperature [K]	289.15	289.15	288.65	286.15
Stagnation Temperature [K]	290.02	313.54	332.98	328.02
Ratio of Specific Heats (γ) [-]	1.27	1.27	1.27	1.26
Post-expansion Temperature [K]	289.83	313.12	332.23	326.51
Post-expansion Velocity [m/s]	26.83	39.84	53.35	74.29
Humidity (%) [-]	53	56	56	56
Wind Speed [m/s]	7.5	7.9	7.4	8
Diameter of discharge point (Do) [m]	1.07	1.07	1.07	1.07

Field Trial-4	Test-4A	Test-4B	Test-4C	
Flowrate [kg/s]	5.6	11.2	22.2	
Molecular Weight [kg/kmol]	16.9	16.9	16.9	
Mach number [-]	0.56	1.03	1.53	
Air Temperature [K]	289.45	287.35	287.45	
Stagnation Temperature [K]	297.51	278.83	267.89	
Ratio of Specific Heats (γ) [-]	1.30	1.30	1.30	
Post-expansion Temperature [K]	284.15	240.57	198.30	
Post-expansion Velocity [m/s]	238.71	403.98	544.83	
Humidity (%) [-]	50	60	51	
Wind Speed [m/s]	8.1	6.3	10.3	
Diameter of discharge point (Do) [m]	0.203	0.203	0.203	

Table 2 Summary of pertinent discharge and ambient data for field trials 3 (tests A-D) and 4 (tests A-C)

A study of the reported molecular weight for natural gas during each field test revealed that at least three different fuel mixtures were employed. Details of the exact composition for each fuel (i.e., natural gas) mixture were not reported. For the purpose of this work, it is assumed that natural gas is made up of methane and ethane only. Hence, the molar composition of each mixture has been calculated from its reported molecular weight. Table 1 shows the estimated compositions (mole %) for each fuel mixture, while Table 1 presents a summary of pertinent JFSH input data for each test case.

Figure 1, Figure 2, Figure 3, and Figure 4 respectively show the variations of predicted frustum length (R_L), flame tip width (W_2), angle between release and frustum axes (α) and flame surface emissive power (SEP) with field data using the JFSH and Chamberlain models. In each plot, the dotted red and blue lines respectively refer to flame characteristics 10% above and below the mean field data. The black line represents the mean field data. A discussion of how the models compare against each other is given in Section 2.1.1, while model predictions against the experimental field data is given in Section 2.1.2.

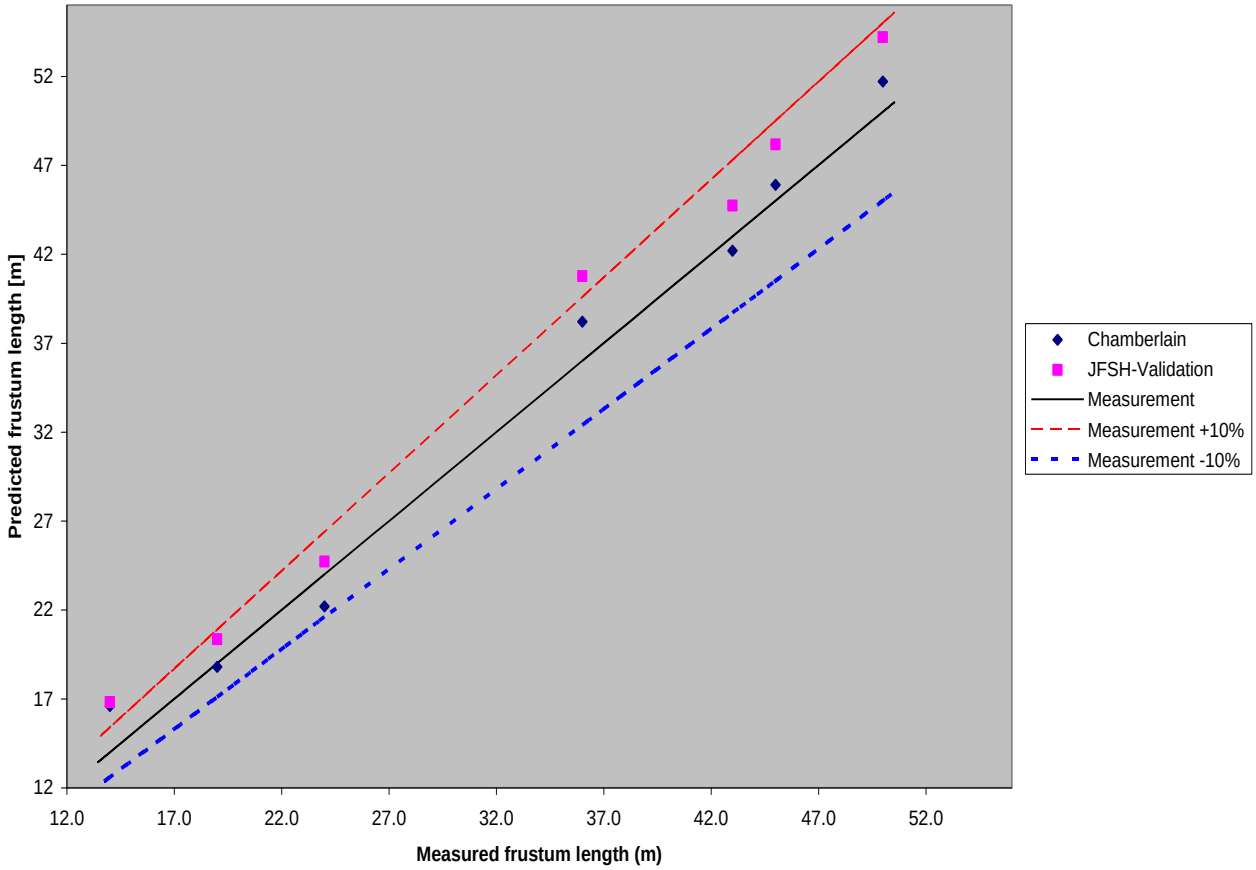

Figure 1 **Variation of predicted flame frustum lengths with field data using the JFSH and Chamberlain models.**
(Field data and predictions from Chamberlain model are obtained from literature[3])

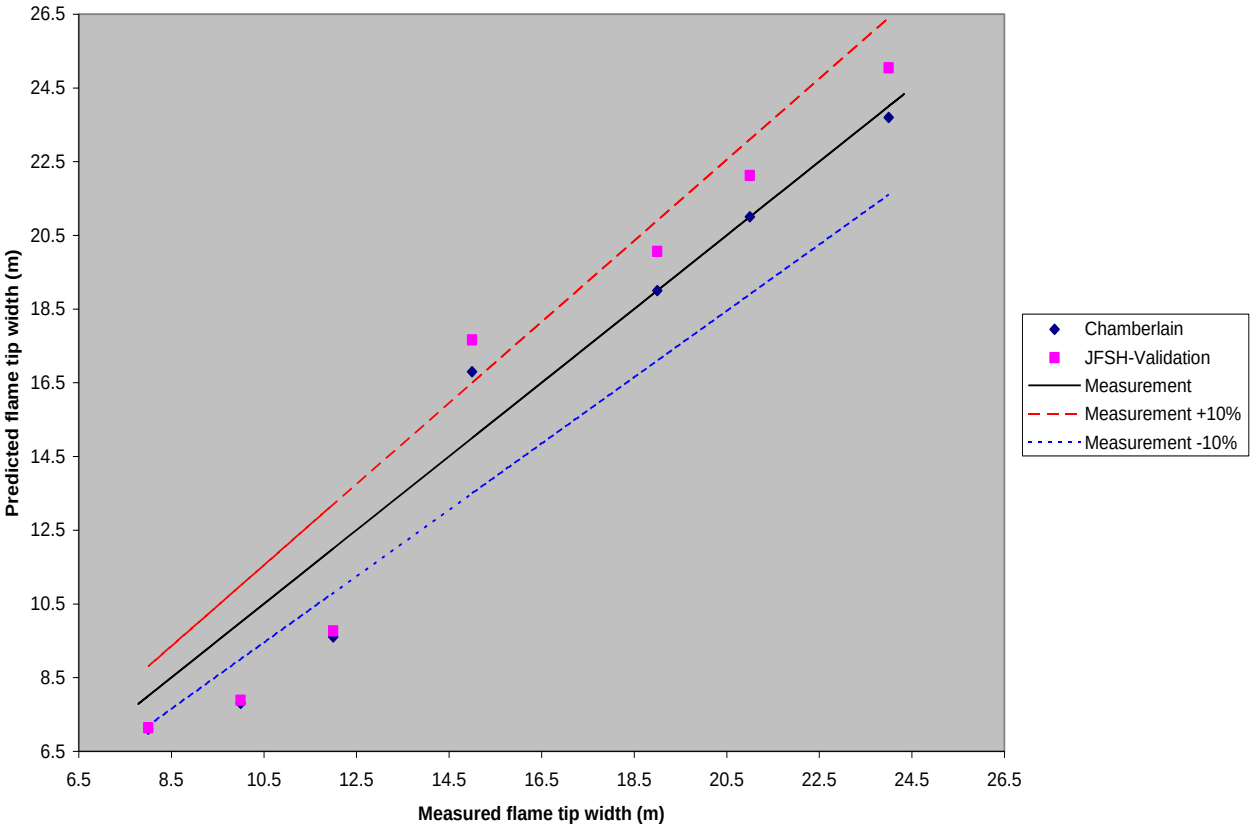

Figure 2 **Variation of predicted flame tip width (W_2) with field data using the JFSH and Chamberlain models.**
(Field data and predictions from Chamberlain model are obtained from literature[3])

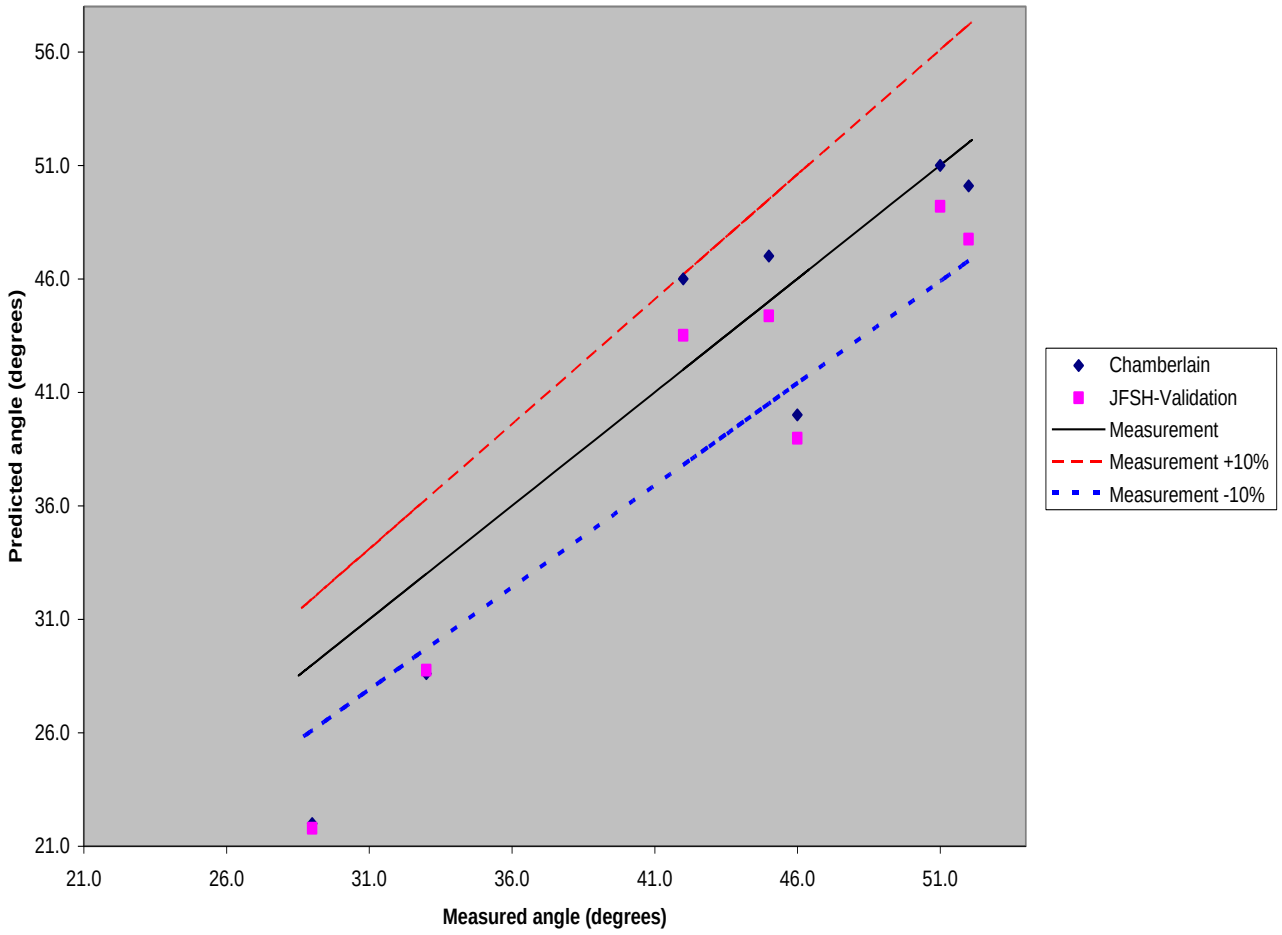

Figure 3 **Variation of predicted angle between release and frustum axes (α) with field data using the JFSH and Chamberlain models.**
(Field data and predictions from Chamberlain model are obtained from literature[3])

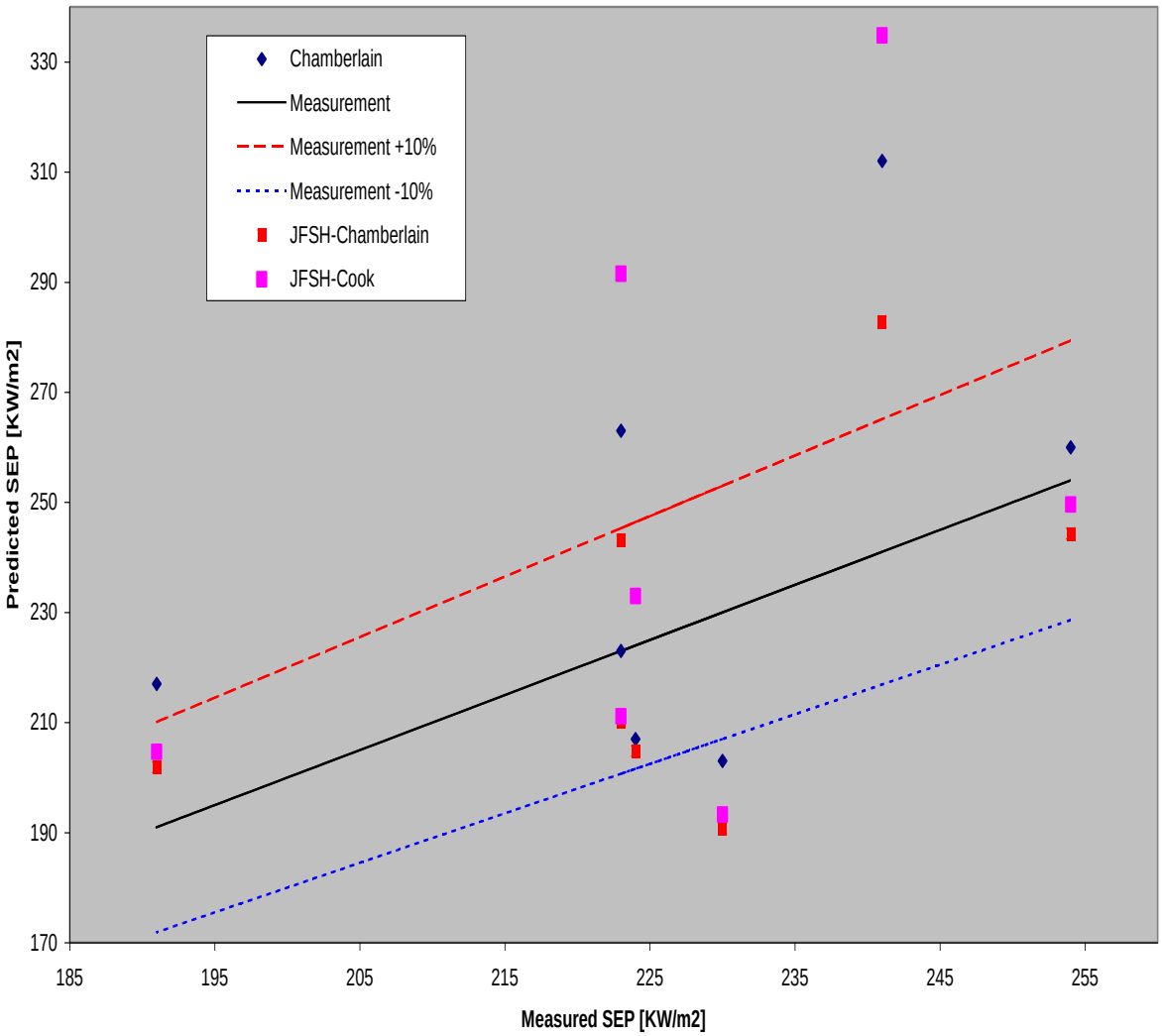

Figure 4 **Variation of predicted surface emissive power (SEP) with field data using the JFSH and Chamberlain models**
(Field data and predictions from Chamberlain model are obtained from literature[1])

2.1.1 Comparison of Cook and Chamberlain models

For the test cases studied, the following are the observations made by comparing the predictions from the JFSH-Cook and JFSH-Chamberlain models with simulated data reported by Chamberlain.

- The JFSH-Cook and JFSH-Chamberlain models give exactly the same results for frustum length, frustum tip width and angle between the release and frustum axes. The only effect of the Cook et al modifications on the Chamberlain model is evident in the surface emissive power predictions.

- Frustum Length [R_L] (Figure 1)
  - Predictions from the JFSH and Chamberlain models are generally in close agreement. The respective maximum and average (absolute) percentage deviations of the JFSH from the Chamberlain model are ca 11% and 6%.
  - The JFSH models generally predict longer (more conservative) frustum lengths when compared with the Chamberlain model

- Differences observed in predictions from the models can be ascribed to:
  - Inaccurate knowledge of the exact input data into the Chamberlain code
  - The use of real as against ideal gas equations of state by the JFSH models in calculating post-expansion characteristics of the escaping fluid. The Chamberlain model and the empirical correlations on which it is based were derived based on the assumption of ideal gas fluid behaviour.

- Flame tip width [W_2] (Figure 2)
  - Predictions from the JFSH and Chamberlain models are in close agreement. The respective maximum and average percentage deviations of the JFSH from the Chamberlain model are ca 6% and 4% respectively.
  - The JFSH models generally predict wider (more conservative) flame tip widths when compared with the Chamberlain model
  - The reasons given above for differences between frustum length predictions from both models are deemed to apply for the observed differences in W_2 predictions

- Angle between release and frustum axes [α] (Figure 3)
  - Predictions from the JFSH and Chamberlain models are in close agreement. The respective maximum and average percentage deviations of the JFSH from the Chamberlain model are ca 6% and 3% respectively.
  - The JFSH models generally predict narrower angles between the release and frustum axes when compared with the Chamberlain model
  - The reasons given above for differences between frustum length predictions from both models are deemed to apply for the observed differences in predicted α

- Surface emissive power [$W_{Surface}$] (Figure 4)

  - Predictions from the JFSH-Chamberlain and JFSH-Cook models are generally in good agreement with predictions reported for the Chamberlain model. Expectedly, predictions from the JFSH-Chamberlain model show closer agreement with predictions from the Chamberlain model than the JFSH-Cook results. The respective maximum/average percentage deviations of predictions from the JFSH-Chamberlain and JFSH-Cook models from the Chamberlain model are ca 9%/6% and 13%/7% respectively.
  - No particular trend can be identified when SEP predictions from the JFSH-Cook and Chamberlain models are compared. However, the JFSH-Chamberlain model generally predicts lower SEP when compared with results from the Chamberlain model.
  - Differences observed in SEP predictions from the JFSH and Chamberlain models can be ascribed to:
    - Differences in predicted flame dimensions. The SEP calculated is a function of the flame's total surface area. The JFSH-Cook model uses a different correlation for the frustum base width (W_1) and generally predicts higher values for the flame frustum length (R_L) and tip width (W_2). These variables have a direct effect on the calculated value of the flame's total surface area.
    - Possible differences in the calculated heat of combustion of the natural gas mixture using the JFSH as compared with the Chamberlain model.

2.1.2 Validation of JFSH-Chamberlain, JFSH-Cook and RADS models against field data

JFSH model

The following discusses the results of validating the JFSH-Cook and JFSH-Chamberlain models against field data reported by Chamberlain[3]. The frustum length, flame tip width and angle between release and frustum axes predictions of the JFSH-Cook and JFSH-Chamberlain are the same.

- Frustum Length [R_L] (Figure 1)
  - Frustum lengths predicted by the JFSH models compare well with field data. The model generally predicts flame frustum lengths to within +10% of measured data.

- In comparison with mean field data, the JFSH models predict longer (more conservative) frustum lengths.

- Flame tip width [W_2] (Figure 2)
  - Flame tip widths predicted by the JFSH models compare well with field data. The models predict flame tip widths to ca ± 10% of mean field data
  - In comparison with mean field data, the models appear to over and under predict flame tip widths above and below 14m in diameter respectively.

- Angle between release and frustum axes [α] (Figure 3)
  - Predictions of α using the JFSH models compare well with measured field data. Most of the model's predictions (> 50%) lie within ±10% of mean field data.
  - In comparison with mean observed data, the models appear to predict narrower values for α

- Surface emissive power [$W_{Surface}$] (Figure 4)
  - Predictions of SEP using the JFSH-Cook model compare averagely well with measured field data while better agreement is obtained using the JFSH-Chamberlain model. Predictions (> 50%) generally lie within ±10% of mean measurements.
  - Model predictions show no apparent trend when compared with mean measurements.

JFSH-RADS model

The following discusses the results of validating the radiation model (RADS), based on the flame characteristics predicted respectively by the JFSH-Cook and JFSH-Chamberlain models, against field and simulated data reported by Chamberlain[3]. Table 3 lists the Cartesian coordinates and orientations at which radiation intensities were measured for different observer (radiometer) positions. The x, y and z axes of the Cartesian coordinate system correspond to the geographic East, geographic North and vertical directions respectively. The origin of the coordinate system is located at the flare tip. The angles ξ and γ refer, respectively, to the angle of inclination of the observer from the vertical, and the horizontal orientation of the normal to the radiometer face from the geographic West direction. For trial 3, the radiometers were oriented to receive maximum radiation.

Trial 3 (Tests A, B, C and D)				
x [m]	y [m]	z [m]	ξ [degrees]	γ [degrees]
34.1	27.7	-100		
13.6	55	-101.7		
31.7	64.9	-103.8		
-1.4	64.4	-92.3		
25.9	6.4	-99		
Trial 4 (Tests A, B and C)				
x [m]	y [m]	z [m]	ξ [degrees]	γ [degrees]
26	-15	-8.6	38.0	75.0
20	-34.6	-8.7	45.0	80.0
0	-30	-8.6	43.0	115.0
-26	-15	-8.7	48.0	160.0
-8.7	-5	-8.8	30.0	160.0
-26	15	-8.6	48.0	-160.0
-8.7	5	-8.6	30.0	-160.0
0	30	-8.5	43.0	-115.0
20	34.6	-8.7	45.0	-80.0
26	15	-8.7	38.0	-75.0
50	0	-8.5	45.0	0.0
58.6	-3.1	5	70.0	3.0

Table 3 **Observer (radiometer) position and orientation with respect to flare tip for field trials 3 and 4 (source: Chamberlain, 1987) [3]**

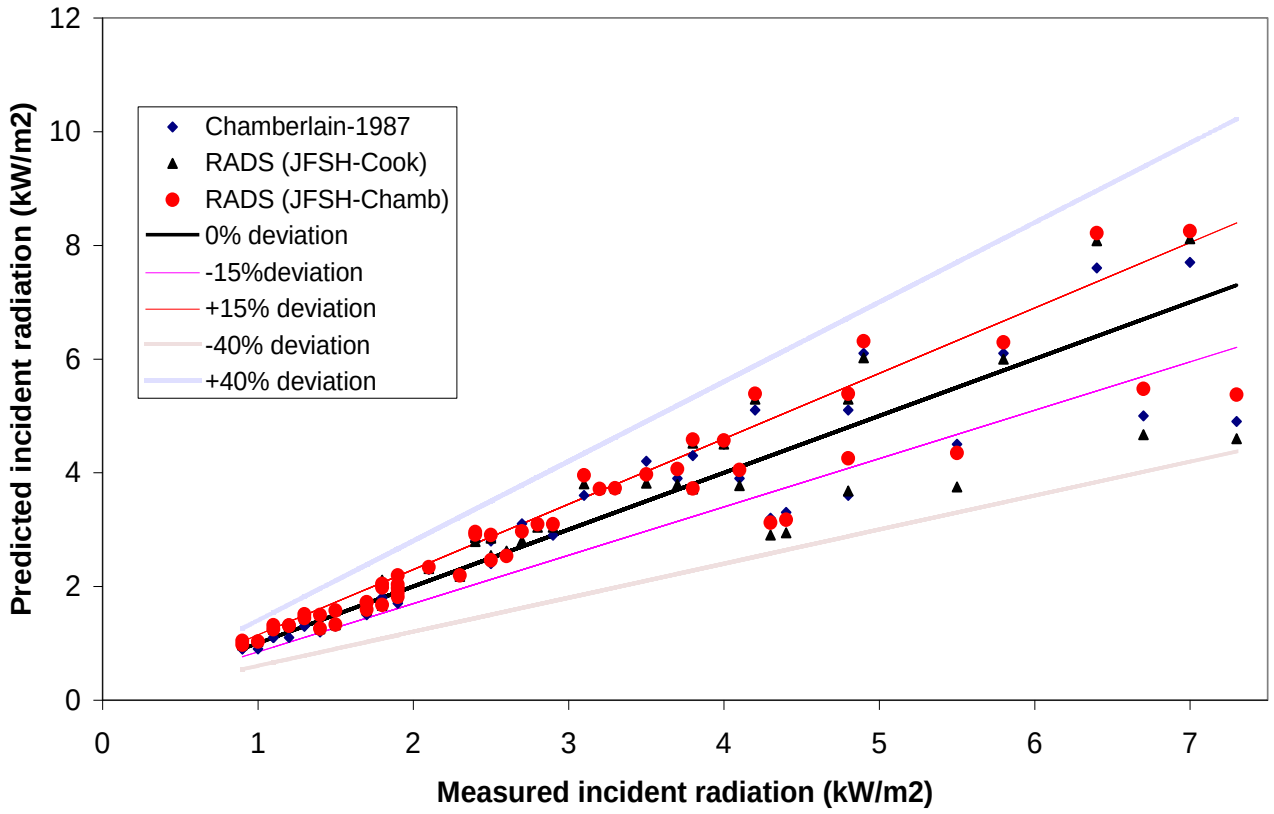

Figure 5 **Variation of predicted against measured incident radiation at different observer positions and orientations using the RADS (JFSH-Cook and JFSH-Chamberlain) and the Chamberlain radiation models.**
(Field data and predictions from the Chamberlain radiation model are obtained from literature[3])

Figure 5 shows the variation of predicted incident radiation [kW/m^2] with measured data for field trials 3 (A-D) and 4 (A-C) based on the flame characteristics predicted by the JFSH-Cook [legend: RADS (JFSH-Cook)] and JFSH-Chamberlain [legend: RADS (JFSH-Chamb)] models. The reported values of incident radiation predicted by the Chamberlain jet flame and radiation model[3] [legend: Chamberlain-1987] at each observer location are also presented. Incident radiations corresponding to 0, ±15 and ±40% from measured data are represented by linear plots on Figure 5. From Figure 5, the following observations are made:

- Within limits of uncertainty and reported discrepancy in measurements[3], good agreement is observed between the predicted and measured incident radiation for the JFSH-RADS models. In addition, there is close semblance in simulated results from the JFSH-RADS and Chamberlain radiation models. All simulated results lie within ±40% of measured data.
- All three models appear to perform better (ca $\leqslant$ ±20% deviation from measured data) when simulating "far field" incident radiation (i.e., incident radiation $\leqslant$ 4kW/m^2).
- On average, the percentage absolute deviation from measured data of the RADS (JFSH-Cook), RADS (JFSH-Chamb) and Chamberlain-1987 simulated results are ca 12.8%, 12.6% and 10% respectively.

2.2 Validation of the JFSH-RADS models against data reported by Bennett et al. (1991) and Johnson et al. (1994)

The following discusses the results of validating the JFSH-Johnson and RADS models against field and simulated data reported by Bennett et al[3] and Johnson et al[2] for jet flames resulting from horizontal natural gas releases. Seven tests (1042, 1040, 1083, 1037, 1033, 1036 and 1089) that relate to free jet flames were

reported. For each test, the flame length was measured and reported. Table 4 shows the measured composition (mole %) for the natural gas mixture employed in the tests, while Table 6 presents a summary of pertinent JFSH input data for each test case. Table 7 lists, for tests 1040, 1083, 1033 and 1089, the Cartesian coordinates and orientations at which radiation intensities were measured for different observer (radiometer) positions. The x, y and z axes of the Cartesian coordinate system are illustrated in the companion theory manual. The origin of the coordinate system is located at the discharge point. The angles ξ and γ refer, respectively, to the angle of inclination of the observer from the vertical, and the horizontal orientation of the normal to the radiometer face from the negative x direction. Incident radiation versus observer location predictions for the RADS (JFSH-Johnson) simulation of tests 1040, 1083, 1033 and 1089 and the corresponding simulated data reported by Johnson et al are presented.

The stagnation temperatures and/or pressures for tests 1033, 1037, 1040, 1042, 1083 and 1089 were obtained or estimated from values quoted by Johnson et al. For test 1036 (high upstream pressure release), the measured static pressure and ambient temperature were used as input for the discharge calculation in place of stagnation pressure and temperature. The data sources for each input data in Table 6 are referenced accordingly.

The post-expansion temperature and expanded radius were estimated from the DISC and ATEX routines in PHAST6.4/7.2 based on the stagnation temperatures and pressures in Table 6. The associated DISC input and DISC results are summarised by Table 5. Default values for the DISC parameters were applied (with no cap applied for post-expansion velocity). It is seen that the flow-rate predictions agree well with the measured data (the input data for tests 1040 and 1042 are very close, and therefore the measured flow rate for test 1042 appears to be too high). However, the measured flow rates for each test were used (in place of predicted values) as input into the JFSH models.

For the wind direction, the release axis is oriented at 270^o from the true north while the declination of the magnetic from the true north (i.e., 16^o) is obtained from reported data published by Selby and Burgan[5].

Component	Mole %
Nitrogen	0.425
Methane	94.0
Ethane	5.31
Propane +	0.265

Table 4 Typical natural gas composition for horizontal jet fire field tests (source: Bennett et al., 1991)[3]

Inputs	DISC orifice' Discharge simulations corresponding to Johnson (1994) horizontal natural gas vapour jet fies										
Input Index	Description	Units	Limits		TC 1042	TC 1040	TC 1083	TC 1037	TC 1033	TC 1036	TC 1089
			Lower	Upper							
	Material										
N	Stream name	-			Natural-Gas						
	Storage state										
3	Gauge pressure	Pa	0		3.00E+04	3.00E+04	2.10E+05	2.10E+05	1.11E+06	1.14E+06	6.60E+06
4	Temperature	K	10	1000	276.4	277	267	279.6	279	279.15	281
	Vessel data										
7	Orifice diameter	m	0.001	50	0.152	0.152	0.152	0.152	0.075	0.075	0.020
	Atmospheric expansion data										
9	Atmospheric pressure	Pa	50000	120000	100000	100000	98413	100000	100000	100000	96973
10	Atmospheric temperature	K	10		276.35	279.15	281.15	279.65	282.35	279.15	285.85
11	Atmospheric humidity	-	0	1	0.95	0.89	0.8	0.88	0.81	0.89	0.91
12	Wind speed	m/s	0		1.5	1.7	0.3	3.5	4	3.5	9
Outputs		**Measured flow rate (kg/s)**			**2.6**	**2.9**	**8.6**	**8.3**	**8.2**	**8.8**	**3.7**
Output	**Description**	**pred./meas. flow rate**			**0.939**	**0.841**	**0.988**	**1.004**	**1.033**	**0.987**	**0.985**
	Release state										
1	Pressure	Pa			130000	130000	308413.333	310000	1210000	1240000	6696973.33
2	Temperature	K			276.4	277	267	279.6	279	279.15	281
3	Liquid fraction (MASS basis)	kg/kg			0	0	0	0	0	0	0
	Orifice state										
5	Pressure	Pa			100000	100000	167282.029	168299.2	656720.997	672999.598	3589843.79
6	Temperature	kg/kg			259.9	260.4	230.5	241.8	240.5	240.6	238.1
7	Liquid fraction (MASS basis)	-			0	0	0	0	0	0	0
8	Velocity	m/s			262.5	262.8	384.9	394.0	389.1	389.1	366.1
9	Vena contracta diameter	m			0.123	0.123	0.137	0.137	0.070	0.070	0.019
	Final (post-expansion) state										
10	Temperature	K			259.9	260.4	203.7	214.3	172.8	172.5	147.5
11	Liquid fraction (MASS basis)	kg/kg			0	0	0	0	0	0	0.01386298
12	Velocity	m/s			262.5	262.8	505.2	515.6	639.8	640.8	627.8
	ATEX outputs										
16	ATEX expansion method (1 = isentropic, 2 = cons momentum)	-			2	2	2	2	2	2	2
17	Expanded diameter	m			0.123	0.123	0.147	0.147	0.119	0.120	0.073
	Other data										
20	Discharge coefficient	-			0.653	0.653	0.818	0.817	0.863	0.864	0.869
21	Mass release rate	kg/s			2.441	2.439	8.500	8.329	8.472	8.686	3.643

Table 5 DISC discharge input and results for natural gas field tests

Test Number	1042	1040	1083	1037	1033	1036	1089
Mass flow rate [kg/s][3]	2.6	2.9	8.6	8.3	8.2	8.8	3.7
Elevation of hole [m][3]	3	1.5	3	1.5	3	1.5	3
Wind direction from magnetic north [°][3]	245	228	340	230	255	240	260
Angle between wind and hole axes [°]	9	26	86	24	1	14	6
Post-expansion temperature [K][6,7]	259.8	260.4	203.7	214.3	172.8	172.5	143.9
Expanded radius [m] [6,7]	0.0614	0.0614	0.0736	0.0734	0.0595	0.06015	0.036395
Stagnation pressure [barg][2, 3]	0.3	0.3	2.1	2.1	11.1	11.4	66
Stagnation temperature [K][2, 3]	276.4	277	267	279.6	279	279.15	281
Wind Speed [m/s][3]	1.5	1.7	0.3	3.5	4	3.5	9
Atmospheric Pressure [mm Hg][3]	750	750	738.1	750	750	750	727.3
Air temperature [K][3]	276.35	279.15	281.15	279.65	282.35	279.15	285.85
Relative Humidity (fraction)[3]	0.95	0.89	0.8	0.88	0.81	0.89	0.91
Discharge Diameter [mm][3]	152	152	152	152	75	75	20

Table 6 Summary of ambient and discharge data employed by the JFSH models for simulating horizontal natural gas jet fires reported by Bennett et al. [3]

Test 1040				
x [m]	y [m]	z [m]	ξ [degrees]	γ [degrees]
15	-10.3	-0.5	0	90
15	-14.3	-0.5	0	90
15	-24.3	-0.5	0	90
15	-30.3	-0.5	0	90
10	-18.3	-0.5	0	90
15	14.3	-0.5	0	90
15	24.6	-0.5	0	90
Test 1083				
x [m]	y [m]	z [m]	ξ [degrees]	γ [degrees]
9	-10.3	-2	0	90
9	-14.3	-2	0	90
9	-18.3	-2	0	90
9	-22.3	-2	0	90
9	-26.3	-2	0	90
9	-30.3	-2	0	90
9	-44.3	-2	0	0
50	-0.3	-2	0	0
55	-0.3	-2	0	0
60	-0.3	-2	0	0
Test 1033				
x [m]	y [m]	z [m]	ξ [degrees]	γ [degrees]
15	-10.3	-2	0	90
15	-14.3	-2	0	90
15	-24.3	-2	0	90
15	-30.3	-2	0	90
5	-18.3	-2	0	90
10	-18.3	-2	0	90
15	14.3	-2	0	90
15	24.6	-2	0	90
Test 1089				
x [m]	y [m]	z [m]	ξ [degrees]	γ [degrees]
15	-10.3	-2	0	90
15	-14.3	-2	0	90
15	-18.3	-2	0	90
15	-22.3	-2	0	90
15	-26.3	-2	0	90
15	-30.3	-2	0	90
15	-44.3	-2	0	90

Table 7 Observer (radiometer) position and orientation with respect to discharge point for Tests 1040, 1083, 1033 and 1089 (horizontal natural gas jet flames) (source: Bennett et al. [3] and Johnson et al[2])

2.2.1 Validation of JFSH-Johnson and RADS models against field data

JFSH-Johnson model [Flame Length, L_B]

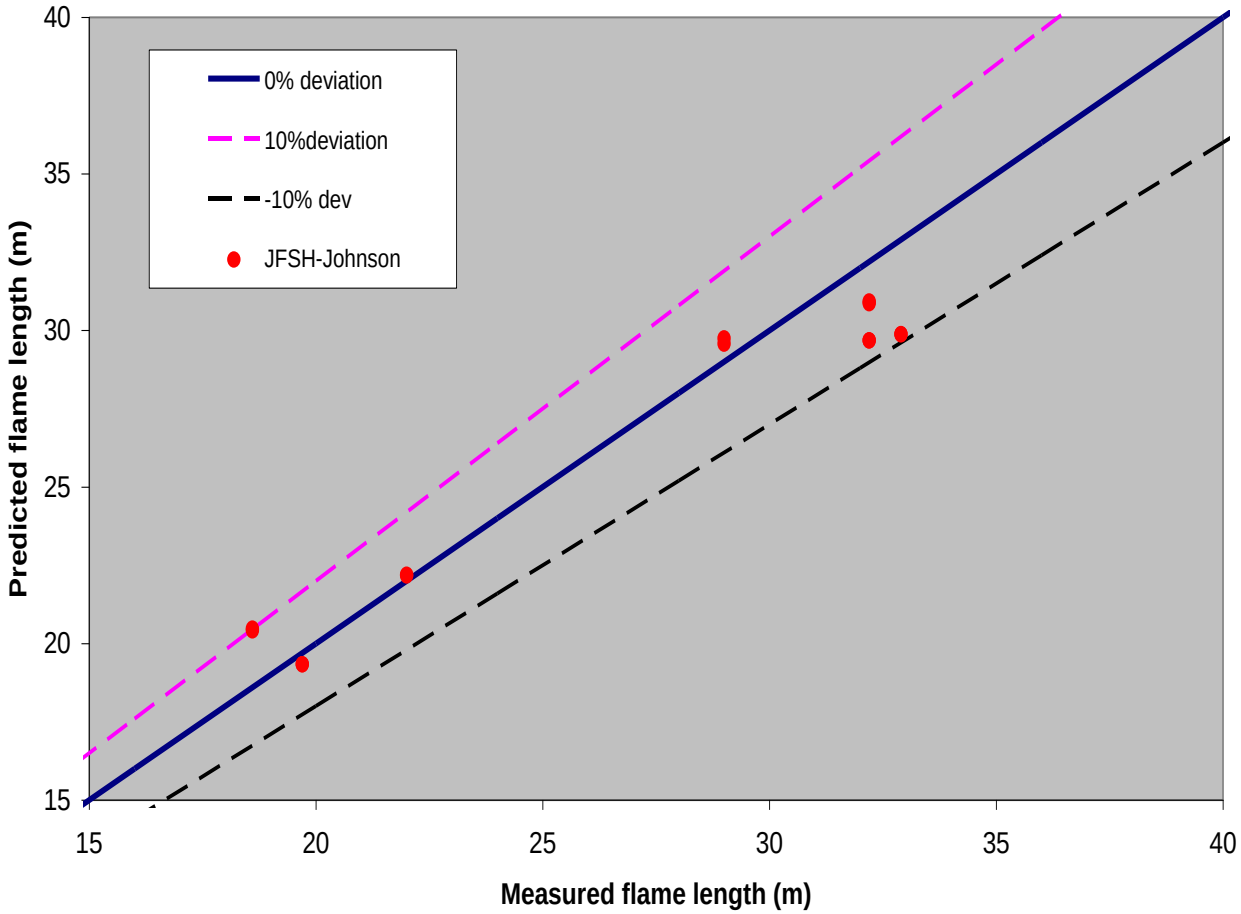

Figure 6: Variation of predicted against measured flame lengths for horizontal natural gas jet flames (field data obtained from literature[3]

Figure 6 shows the variation of the predicted flame lengths against measured data. The simulated results are based on the JFSH-Johnson (legend: JFSH-Johnson) model. The following can be observed:

- Close agreement is observed between simulated and measured data with simulated results generally lying within ±10% of measured data.
- On average, the percentage absolute deviation of simulated results from measured data is ca 5%.

In general, results from the JFSH-Johnson model compares very well with measured data for horizontal natural gas flares. This is expected as the Johnson et al model was specifically developed for flares resulting from horizontal vapour phase releases.

JFSH-Johnson-RADS model

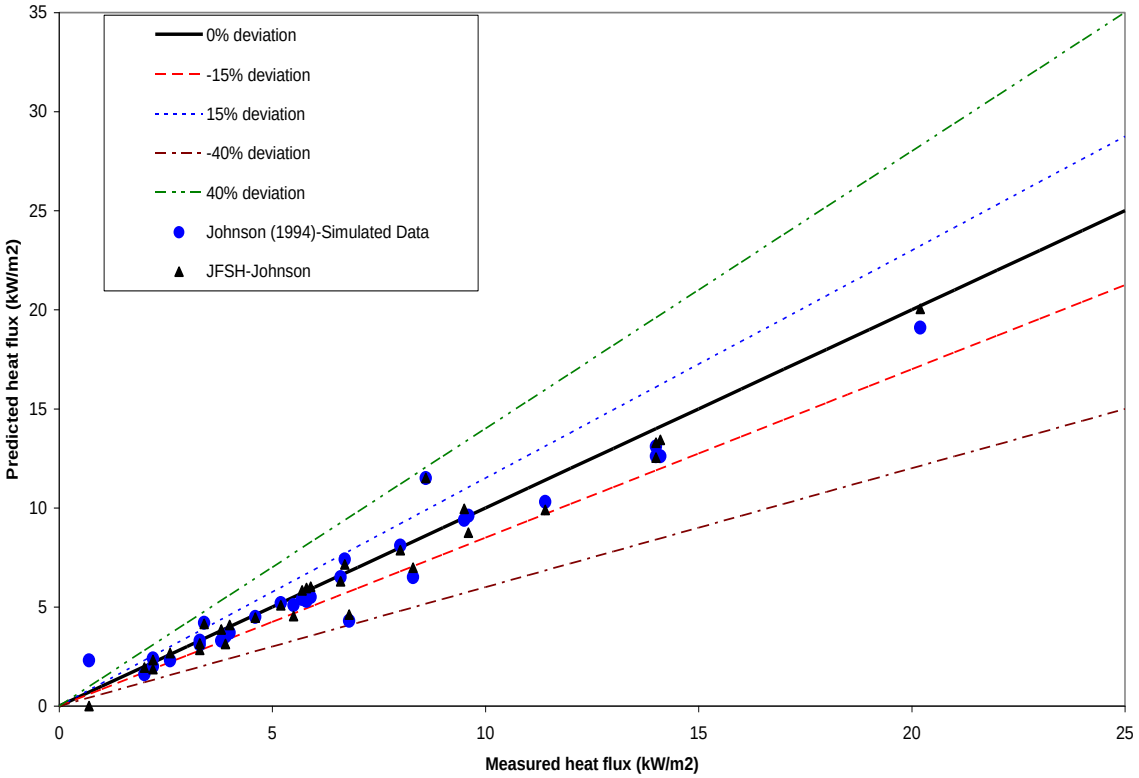

Figure 7 **Variation of predicted against measured incident radiation at different observer positions and orientations using the RADS (JFSH-Johnson) and simulated data reported by Johnson et al. (1994)**

Figure 7 compares the variation of predicted incident radiation [kW/m^2] with measured data for Tests 1040, 1083, 1033 and 1089 based on the flame characteristics predicted by the JFSH-Johnson model [legend: JFSH-Johnson]. The reported values of incident radiation predicted by the Johnson et al. (1994) flame shape and radiation models [legend: Johnson (1994)-Simulated Data] at each observer location are also presented[2]. Incident radiations corresponding to 0, ±15 and ±40% from measured data are represented by linear plots on Figure 7. Within limits of uncertainty in measured data, the following observations are made:

- Good agreement is observed between the predicted and measured incident radiation for the JFSH-Johnson-RADS model. In addition, there is close semblance in simulated results from the JFSH-Johnson-RADS and the Johnson et al. (1994) radiation models. All simulated results lie within ±40% of measured data.
- On average, the percentage absolute deviation from measured data for the JFSH-Johnson-RADS and Johnson et al. (1994) simulated results is ca 12.1%, and 17.3% respectively.

3 VALIDATION OF THE LIQUID/TWO-PHASE JET FIRE MODEL

3.1 Original validation

The following discusses the results of validating the JFSH-Cook models against field data reported by Bennett et al[3] and Selby and Burgan (1998)[5] for jet flames resulting from horizontal liquid/two-phase releases. Bennett et al report five tests that relate to free two-phase jet flames, while the Selby and Burgan data (also referred to as JIP-1 and JIP-2 tests) relate to jet flames resulting from liquid-phase (crude-oil) releases. For each test, the flame length and surface emissive power were measured and reported. Table 8 shows the measured composition (mole %) for the LPG mixture employed in the Bennett et al tests, while Table 9 presents a summary of pertinent JFSH input data for each test case. The specific composition of the crude-oil mixture in the Selby and Burgan test is unknown, as such, the fluid is assumed to be n-octane.

For the Bennett et al tests, no information was provided with respect to the fluid's stagnation pressure or temperature. Based on data provided, it is assumed that the ambient and stagnation temperatures are equal. Also, for the discharge calculations, the drive (upstream) pressure is used in place of the stagnation pressure. The post-expansion temperature and expanded radius were estimated from the DISC[6] and ATEX[7] routines in PHAST6.4 based on the assumed stagnation temperatures and pressures. With the exception of tests 3026 and 3029, flow-rate predictions from the discharge routines for each test case showed good agreement with measured data. However, the measured flow-rates for each test were used (in place of predicted values) as input into the JFSH models.

Component	Mole %
Methane	0.0
Ethane	0.2
Propane +	97.4
Iso-butane	1.6
N-butane	0.8

Table 8 Typical LPG composition for horizontal two-phase jet fire field tests (source: Bennett et al., 1991)[3]

Test Number	3007	3006	3028	3026	3029	JIP-1	JIP-2
Mass flow rate [kg/s][3, 5]	1.8	1.5	5.7	16.1	18	5.0	5.0
Elevation of hole [m][3, 5]	3	1.5	3	3	1.5	3	3
Wind direction from magnetic north [°][3, 5]	255	260	243	270	245	249	258
Angle between wind and hole axes [°]	1	6	11	16	9	5	4
Post-expansion temperature [K] [6,7]	230.8	230.9	230.1	231	231	294	295.2
Expanded radius [m] [6,7]	0.018	0.018	0.035	0.085	0.084	0.005	0.007
Drive/Stagnation Pressure (barg) [3, 5]	9.7	9.7	7.7	6.5	6.3	20	7.1
Stagnation temperature [K] [3, 5]	288.85	286.35	278.45	286.85	281.15	294.45	295.35
Wind Speed [m/s][3, 5]	4.5	5.8	1.5	3.7	2	3.1	2.5
Atmospheric Pressure [mm Hg][3, 5]	744.5	746.3	721.3	750	750	744.1	744.1
Air temperature [K][3, 5]	288.85	286.35	278.45	286.85	281.15	294.45	295.35
Relative Humidity (fraction)[3, 5]	0.69	0.79	0.92	0.59	0.82	0.548	0.49
Discharge Diameter [mm][3, 5]	10	10	20	52	52	14	18

Table 9 **Summary of ambient and discharge data employed by the JFSH-Cook model for simulating horizontal two-phase LPG and liquid-phase n-Octane jet fires reported by Bennett et al. [3] and Selby and Burgan[5] (i.e., JIP-1 and JIP-2) respectively**

Observations from the two-phase validation exercise

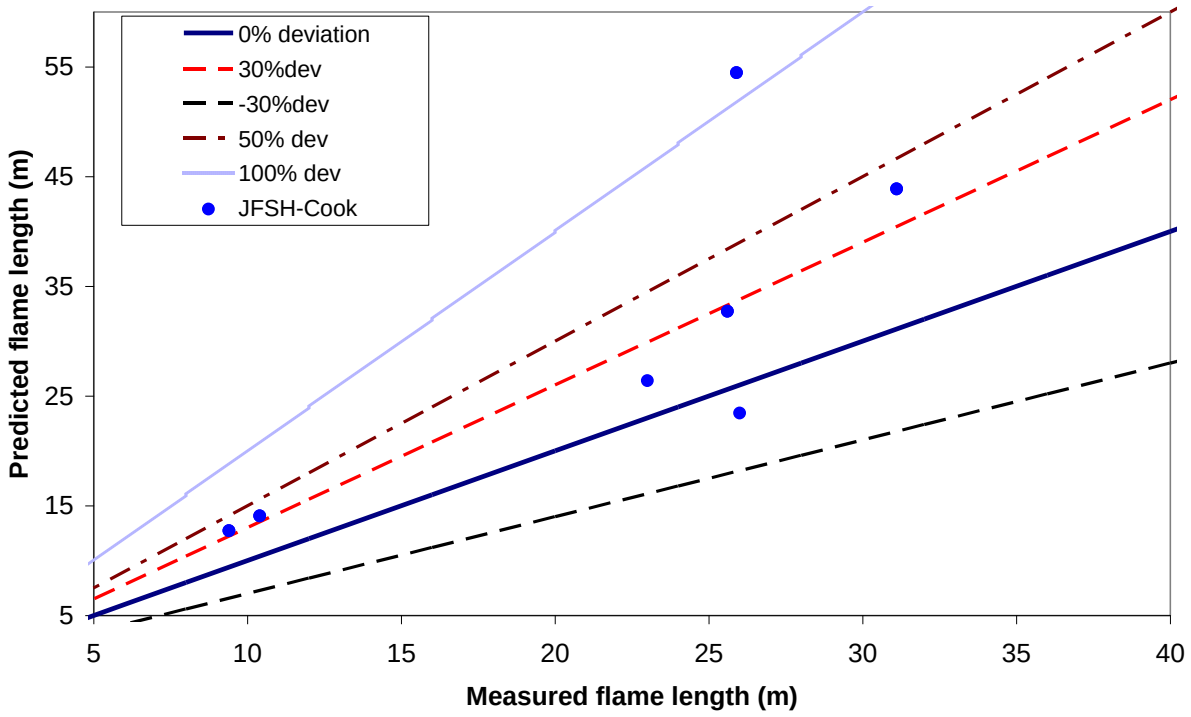

Figure 8 **Variation of predicted against measured flame lengths for horizontal liquid and two-phase jet flames (field data obtained from literature[3, 5])**

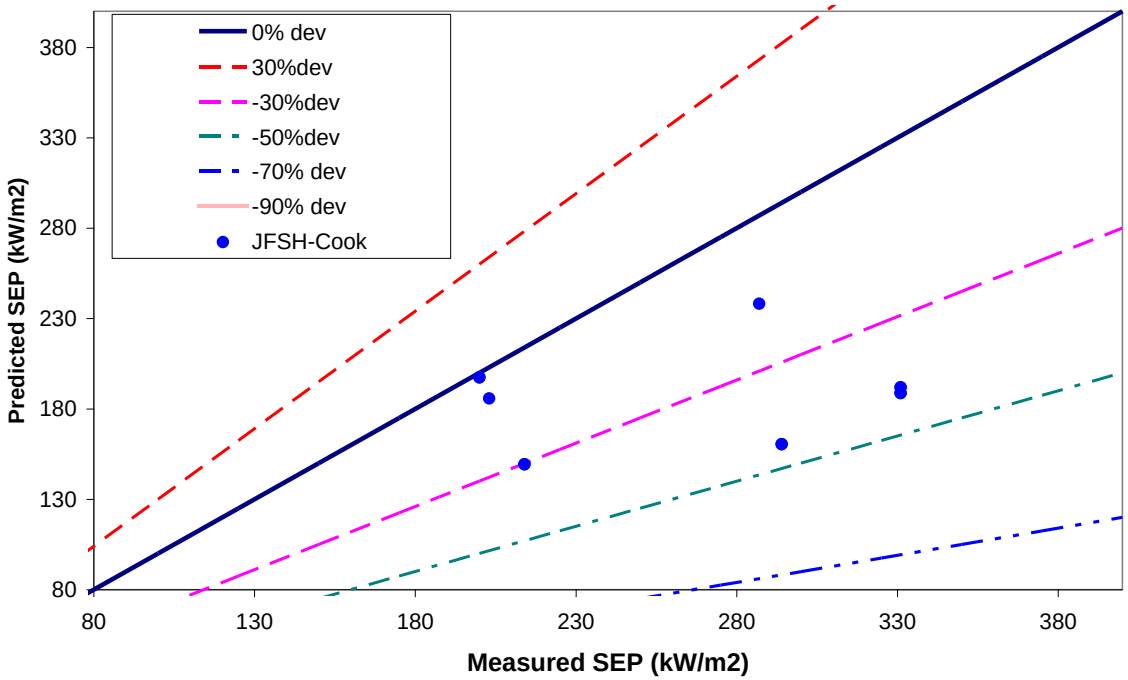

Figure 9 **Variation of predicted against measured surface emissive power (SEP) for horizontal two-phase LPG jet fires (field data obtained from literature[3])**

Figure 8 and Figure 9 show the variation of the predicted flame lengths and surface emissive power against measured data respectively. The simulated results are based on the modified JFSH-Cook (legend: JFSH-Cook) liquid/two-phase jet fire model (see companion theory manual)

- Flame Length [L_B]
    - With the exception of two data points (Tests 3026 and 3029), the JFSH-Cook model generally estimates flame lengths to within ca ±30% of measured data.
    - Simulated flame lengths based on the JFSH-Cook model are generally conservative (i.e., longer than is observed in reality)
    - On average, the percentage absolute deviation from measured data of simulated results from the JFSH-Cook model is ca 43.7%.

- Surface emissive power (SEP) [$W_{Surface}$]
    - The JFSH-Cook model generally underestimates flame SEP to within ca -50% of measurements. This is probably due to the model's overestimation of flame-lengths which would generally lead to underestimation of flame SEP.
    - On average, the percentage absolute deviation from measured data of simulated results from the JFSH-Cook model is ca 29.1%.

In all, for the cases studied, simulated results from the JFSH-Cook liquid/two-phase jet fire model compare relatively well with measured data. The flame length predictions, generally, are conservative and lie within ±30% of measured data while average estimates of flame SEP is within -30% of measured data[i].

3.2 Revised validation

The current section constitutes an update of the validation for 2-phase jet fires documented in the previous section following on an update and further extension of previous validation work by Eelke Kooi[8]. This work includes validation against the following experiments:

[i] Care should be taken in simulating jet flames resulting from liquid-phase releases. Experimental evidence suggests that pure non-flashing liquid releases rarely result in stable jet flames[5].

- 2-phase LPG jet-fire experiments B3006, B3007, B3026, B3028 & B3029 carried out by Shell and British Gas at Spadeadam (late eighties and early nineties) as part of the CEC Project AA.

    - Data are obtained from the overview report by Bennett et al. (1991)[3] and the test reports[9,10,11,12,13] for these tests
    - The LPG is now modelled as pure propane instead of a mixture, since the mixture primarily consists of propane (typical composition[3] 97.4% propane, 1.6% isobutene, 0.8% n-butane, and 0.2% ethane).
    - Attached to the storage vessel of 2m^3 is a 67m supply line (152mm inner diameter) and a 13m pipe (52mm). Quoted value of surface roughness of all pipework is 1.5µm[ii] with pressure and temperature sensors at 150mm upstream from the orifice (no pressure reading for test B3026).
    - For tests B3026 and B3029, the DISC line rupture model is used with a 150mm length with upstream pressure varied such as to match the observed flow rate. This is different from our original approach where the orifice model was applied. Also it was incorrectly assumed for our original approach that the stagnation temperatures were equal to the ambient temperatures.
    - For tests B3006, B3007 and B3028, an orifice is attached at the end of the discharge pipe, and therefore the DISC orifice discharge model is used. The orifice diameter is 10mm for tests B3006 & B3007 and 20mm for test B3028. The measured storage temperature and pressures are specified as input of vessel temperature and pressures (assumed value of temperature for B3006). Thus, since the calculated flow rate was shown to be close to the predicted flow rate, the pressure was NOT varied to match the observed flow rates for these simulations.

- Three 2-phase butane experiments carried out by Sekulin and Acton at British Gas at Spadeadam (Cumbria, UK) as part of the CEC project JIVE (July 1992 – December 1993).

    - Data are obtained from the test report by Sekulin and Acton[14] for the three tests of liquid butane release, i.e. SA 8050, SA8051 & SA8052.
    - The butane is modelled as pure n-butane instead of a mixture, since the mixture primarily consists of butane (given composition 95.56% n-butane, 2.19% isobutane, 1.42% isopentane, 0.59% propane, 0.14% butenes, 0.06% ethane, 0.03% n-pentane, 0.01% ethene).
    - Attached to the storage vessel (unknown size) is a 79m supply line (152mm inner diameter) and a 1.850m pipe (40mm). The value of the surface roughness of all pipework is 1.5µm[ii] with no pressure and temperature measurements available near upstream to the orifice. The DISC line rupture model is used with a 1.85m length with upstream pressure varied such as to match the observed flow rate.
    - Two sets of wind measurements are available for the tests, i.e. measurements from a sonic anemometer by BG and measurements from a vane anemometer by Shell. The sonic anemometer is 50-60m upstream of the release point at 10m height and the vane anemometer is just upstream of the test rig at 1.1m height. Because the measurements by Shell were taken at a position much closer to the release point, the Shell wind data are used for results presented here.

- Liquid crude-oil jet-fire experiments SB1,SB2 carried out by British Gas at Spadeadam (May-June 1995) for the Steel Construction Institute (SCI) as part of Phase 2 of the Blast and fire engineering project.

    - Data are obtained from the overview report by Selby and Burgan (1998)[5] and the test reports[15,16] for tests SB1 and SB2.
    - The crude oil is now modelled as pure nonane instead of pure octane following analysis by Eelke Kooi[8] of the oil composition.
    - Attached to the storage vessel (unknown size) is a supply line (unknown length, 55mm inner diameter) and connected to this a 4.4m pipe (also 55mm). The release was from an orifice at the end of the pipe with varying diameter (14mm for SB1 and 18mm for SB2). Hence the DISC orifice model ('Leak' scenario) is used. Using the measuring stagnation pressure, the flow rate was found to be predicted very accurately (5% over-prediction for Test 1 and 2% under-prediction for Test 2. Subsequently the stagnation pressure input to DISC was varied to match the flow rate, and the DISC post-expansion discharge results thus derived where input to the JFSH jet-fire model.

In addition to validation of flame length and SEP, also validation of radiation data has been added.

[ii] TNER.91.022 (Bennett 3026/3029) and GRC R0367 (Sekulin 8051) both quote a value of 0.0015m (or 1.5mm) for the surface roughness, while referring to *stainless steel pipe having an internal surface which is clean, smooth and free from irregularities*. The website http://www.engineeringtoolbox.com/surface-roughness-ventilation-ducts-d_209.html quotes a value of pipe roughness for stainless steel as 0.015mm=15 µm m and not 1.5mm. Recent communication with the Author confirmed the roughness should be 1.5 µm and not 1.5mm. Sensitivity of model predictions are tested for pipe roughness of 1.5 µm & 15 µm. When flow rate is maintained in the discharge predictions to provide input for the jet-fire model, the jet-fire predictions are proved to be insensitive to this parameter.

Table 12 summarises the experimental conditions for the above tests, and indicates input used for the Phast discharge model DISC (pipe or orifice scenario), the Phast dispersion model UDM, and the Phast jet-fire model JFSH (Cook model). Table 13 shows the calculated model results. The DISC post-expansion data (temperature, liquid fraction, velocity) are input to the JFSH jet-fire model. For all experiments except SB2 the input flow rate Q_{JFSH} to JFSH equals the entire flow rate $Q_{discharge}$, since the rainout liquid mass fraction $\eta_{rainout}$ is less than 2/3. For SB2, a reduced flow rate is applied $Q_{JFSH} = 3(1- \eta_{rainout}) Q_{discharge} < Q_{discharge}$, since $\eta_{rainout} > 2/3$ (see Table 13) while retaining the calculated DISC post-expansion velocity (i.e. effectively reducing the post-expansion radius).

Lowesmith, Henkinson, Acton and Chamberlain[17] developed a flame-length correlation based on a best fit against a large amount of jet fire tests. Here the flame length was expressed as a function of the flame power Q (MW), where the flame power is defined as the product of the mass release rate (kg/s) and the heat of combustion (J/kg).

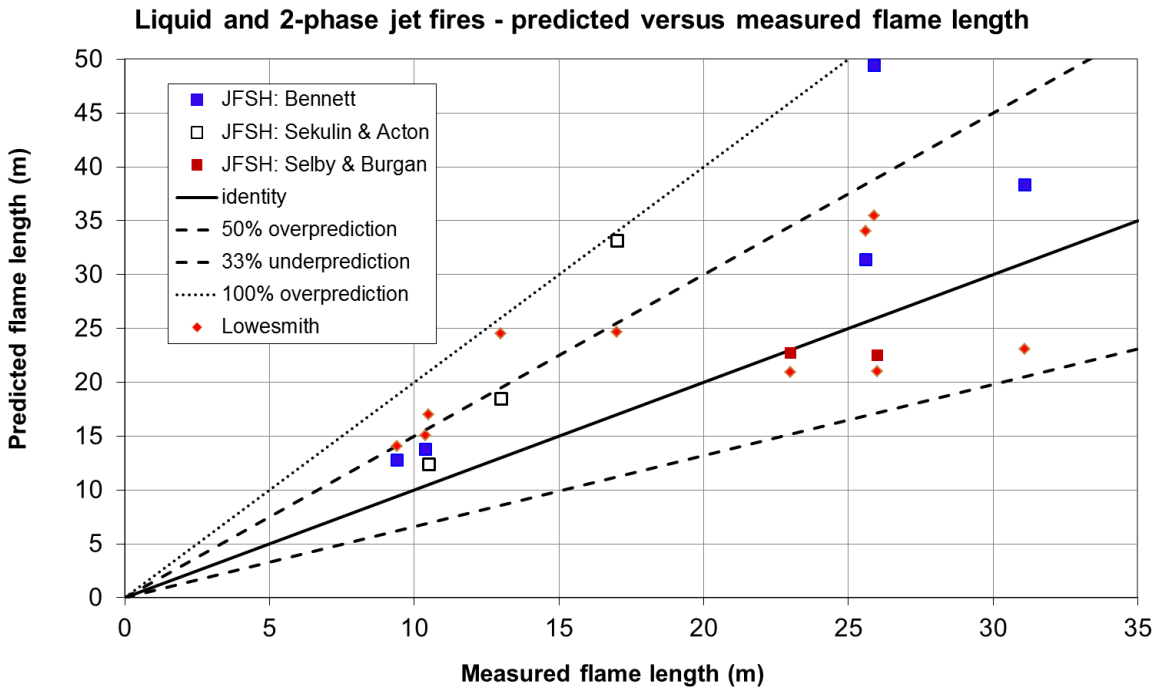

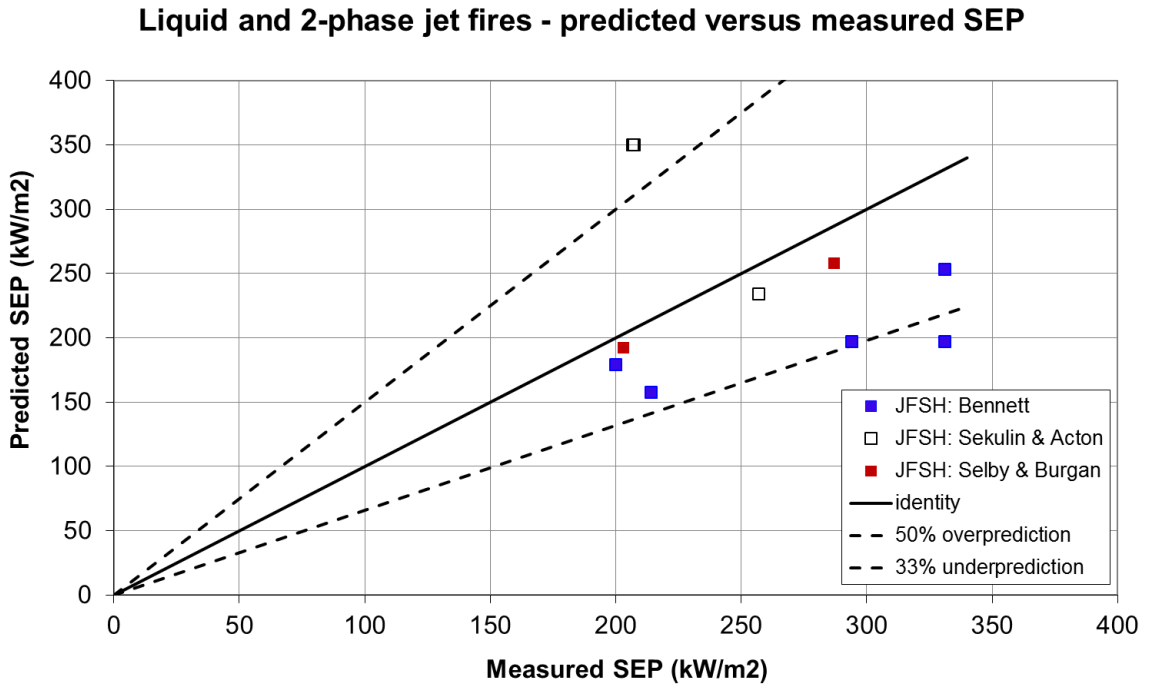

Figure 10. Two-phase fire tests - predicted versus measured flame length and SEP

Figure 10 graphically compares the predicted versus measured flame length and SEP for the liquid and 2-phase experiments (as derived from the measured results given by Table 12 and the predicted results given by Table 13). Flame lengths estimated using Lowesmith correlation are also included to assess the accuracy of the predictions by JFSH-Cook. The following conclusions can be drawn:

- Overall the flame length is accurately predicted (mostly within 33%) by JFSH, with the JFSH model producing more accurate results than the Lowesmith correlation.
- On average, the percentage absolute deviation from measured SEP of the predictions by the JFSH-Cook model is 37.52%. Please be aware that the SEP is over-predicted nearly 70% for SA8050 & SA8052 and the measured SEP is only reported at NAR1 in these cases. When measurements are reported at both NAR1 and NAR2 in SA8051, the SEP at NAR1 is much lower than at NAR2 as shown in Table 12 and please refer to Table 12 for the location of NAR1 & Nar2. So the over-prediction of 70% for SA8051& 8052 may be overstated because of the missing measurements. For SA8051 and SA8052, the predicted SEP is cut-off by the JFSH maximum SEP of 350 kW/m^2 (corresponding to the maximum value proposed by Geoff Chamberlain – private communication).

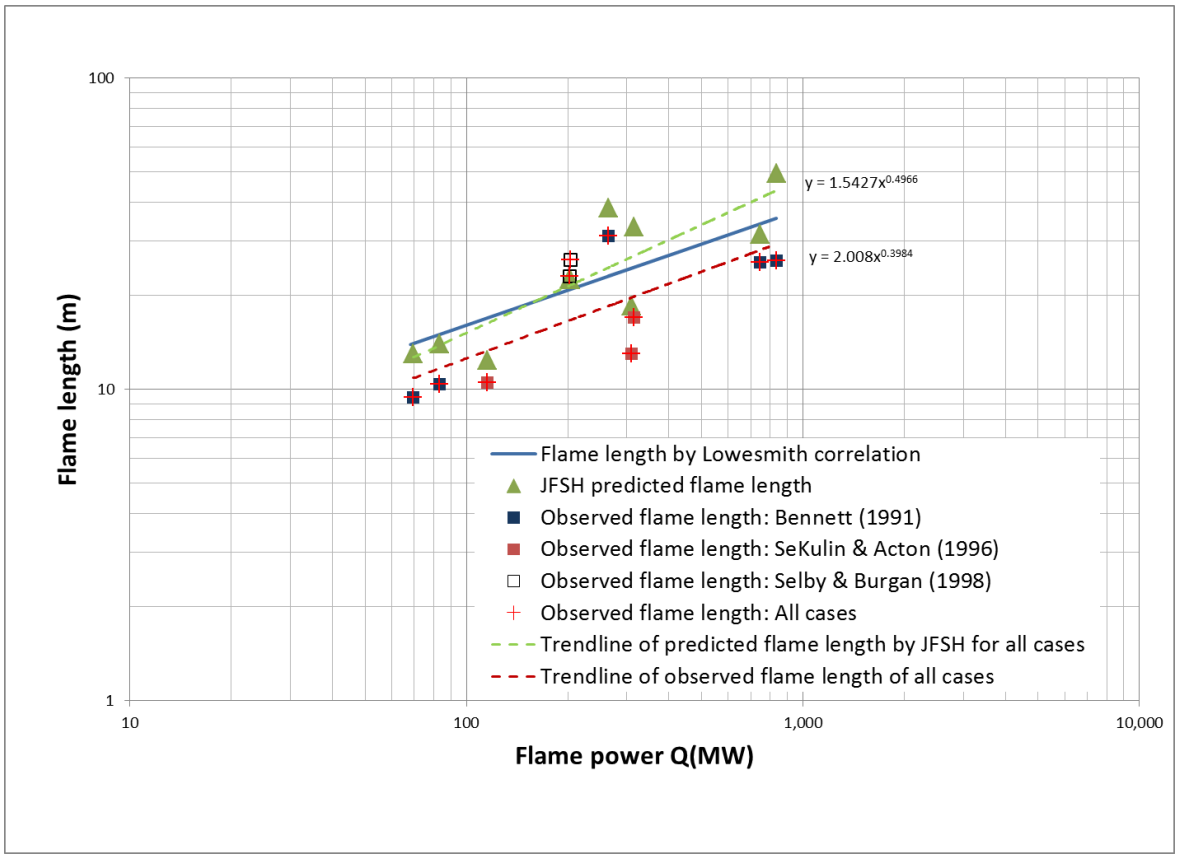

Figure 11 JFSH predictions of flame length versus observed data and Lowesmith correlation

Figure 11 plots the flame length (m) as function of the flame power Q (MW). For each of the experiments, the figure compares the flame lengths predicted by JFSH-Cook (denoted by green triangular markers) and estimations using the Lowesmith correlation (blue solid line) against the observed data (denoted by square markers). In general, the predictions by JFSH-Cook are conservative and in reasonable agreement with the measurements. The agreement is better than the Lowesmith correlation for releases with flame power less than 300MW, i.e. small/medium releases. This may be because the correlations of JFSH-Cook are largely based on measurements of small/medium releases. The figure illustrates that the Lowesmith correlation does NOT provide overall closer agreement (also not for the larger scale releases), and therefore the JFSH-Cook flame length correlation was not modified.

Test	Radiometer	downstream X	crossstream Y	vertical Z	Observed	JFSH-Cook	JFSH-Cook	Average
		m	m	m	kW/m2	kW/m2	deviation	deviation
Bennett 3026	**3026-1**	15	10	1	48.7	61.7	27%	
Bennett	**3026-2**	15	14	1	45.2	44.3	-2%	
	3026-3	15	18	1	20	33.5	68%	
	3026-4	15	24	1	18.2	23.3	28%	
	3026-5	15	30	1	14.7	16.7	14%	
	3026-9	5	18	1	22.8	19.3	-15%	
	3026-10	10	18	1	29.5	26.3	-11%	
	3026-12	15	-14.6	1	27.8	42.4	52%	
	3026-13	15	-24.9	1	14.2	22.1	56%	24%
Bennett 3029	**3029-1**	15	10	1	24.6	44.8	82%	
	3029-2	15	14	1	23.8	32.5	36%	
	3029-4	15	24	1	12.7	18.7	47%	
	3029-5	15	30	1	10.5	14.4	37%	
	3029-10	10	18	1	21.9	19.5	-11%	
	3029-12	15	-14.6	1	35.3	31.2	-12%	
	3029-13	15	-24.9	1	16.8	17.9	7%	27%
Bennett 3006	**3006-1**	10	8.7	1	6	20.8	246%	
	3006-2	10	10.8	1	5.7	13.8	141%	
	3006-4	10	12.8	1	3.3	6.6	100%	
	3006-5	10	20.8	1	2.6	3.8	46%	
	3006-9	6	20.8	1	1.8	4.0	122%	
	3006-10	8	20.8	1	2.7	4.0	46%	
	3006-11	12	20.8	1	1.8	3.6	99%	
	3006-12	14	20.8	1	1.5	3.4	128%	
	3006-13	30	0	1	1.5	3.2	112%	
	3006-14	20	-15	1	4.4	4.6	4%	104%
Bennett 3007	**3007-2**	10	10.8	1	4.8	13.9	189%	
	3007-4	10	12.8	1	2.9	6.7	132%	
	3007-5	10	20.8	1	2.3	3.8	67%	
	3007-9	6	20.8	1	1.5	4.0	163%	
	3007-10	8	20.8	1	2.3	4.0	72%	
	3007-11	12	20.8	1	1.6	3.6	128%	
	3007-12	14	20.8	1	1.4	3.4	144%	
	3007-13	30	0	1	1.3	3.5	168%	
	3007-14	20	-15	1	3.6	4.7	31%	122%
Bennett 3028	**3028-1**	15	10	1	13.5	31.4	133%	
	3028-2	15	14	1	12.5	21.3	70%	
	3028-4	15	18	1	7.4	9.6	30%	
	3028-5	15	24	1	5.4	6.5	21%	
	3028-10	5	18	1	12.2	12.1	-1%	
	3028-12	15	-14.6	1	17.5	20.2	15%	
	3028-13	15	-24.9	1	8.7	9.1	4%	39%

Table 10. Two-phase fire tests –Phast radiation predictions versus observed data for Bennett Tests (i.e. B3006, B3008, B3026, B3028 & B3029)

Test	Radiometer	downstream X	crossstream Y	vertical Z	Observed	JFSH-Cook	JFSH-Cook	Average
		m	m	m	kW/m2	kW/m2	deviation	deviation
SA 8050	8050-1	14	10	1	10.29	17.0	65%	
Sekulin&Acton	8050-2	14	15	1	6.92	10.7	54%	
	8050-3	14	20	1	5.1	7.6	49%	
	8050-4	14	25	1	3.46	5.6	61%	
	8050-5	14	30	1	2.8	4.3	52%	
	8050-6	14	35	1	2.14	3.3	56%	
	8050-13	35	0	1	6.74	8.2	22%	
	8050-14	40	0	1	3.82	6.2	61%	
	8050-SH1	-10.2	-1.7	5.4	12.17	16.1	32%	
	8050-SH2	-10.2	28.3	2.3	2.63	2.2	-17%	
	8050-SH3	14	28.3	1	3.03	4.6	53%	
	8050-SH4	40	28.3	1	2.31	3.1	33%	
	8050-SH5	40	0.3	0.5	3.41	6.1	79%	
	8050-SH6	14	-27.7	1	8.24	20.6	150%	54%
SA 8051	8051-1	14	10	1	23.76	42.6	79%	
	8051-2	14	15	1	15.82	27.3	73%	
	8051-3	14	20	1	11.14	18.8	69%	
	8051-4	14	25	1	7.5	13.5	80%	
	8051-5	14	30	1	5.77	10.0	74%	
	8051-6	14	35	1	4.45	7.7	73%	
	8051-13	35	0	1	7.95	137.4	1628%	
	8051-14	40	0	1	4.74	51.2	979%	
	8051-SH1	-10.2	-1.7	5.4	7.1	3.7	-47%	
	8051-SH2	-10.2	28.3	2.3	3.47	4.3	23%	
	8051-SH3	14	28.3	1	6.36	11.1	74%	
	8051-SH4	40	28.3	1	3.29	8.1	145%	
	8051-SH5	40	0.3	0.5	3.99	47.0	1079%	
	8051-SH6	14	-27.7	1	9.77	13.0	33%	312%
SA 8052	8052-1	14	10	1	5.91	10.3	74%	
Sekulin&Acton	8052-2	14	15	1	3.97	6.4	60%	
	8052-3	14	20	1	2.98	4.3	46%	
	8052-4	14	25	1	2.01	3.1	55%	
	8052-5	14	30	1	1.65	2.3	41%	
	8052-6	14	35	1	1.22	1.8	46%	
	8052-13	35	0	1	3	3.6	19%	
	8052-14	40	0	1	1.98	2.6	33%	
	8052-SH1	-10.2	-1.7	5.4	7.53	11.5	53%	
	8052-SH2	-10.2	28.3	2.3	1.51	1.3	-15%	
	8052-SH3	14	28.3	1	1.74	2.6	47%	
	8052-SH4	40	28.3	1	1.19	1.4	19%	
	8052-SH5	40	0.3	0.5	1.99	2.6	32%	
	8052-SH6	14	-27.7	1	4.53	5.5	21%	38%
SB1	SB1-1	14	10	1	35.9	55.7	55%	
Selby & Burgan	SB1-2	14	15	1	21.3	29.5	39%	
	SB1-3	14	20	1	13.7	17.5	27%	
	SB1-4	14	25	1	9.2	11.3	23%	
	SB1-5	14	30	1	6.8	7.8	15%	
	SB1-6	14	35	1	5.1	5.7	12%	
	SB1-7	14	40	1	3.7	4.3	17%	
	SB1-8	14	45	1	3.1	3.4	9%	
	SB1-9	14	-10	1	30.8	55.7	81%	
	SB1-10	14	-20	1	12.8	17.5	36%	
	SB1-11	14	-30	1	6.4	7.8	22%	
	SB1-12	14	-40	1	3.7	4.3	17%	
	SB1-13	34	0	1	9.2	24.6	167%	
	SB1-14	39	0	1	3.8	13.4	252%	55%
SB2	SB2-1	14	10	1	39.8	44.4	11%	
	SB2-2	14	15	1	21.4	23.8	11%	
	SB2-3	14	20	1	12.7	14.1	11%	
	SB2-4	14	25	1	8	9.2	14%	
	SB2-5	14	30	1	5.5	6.3	15%	
	SB2-6	14	35	1	4	4.6	16%	
	SB2-7	14	40	1	2.8	3.5	25%	
	SB2-8	14	45	1	2.3	2.7	19%	
	SB2-9	14	-10	1	19.5	44.4	128%	
	SB2-10	14	-20	1	7.9	14.1	79%	
	SB2-11	14	-30	1	4.1	6.3	55%	
	SB2-12	14	-40	1	2.4	3.5	46%	
	SB2-13	34	0	1	6.5	20.4	214%	
	SB2-14	39	0	1	2.5	11.2	350%	
	SB2-15	0	0	1	12.4	24.9	101%	73%

Table 11 **Two-phase fire tests –Phast radiation predictions versus observed data for Sekulin & Acton and Selby & Burgan**

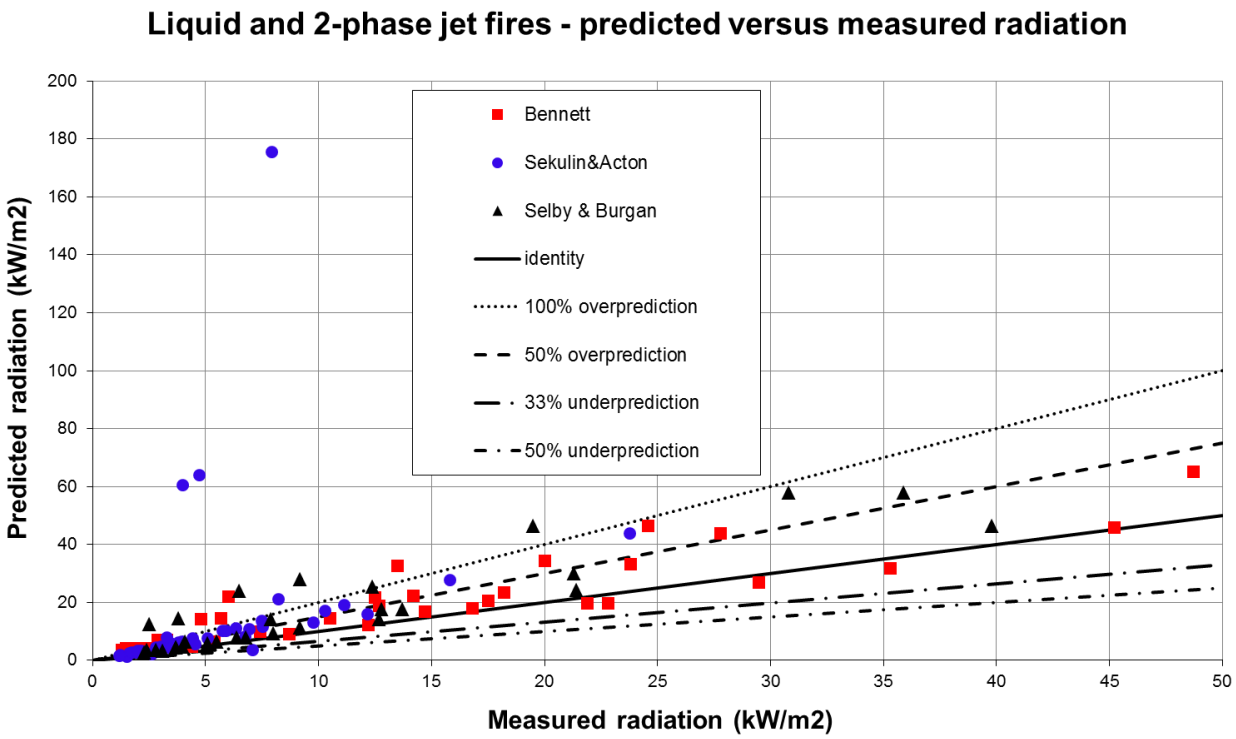

(a) Before flame adjustment for ground effects

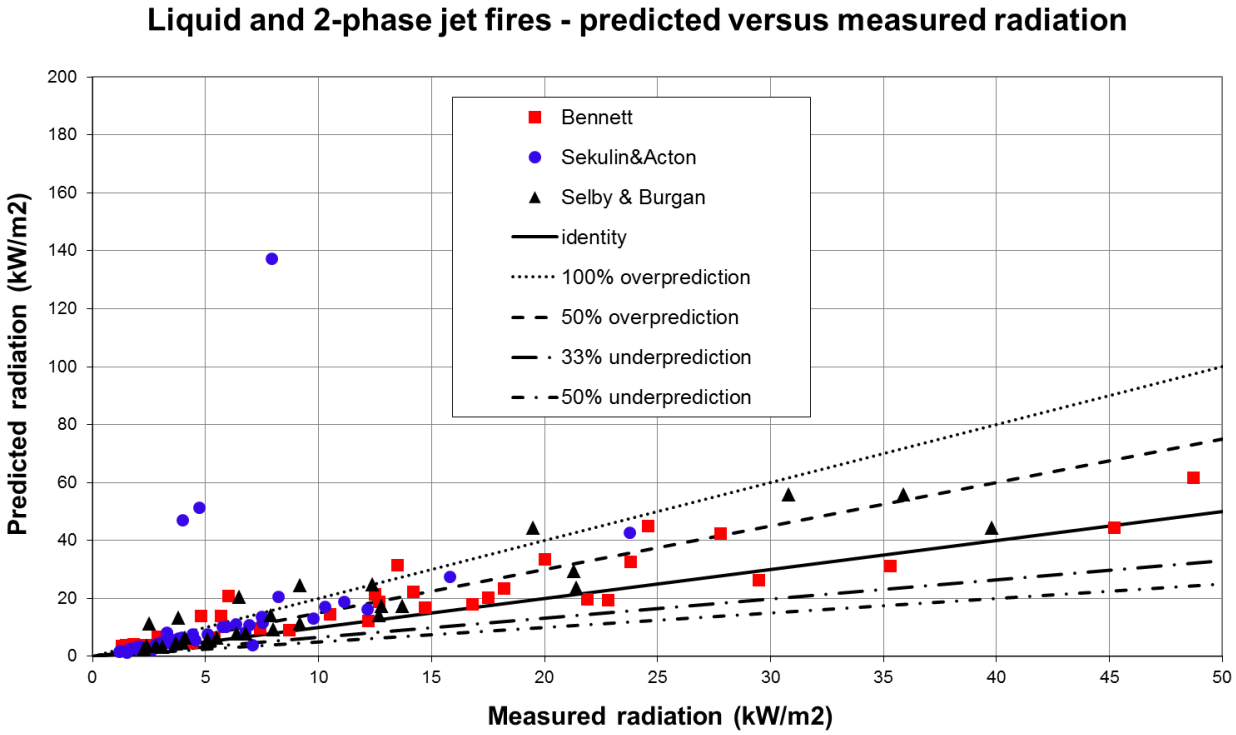

(b) After flame adjustment for ground effects

Figure 12. Two-phase fire tests - predicted versus measured incident radiations

Figure 12 graphically compares the predicted versus measured radiation. Figure 12a includes results before the flame adjustment for ground effects. Figure 12b includes results after the flame adjustment (see companion theory manual) corresponding to the measured and predicted results given by Table 10 and Table 11. Prior to the adjustment (Figure 12a), the overall overprediction of all measurements is 105%, while after the adjustment (Figure 12b) the overprediction is reduced to 91%. In Figure 12b most data points over-predict the observed data between 0 and 50%. This is with the exception for the SA 8051 sensors located along the release axis (y=0) for which a dramatic over-prediction is observed. This appears to be caused by an over-predicted flame length as well as insufficient fire lift-off.

Summary of the results

- Flame Length [LB]
  - Flame lengths predicted by the JFSH-Cook model are generally conservative (i.e., longer than the observed flame length), except a small under-prediction for the Selby & Burgan cases (i.e. SB1 & SB2).
  - On average, the percentage absolute deviation from measurements of simulated results by the JFSH-Cook model is 38% for liquid/2-phase releases.
- Surface emissive power (SEP)
  - The JFSH-Cook model generally predicts flame SEP within 50% of measurements, except SA8050 & SA8052 which are over-predicted by 70% and this may be overstated because of the missing measurements.
  - On average, the percentage absolute deviation from measured data of simulated results by the JFSH-Cook model is about 30%.
- Radiations
  - EXPS, the model for predicting radiation on Phast/Safeti, generally over-predicts radiations for these test cases of liquid/2-phase releases.
  - On average, the percentage absolute deviation from measured data is 91% when the predicted jet-fire cone is adjusted if the cone penetrates the ground.

Thus overall the results for the two-phase jet fires are found to be very satisfactory and to provide conservative predictions. Possible improvement may be considered in the future (resulting in reduced over-predictions) by e.g. using the methodology from the latest Shell jet-fire models (if made non-confidential).

Input	B3006	B3007	B3026	B3028	B3029	SA8050	SA8051	SA8052	SB1	SB2	Input for models
Discharge data											
Fuel	propane	propane	propane	propane	propane	butane	butane	butane	nonane	nonane	DISC,UDM,JFSH
orifice/line-rupture (pipe)	orifice	orifice	pipe	orifice	pipe	pipe	pipe	pipe	orifice	orifice	DISC scenario
supply line diameter (mm)	52.15	52.15	52.15	52.15	52.15	40	40	40	55	55	input DISC pipe only
pipe length modelled (m)	-	-	0.15	-	0.15	1.85	1.85	1.85	-	-	DISC
pipe roughness (micrometer)	-	-	1.5	-	1.5	1.5	1.5	1.5	-	-	DISC
orifice diameter (mm)	10	10		20					14	18	DISC
vessel pressure (barg)	9.7	9.7	6.5 vary in DISC	7.66	6.3 vary in DISC	- vary in DISC	- vary in DISC	- vary in DISC	-	-	DISC orifice, not used for DISC pipe (vary to match flow rate)
vessel temperature (C)	10	10	5.5	3.2	3.2	14.02	13.86	14.05	-		DISC
release elevation (m)	1.5	3	3	3	1.5	3	3	3	3	3	UDM,JFSH
pressure upstream of orifice (barg)[iii]	--	--	0.03	8.28	4.6	1.91	1.62	12.47	19	6.1	DISC orifice, not used for DISC pipe
temperature upstream of orifice (C)[iii]	--	--	--	--	--	-	-	-	21.4	29.2	DISC
Observed release rate (kg/s)	1.5	1.8	16.1	5.7	18.0	6.75	6.86[iv]	2.52	5.03	5	DISC and JFSH (excl. B3006, B3007, B3028)
averaging period (s) – radiation – flame shape, SEP	27-33	30-40	15-35	7-20	13-35 20-30	25-35	25-40	15-30	107-119	138-158	
Exit pressure											
Ambient data											
ambient temperature (C)	13.2	15.7	13.7	5.3	8.0	8.53	8.7	7.97	21.3	22.2	DISC,UDM,JFSH
ambient pressure (mbar)	995	993	1000	962	1000	995	995	995	992	992	DISC,UDM,JFSH
relative humidity (%)	79	69	59	92	82	34.2	35	38.5	0.548	0.49	UDM,JFSH
release direction from magnetic north (°)	74	74	74	74	74	74	74	74	74	74	
wind direction from magnetic north (°)	260	255	270	243	245	143v	181[v]	152[v]	249	258	
cross-wind angle wind and hole axis (°)	-6	-1	-16	11	9	111	73	102	5	4.98	JFSH
wind speed (m/s)	5.8	4.5	3.7	1.5	2	2.96[v]	0.5[v]	3.5[v]	3.1	2.5	UDM,JFSH
Jet-fire measurements											
Flame length (m)	9.4	10.4	31.1	25.6	25.9	13[vi]	17[vii]	10.5	26	23	
SEP (kW/m^2)	331	200	331	214	294	207 ---[viii]	151(NAR1) 257[viii](NAR2)	207 ---[viii]	287	203	

Table 12. Two-phase fire tests - experimental conditions and measurements

[Above data marked in red are not actually used as input data]

[iii] Upstream pressure/temperature: Bennett - 0.15m upstream of orifice, JIVE - 1.85m at start of 40mm pipe, SB – 0.13m upstream of orifice

[iv] SA 8051 report mostly mentions 6.86 kg/s, but in summary (page 1) it inconsistently mentions 6.67 m/s

[v] SA 8051 report at start mentions wind direction (Shell) of 181 degrees corresponding to 254-181=73 degrees. Page 1 of JIVE 8051 report however mentions angle of 40^0!

[vi] SA8050 report does not give value of measured flame length, Flame length is estimated according to SEP map in the report

[vii] SA 8051 report does not specify value of measured fire length; estimate adopted from Eelke Kooi

[viii] Spot SEP was measured using two narrow angle radiometers (i.e. NAR1 & NAR2) in JIVE tests. NAR1 aimed at a point 8.5m from the release point and 0.5m above the release axis. NAR2 aimed at a point 10.5m from the release point and 1.2m above the release axis. No flame SEP was reported in the JIVE reports, the adopted value are taken as reported value at NAR2 for SA8051 and at NAR2 for SA8050 & SA8052 which has no SEP reported at NAR1. Values in the summary sheets are used, which may differ from the values in the tables slightly.

Result	B3006	B3007	B3026	B3028	B3029	SA8050	SA8051	SA8052	SB1	SB2	Input for models
DISC discharge results											
drive pressure to match flow rate (barg)	NA use9.70	NA use9.70	4.6731	NA use7.66	4.31997	0.885	0.875	0.730	17.22	6.31	
flow rate (without matching flow rate)	1.55	1.55		5.53	-	-	-	-	5.25	4.90	
post-expansion temperature (K)	230.7	230.6	230.51	230	230.51	272.14	272.14	272.14	294.14	302.23	JFSH
post-expansion liquid fraction (-)	0.737	0.737	0.768	0.768	0.769	0.912	0.913	0.912	1	1	JFSH
post-expansion radius (m)	0.018	0.018	0.059	0.035	0.062	0.04	0.040	0.025	0.0054	0.0070	JFSH
post-expansion velocity (m/s)	171	171	152.74	151	146.47	46.66	46.22	45.93	75.47	45.84	
UDM Dispersion results											
rainout fraction	0	0	0	0	0	0.155	0.248	0.056	0.4936	0.7647	JFSH
JFSH-Cook results											
flame length (m)	12.74	13.80	38.9	31.4	50.0	18.5	33.2	12.4	22.5	22.7	
SEP (kW/m2)	197.2	179.3	245.9	158.1	192.5	350	234.9	350	258.2	192.1	

Table 13. Two-phase fire tests - Phast DISC/UDM/JFSH predictions

3.3 Two-Phase Hydrogen Fires

3.3.1 Introduction

A total of seven tests were performed at Spadeadam on behalf of Forsvarets forskningsinstitutt (FFI) Norwegian Defence Research Establishment[18]. However only two of these were ignited tests. Test 6 (Figure 14) was horizonal and therefore a good match to the jet fire modelling that is in Phast and Safeti. Test 5 (Figure 13) was configured to project downwards with the release point only 0.32m from the concrete pad so it was not a conventional 'free-field jet fire'.

Figure 13 - Test 5 taken from behind the release point

Figure 14 - Test 6 taken from behind the release point (after dark)

Jet fire input data	Test 05	Test 06	Comments
Averaging start time [s]	330.0	180.0	This averaging period is defined in the "Report" worksheet. Averaging periods may vary for concentration, radiation etc.
Averaging end time [s]	350.0	200.0	
AMBIENT DATA			
Wind_Direction_High [°]	264	232	Values taken from "Report" worksheet and based on averaging period at start of this table.
Wind_Direction_Low [°]	272	247	
Wind_Speed_High [m/s]	4.6	2.8	
Wind_Speed_Low [m/s]	1.9	2.8	
Air temperature [°C]	3.77	3.77	Values taken from "Raw Data" worksheet and based on averaging period given in the final row of column A in said worksheet.
Pressure [Pa]	94354	94337	
Relative humidity [%]	122.5	125.4	
SOURCE TERM			
Release direction	Vertical down	Horizontal towards East	
Elevation [m]	0.320	0.490	From official report, Section 4.1
Release duration [s]	?	201.7	Taken from "Raw Data" spreadsheet, final row column AM.
Release rate [kg/s]	0.725	0.688	
Pressure pipe end [barg]	2.240	2.405	
IGNITION			
Ignited?	Yes	Yes	
Ignition distance [m]	18.0	30.0	
Ignition time [s]	326	138	

Table 14. Key experimental data used as input to the Phast and Safeti jet fire models

Wind speed and direction referenced in Table 14 were measured using two Gill Windsonic anemometers located at 5 m and 10 m height from the local ground level. The wind tower was situated nominally 15 m south of the release point.

3.3.2 Test 6 – ignited horizontal release

We discuss this test first as it is the more conventional jet fire. There were 12 radiometers though two of them were not working properly (Rad_01 and Rad_5). The locations are given in Table 15 and Figure 15. The coordinate system is defined as x=distance from release point in the direction of the release, y=distance from x axis normal to the release direction, z= vertical distance from ground. The radiometers are 'wide angle' so we can assume that all radiation is being received.

Fire/Explosion Instruments	x	y	z
Rad_01	5000	5000	1200
Rad_02	5000	10000	1200
Rad_03	10607	10607	1200
Rad_04	14142	14142	1200
Rad_05	5000	0	1200
Rad_06	21000	-20000	1200
Rad_07	21000	-5000	1200
Rad_08	21000	-10000	1200
Rad_09	5000	-5000	1200
Rad_10	5000	-10000	1200
Rad_11	5000	-15000	1200
Rad_12	21000	-15000	1200

Table 15. Location of radiometers for Test 6 (Rad_0 and Rad_5 were faulty)

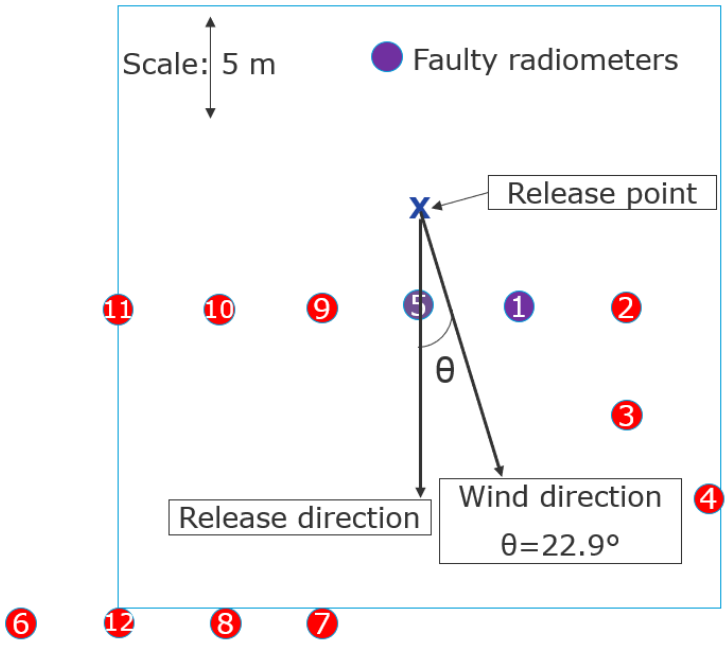

Figure 15: Schematic overview of radiometer locations for Test 6.

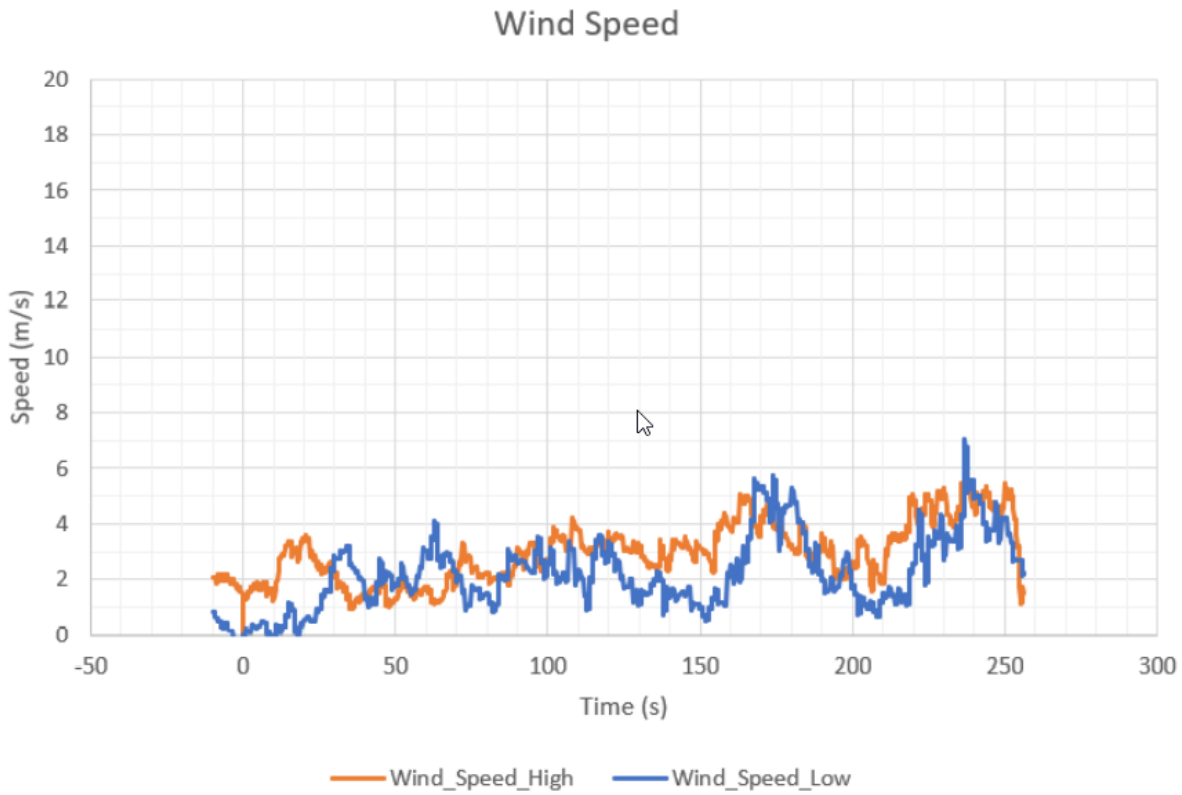

Figure 16:Wind speed measurements during Test 6

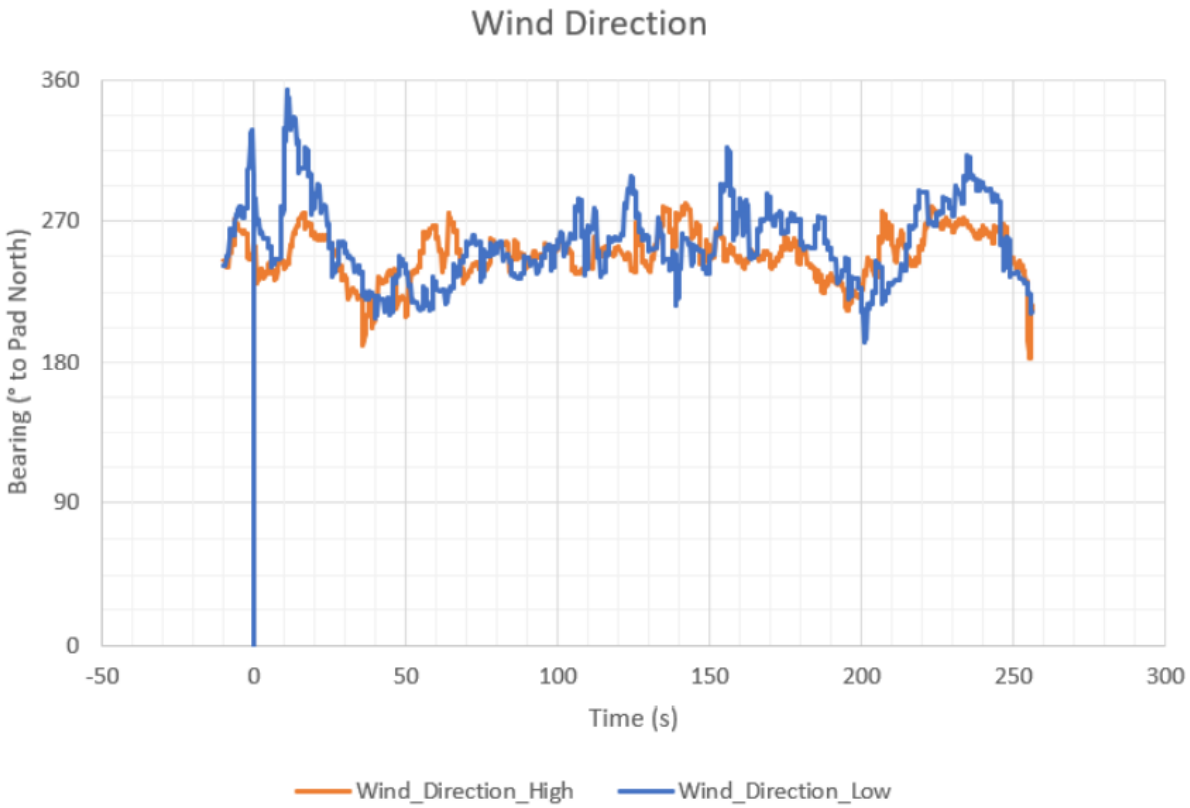

Figure 17 – Wind direction measurements during Test 6

The ignition was delayed, 138 s after the start of the release. The period used for validation purposes is 180 s to 200 s. It can be seen that wind speed (Figure 16) and wind direction (Figure 17) changed significantly in the period. Speed starts as high as 5 m/s and by the end of the period is below 2 m/s. Direction starts close to 270 deg which meant the wind was directly aligned with the release direction. By the end of the period the wind direction was approximately 45 deg away from the release direction.

The case has been modelled using the standalone jet fire model with default options and this invokes the Cook version of the cone model because the release is two-phase. It is also modelled using the Miller model. There is no claim that this latter model should be applicable to a two-phase release and yet it does have the interesting feature in that the flame shape seems to represent the observed flame rather well with a momentum-dominated start to the flame and subsequent buoyancy-dominated section.

Wind speeds of 2,3,4 and 5 m/s combined with cross-wind directions of 0, 22.5 and 45 deg were used in conjunction with these two models.

3.3.2.1 Cook Cone Model

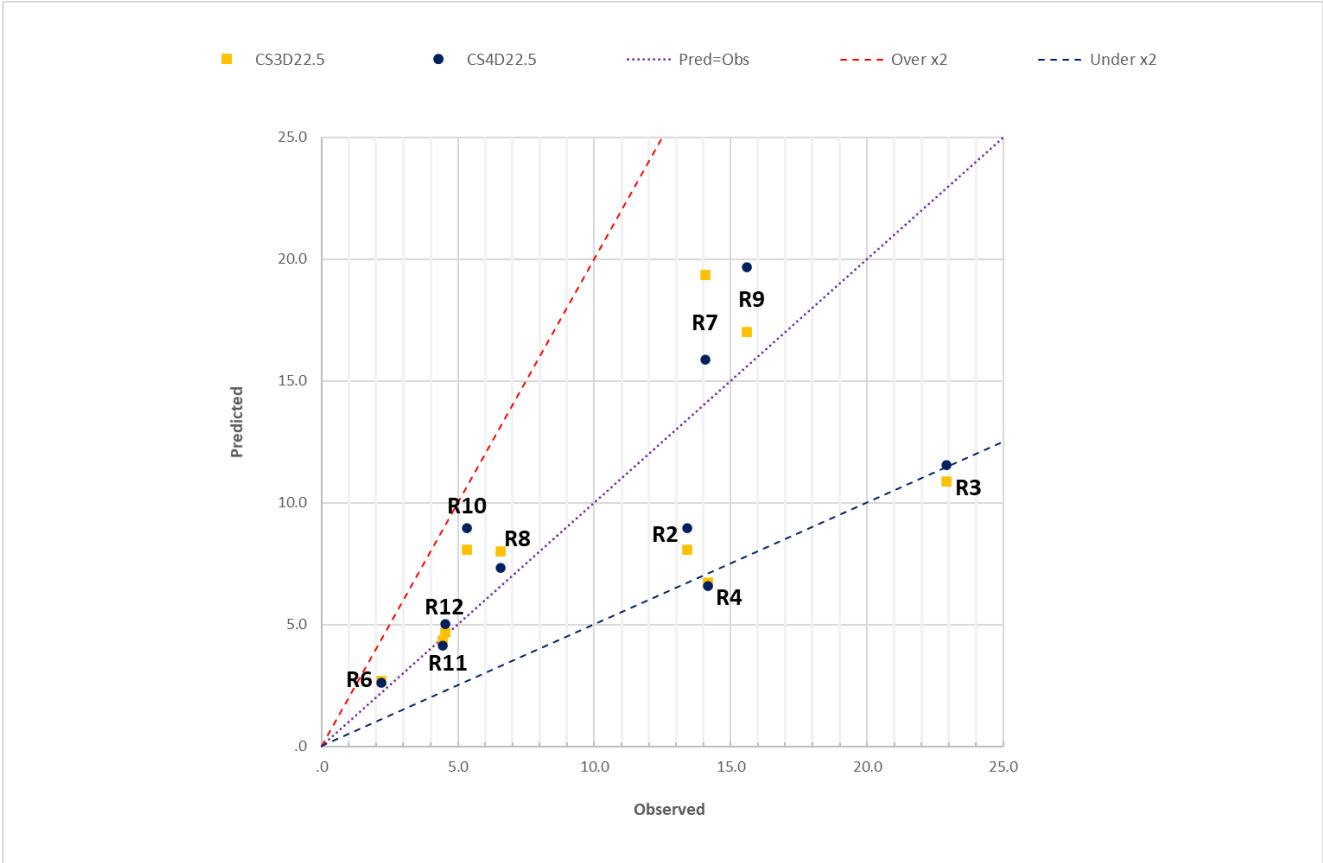

Figure 18 – Cook cone jet fire model predictions for wind speeds 3 and 4 m/s with 22.5 deg cross-wind compared against experimental for Test 6.

The better results are obtained with a cross-wind angle of 22.5 deg and wind speeds in the range 3 to 4 m/s. These correspond approximately to the mean values in the period 180 to 200 s. We see a mix of over and underprediction. Predictions for radiometers 6, 11 and 12 are excellent and 7,9,8 and 10 are quite good and overpredict somewhat. Modelled radiation for radiometer 2 is underpredicted whilst 3 and 4 are underpredicted by a factor of 2. Points 3 and 4 are at an angle of 45degs from the release point at different distances. Point 2 is also on this side of the flame. This is in the direction of the cross-wind as seen in Figure 15. When we plot the footprint of the fire we notice that there is no angling of the flame in the direction of the cross-wind. It seems likely that this is reason for this underprediction for these three radiometers. It does suggest that we should allow some angling of the flame in the presence of the cross-wind as we do for Johnson and Miller models.

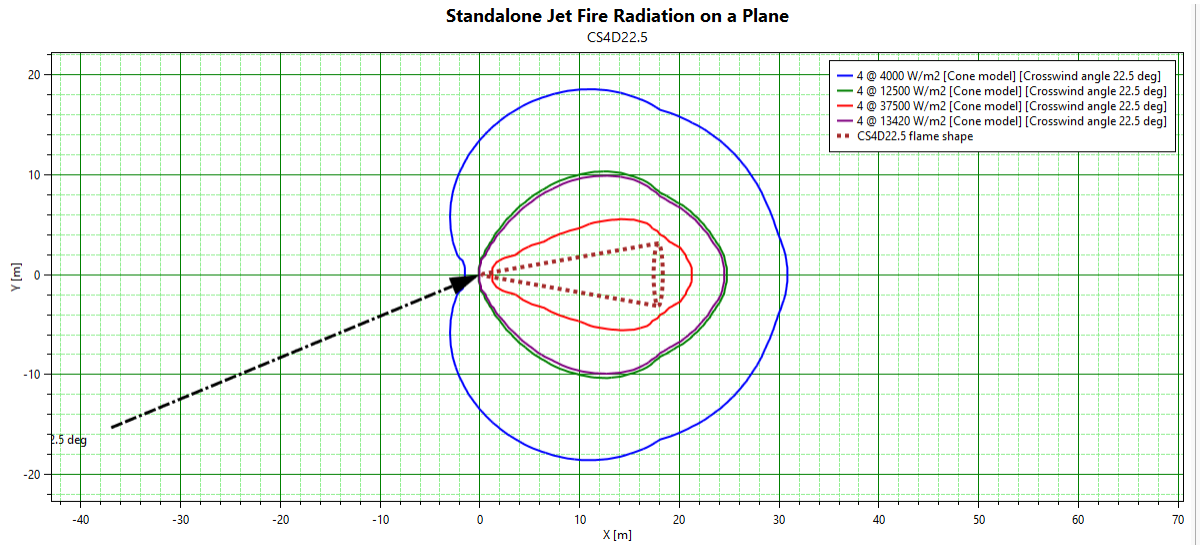

Figure 19: Cook jet fire model footprint (z=0) predictions for Test 6 based on wind speed 4 m/s and wind direction 22.5 degrees with the release direction.

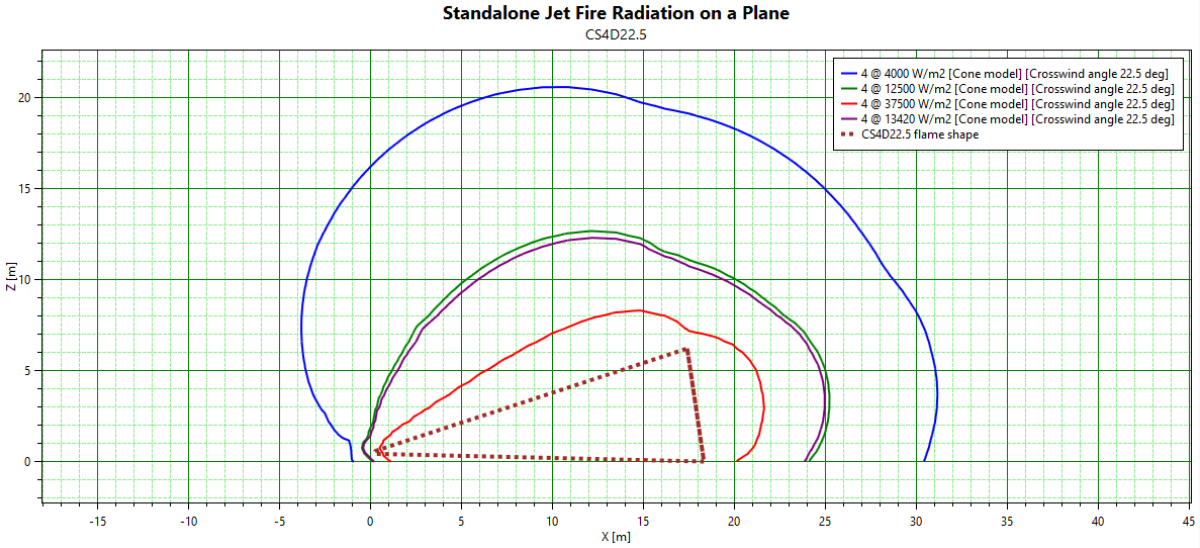

Figure 20: Cook jet fire radiation predictions in a vertical plane (y=0) for Test 6 based on wind speed 4 m/s and wind direction 22.5 degrees with the release direction.

The side-view in Figure 20 shows that there is no flame uplift. This may explain the overprediction of some of the points. The MG-VG plot in Figure 21 shows that there is a small bias towards underprediction. Overall though this is a satisfactory result and suggests that the default settings in Phast are correct for such a two-phase jet fire.

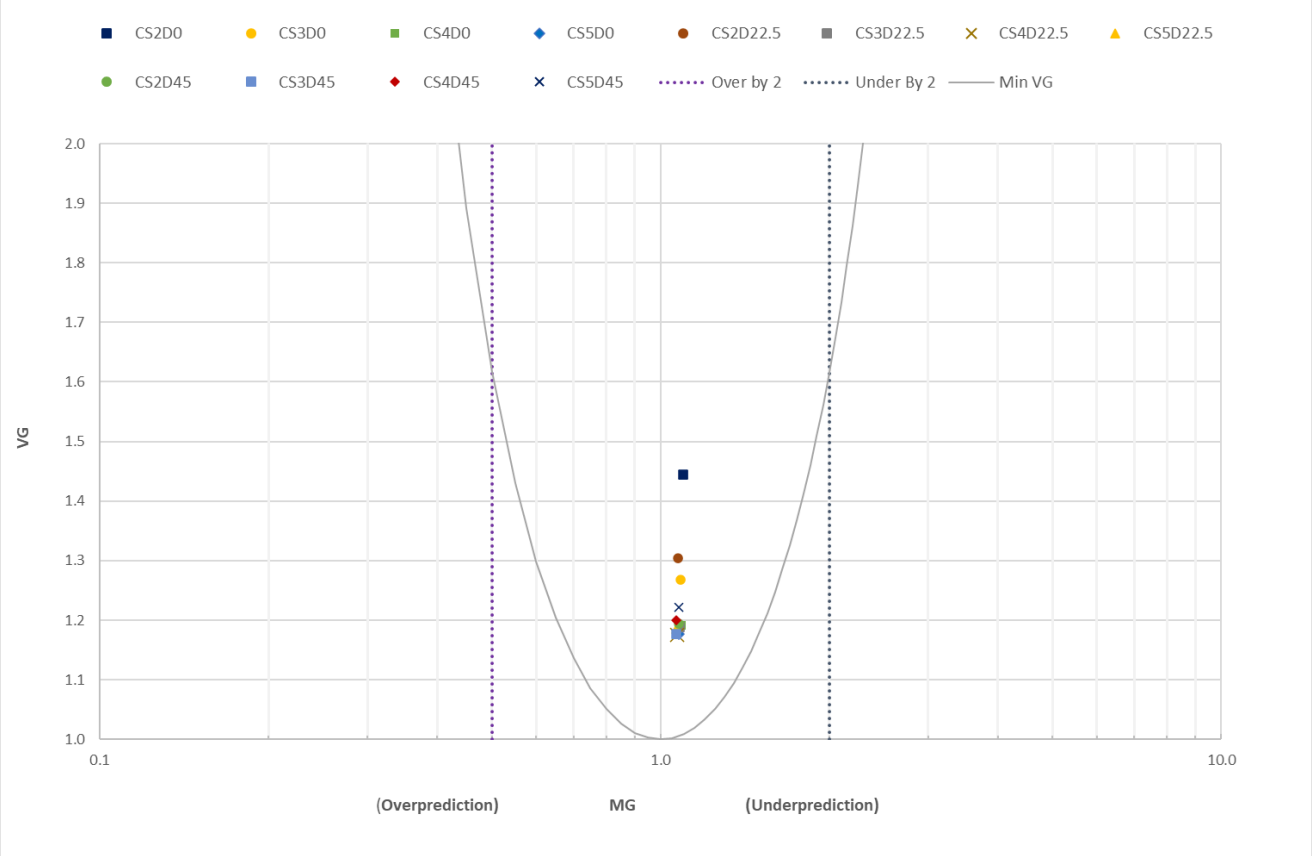

Figure 21 – Geometric bias for each permutation applied using the Cook model for Test 6

3.3.2.2 Miller Model

The cross-wind angle of 22.5degs seems to give the best match for the Miller model. A side view plot shows the sections of flame in Figure 22 – in this case for a wind speed of 4 m/s.

Figure 22 – Radiation contours in a vertical plane using the Miller model for Test 6

In Figure 23 we can see that the results of the Miller model mostly underpredict the data by a factor of 2. An exception is at R10 where the prediction is excellent. This position is 5 m in the direction of the release and at

a distance of 10 m from the axis. R9 is also quite good, and this is also at 5 m in the direction of the release but in this case 5 m from the axis.

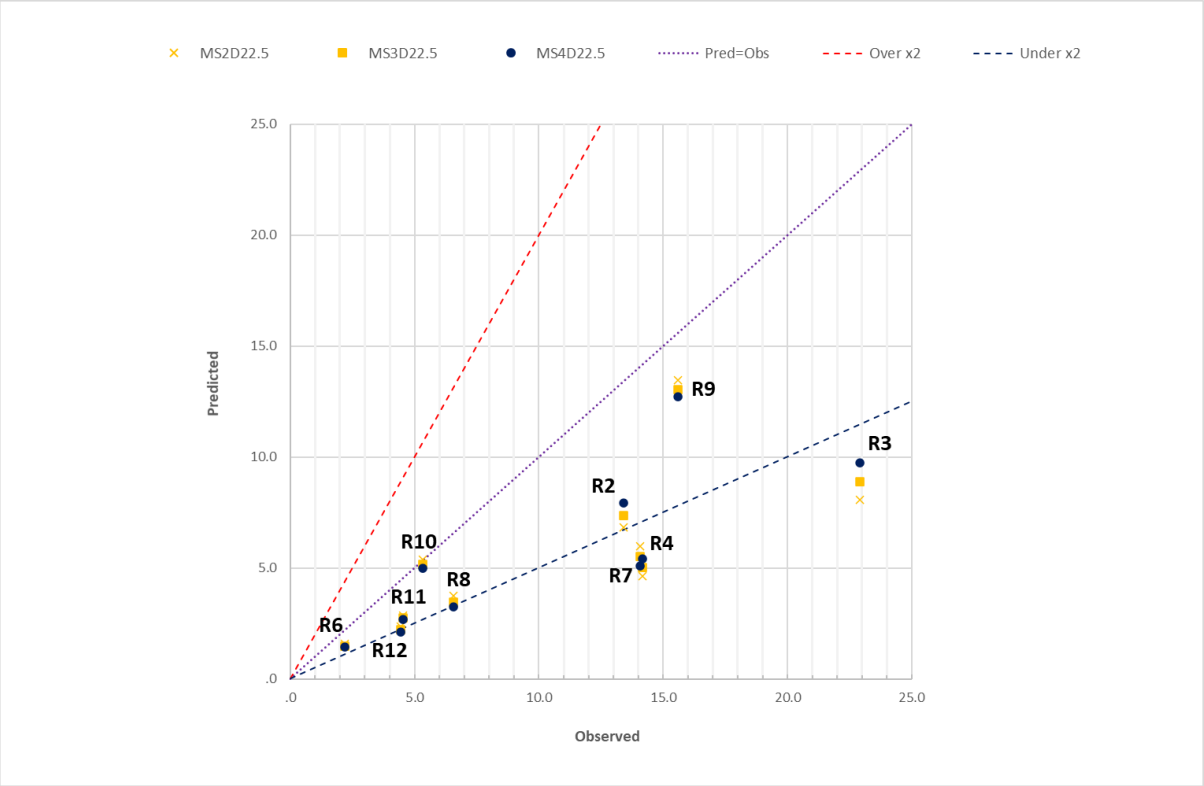

Figure 23 – Prediction vs Observed – Miller model based on 22.5 deg crosswind and 2, 3 and 4 m/s wind speed for Test 6

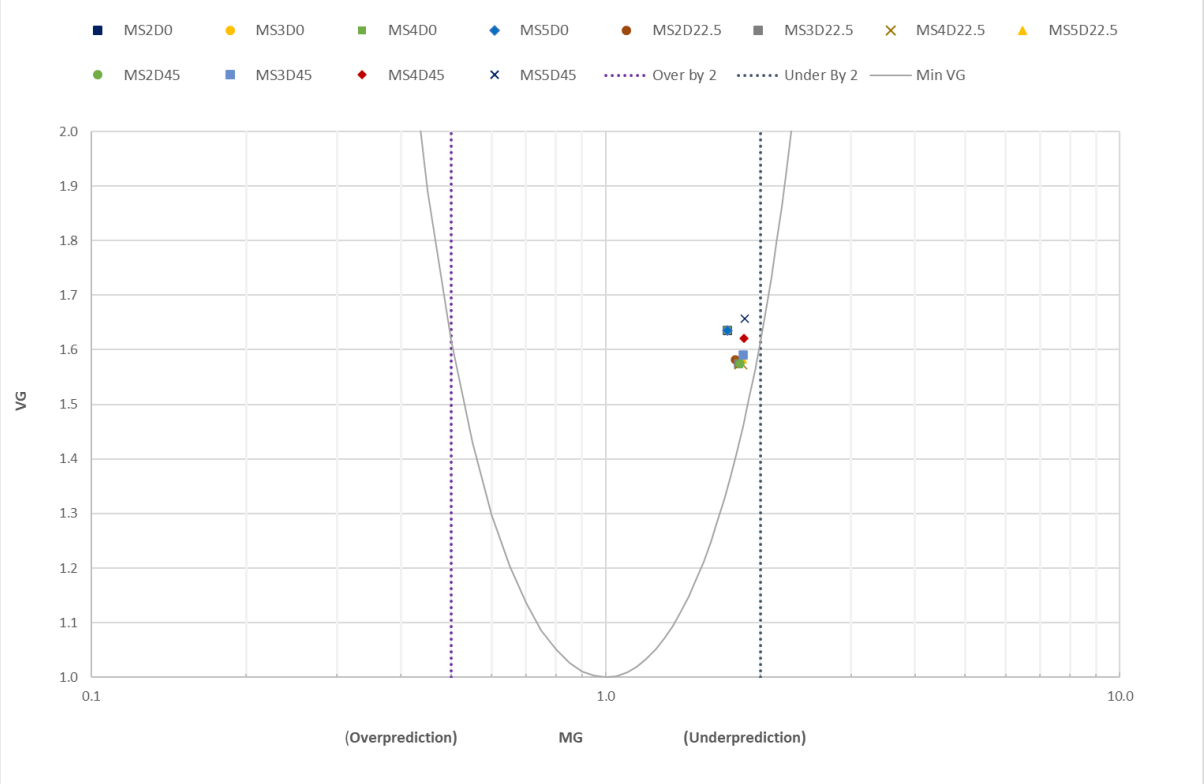

Figure 24 – Geometric bias for each permutation applied using the Miller model for Test 6

The MG-VG plot in Figure 24 shows the underprediction bias very clearly. We speculate that an adjustment to the fraction of energy radiated would give good model results and this could be justified by the presence of liquid increasing the optical thickness of the flame compared to a vapour hydrogen flame. A user could make this adjustment manually by specifying the radiative fraction as an input.

3.3.3 Test 5 – ignited downwards impinging release

In this test again there were two faulty radiometers, in this case R1 (ie labelled Rad_01) and R10. The layout prescribes three lines angled from the west at -45 deg, 0 deg and 45 deg with radiometers stationed with intervals of 5 m up to 20 m from the release point.

A plan view of the test pad is shown in Figure 25 below with the associated coordinates given in Table 16.

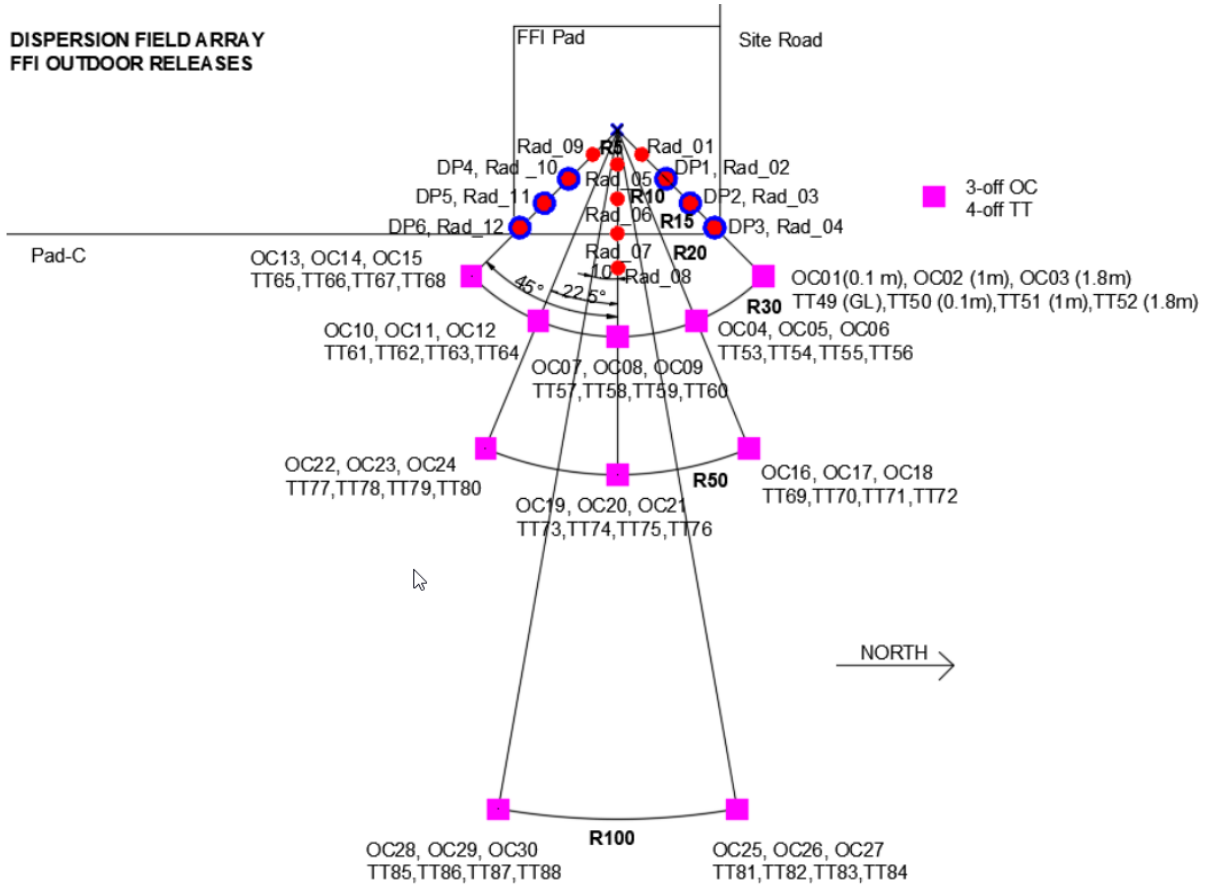

Figure 25 – Plan view of the radiometer layout during Test 5

Fire/Explosion Instruments	x	y	z
Rad_01	3536	3536	1200
Rad_02	7071	7071	1200
Rad_03	10607	10607	1200
Rad_04	14142	14142	1200
Rad_05	5000	0	1200
Rad_06	10000	0	1200
Rad_07	15000	0	1200
Rad_08	20000	0	1200
Rad_09	3536	-3536	1200
Rad_10	7071	-7071	1200
Rad_11	10607	-10607	1200
Rad_12	14142	-14142	1200

Table 16. Radiometer positions for Test 5 (Rad_01 and Rad_10 were faulty)

It should be noted that the ignition did not occur until 326 s and after a while a barrel at the site started burning with quite a luminous flame, and it was felt that this could contribute towards the radiation measurement. For this reason, an early and quite narrow time period is being used for these results comparisons, 330-350 s.

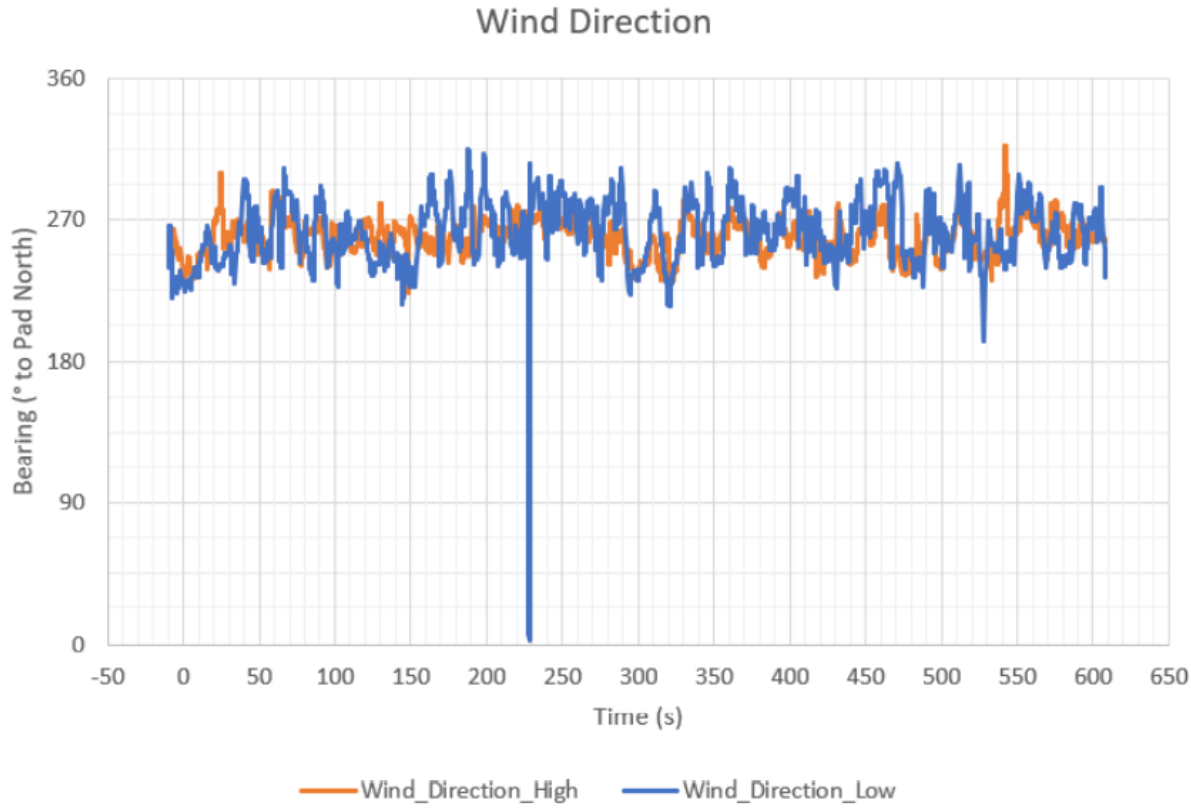

Figure 26: Wind direction measurements during Test 5.

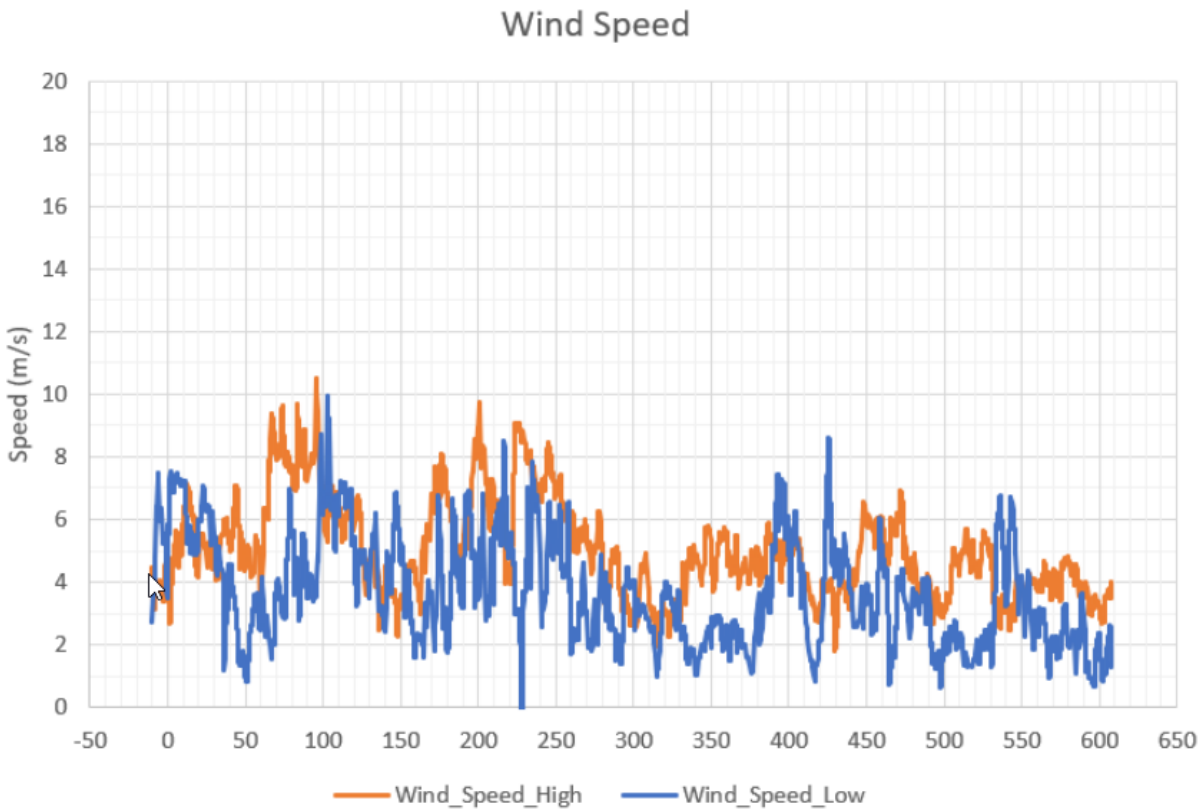

Figure 27: Wind speed measurements during Test 5.

We can see in Figure 26 that the wind direction was approximately aligned with the 0 deg radiometers but did fluctuate. We can also see in Figure 27 that in this period there was a distinct difference between the wind speed at the high and low elevation sensors. We also see from the video evidence that there was an apparent directional bias of the flame towards the north and this suggests that the wind was blowing towards that direction at the pad even if this is not clearly shown in the wind direction data measured nearby.

The radiation measurements have been time averaged over the 330-350 s period. Plotting the values against distance from the release point Figure 28 reveals some distinct directional bias at 5 and 10 m whilst at 15 and 20 m there is none at all. Unfortunately, the two failed radiometers would have been able to confirm this direction bias because there were at 45 deg and -45degs. We can see that at 5 m the highest reading is at 0deg and at 10 m the 45 deg radiometer records the highest value. The -45 deg reading at 5 m is a surprising low value of under 9 kWm-2.

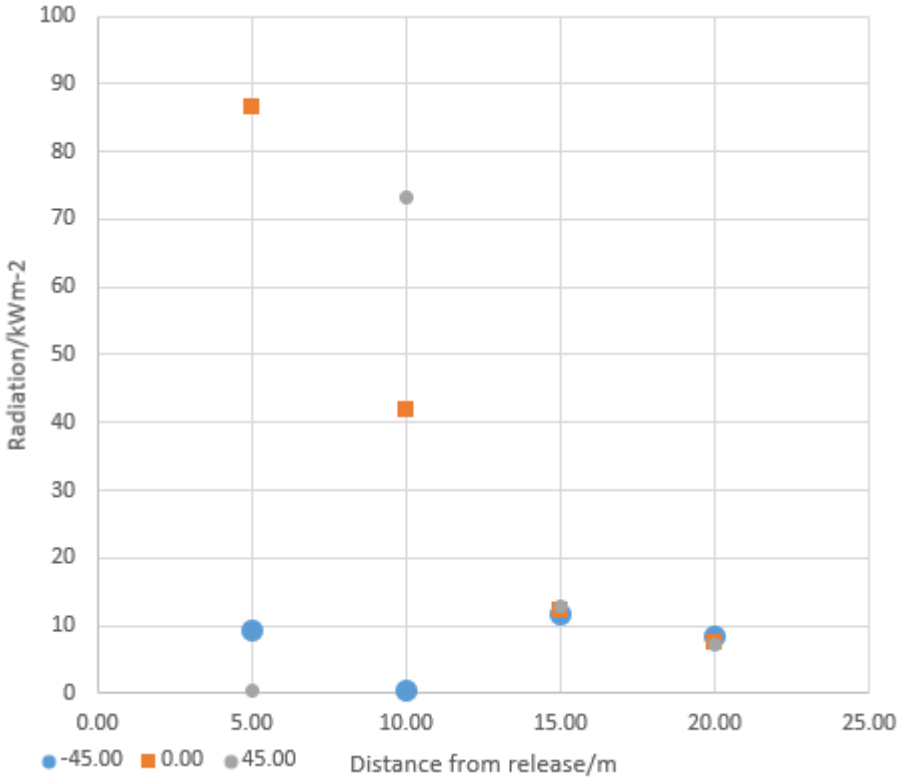

Figure 28 – Test 5 radiation readings averaged over period 330 s to 350 s vs distance from source.

3.3.3.1 Cook Cone Model

The Phast/Safeti jet fire models are based on free-jets so there is no ideal way to correctly represent this experiment. Because of this a number of permutations of modelling approaches have been taken in order to observe trends and with the aim of obtaining insight in how best to model such fires. It may also be considered that running KFX would be a helpful exercise. This has not been done yet but is suggested as future work.

Predictions from various applications of the Cook cone model do not give a close match to the measured data. Results from two jet fire approaches are shown in Figure 29 and illustrate the limitations of the jet fire modelling for this type of scenario. The case CSD0HI case models the flame as horizontal but with a velocity reduced by a factor of 4, no cross wind. This has the effect of extending the length of the flame. The other case shown is set at a release angle of -90 deg and with a crosswind angle of 22.5 deg. Both cases use a wind speed of 1.9 m/s which corresponds to the wind speed recorded by the anemometer at the lower elevation.

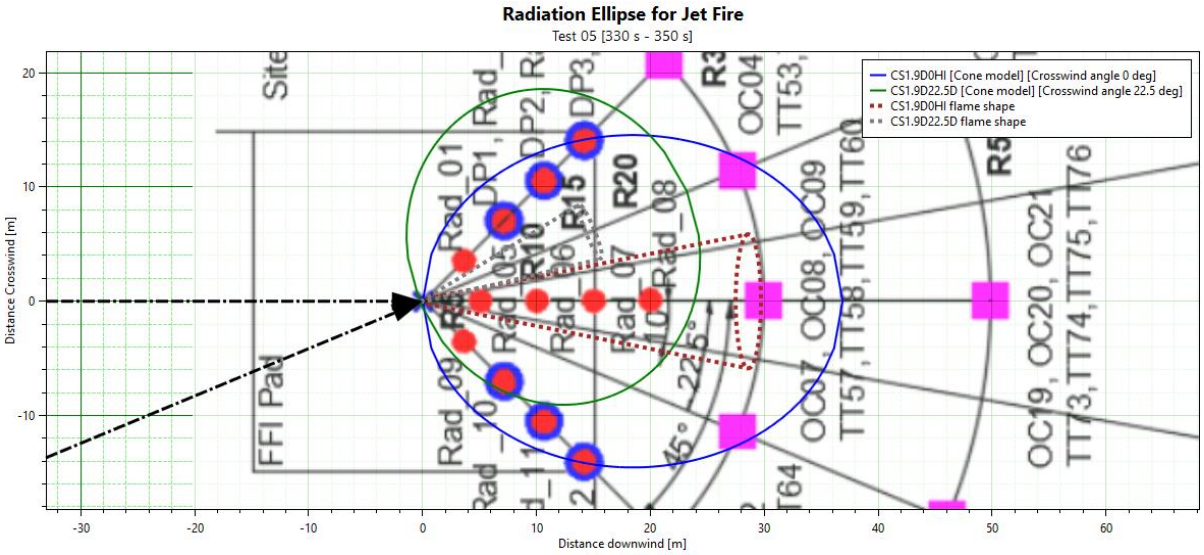

Figure 29: Test 5 radiometer locations and 7 kWm-2 ellipses and flame shapes as predicted by two modelling approaches in Phast.

The plot in Figure 29 shows ellipses at 7 kWm-2 which corresponds to the measurements at 20 m. We can see that the horizonal impinge gives good results at the angle of ±45 deg but not directly downwind where the radiation is higher than measured radiation. If we consider the modelling logic that centres these ellipses around the release point, it looks as this is a non-conservative approach. The downwind radiation may be reasonable, but the lateral dimension of the ellipse will be too small for such a release.

The scatter plot in Figure 30 shows outliers that also demonstrate limitations of the free-field jet fire model for this type of downward impinging release.

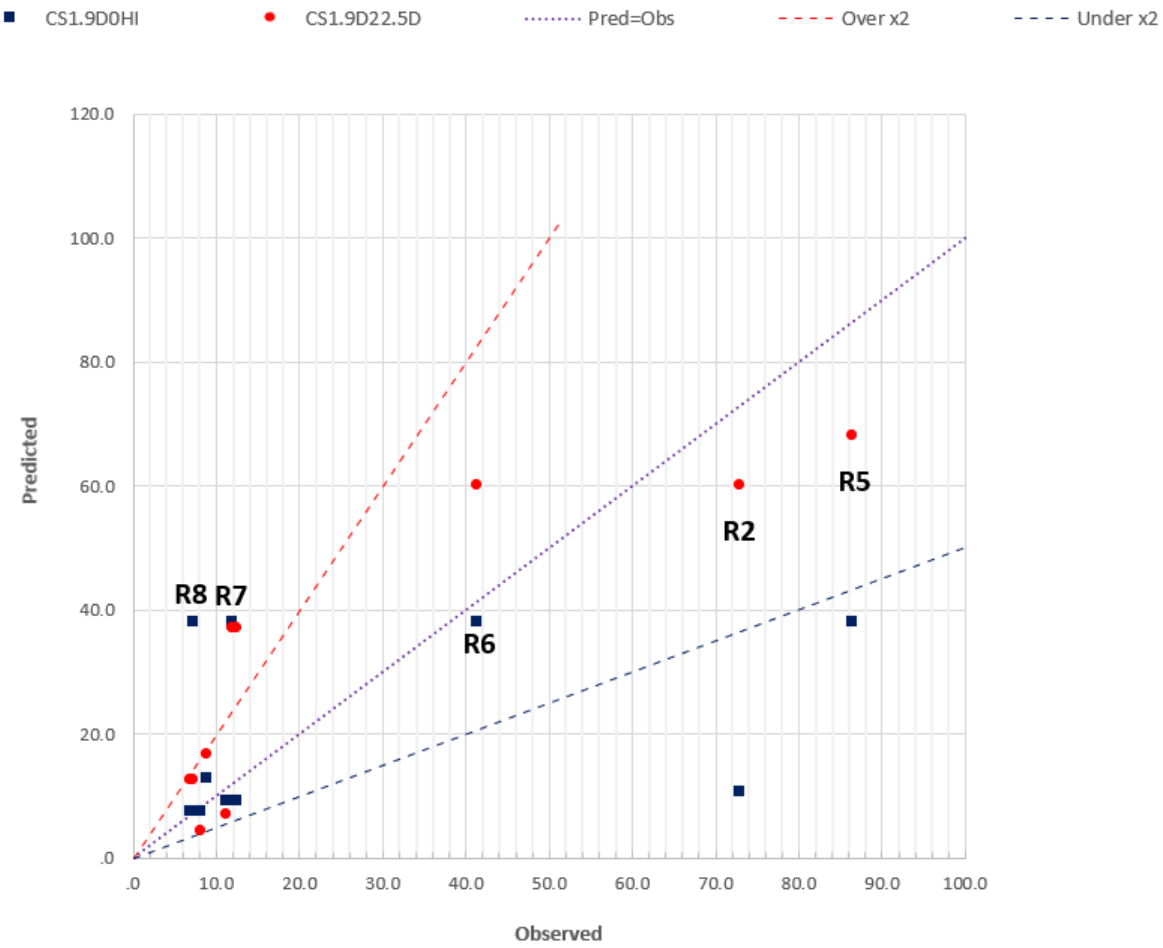

Figure 30 – Prediction vs Observed – Cook model with two permutations and 1.9 m/s wind speed for Test 5.

3.3.3.2 Use of the Pool Fire Model

It was speculated that the pool fire flame shape may be more representative of this type of flame. Certainly, the radiation we would expect to be project upwind more and have a more circular shape. On the other hand, this is a use outside the scope of the model validation.

To set up such a pool fire the radius was adjusted to obtain a pool fire burn rate equal to the total release rate. There is no attempt to model an actual pool, we are assuming complete combustion of the hydrogen.
The results seen in Figure 31 are in quite good agreement with the measured radiation and a clear improvement to the Cook jet fire results from the previous section.

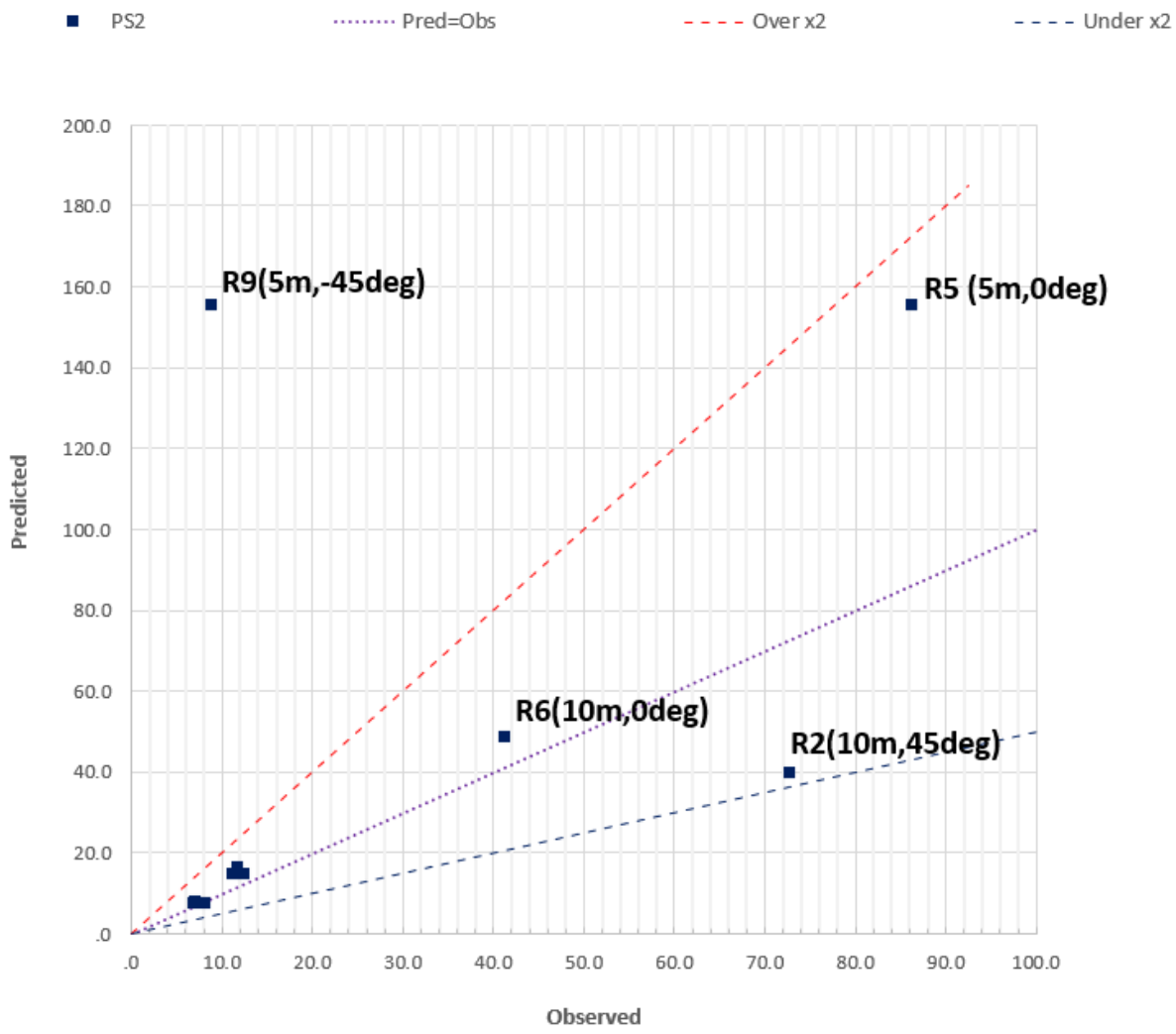

Figure 31 – Prediction vs Observed – Equivalent burn-rate pool fire model based on 2 m/s wind speed for Test 5

We can see that the radiation at 15 and 20 m from the source is close and with a bias towards overprediction. At 10 m downwind the prediction is also a bit high. At 45 deg there is an underprediction but then the experimental values may be affected by additional materials being burned or directional effects. At 5 m there is overprediction and again an anomaly is observed in the data with the point at -45 deg and only 5 m from the release. The measured value of under 9 kWm-2 does seem low.

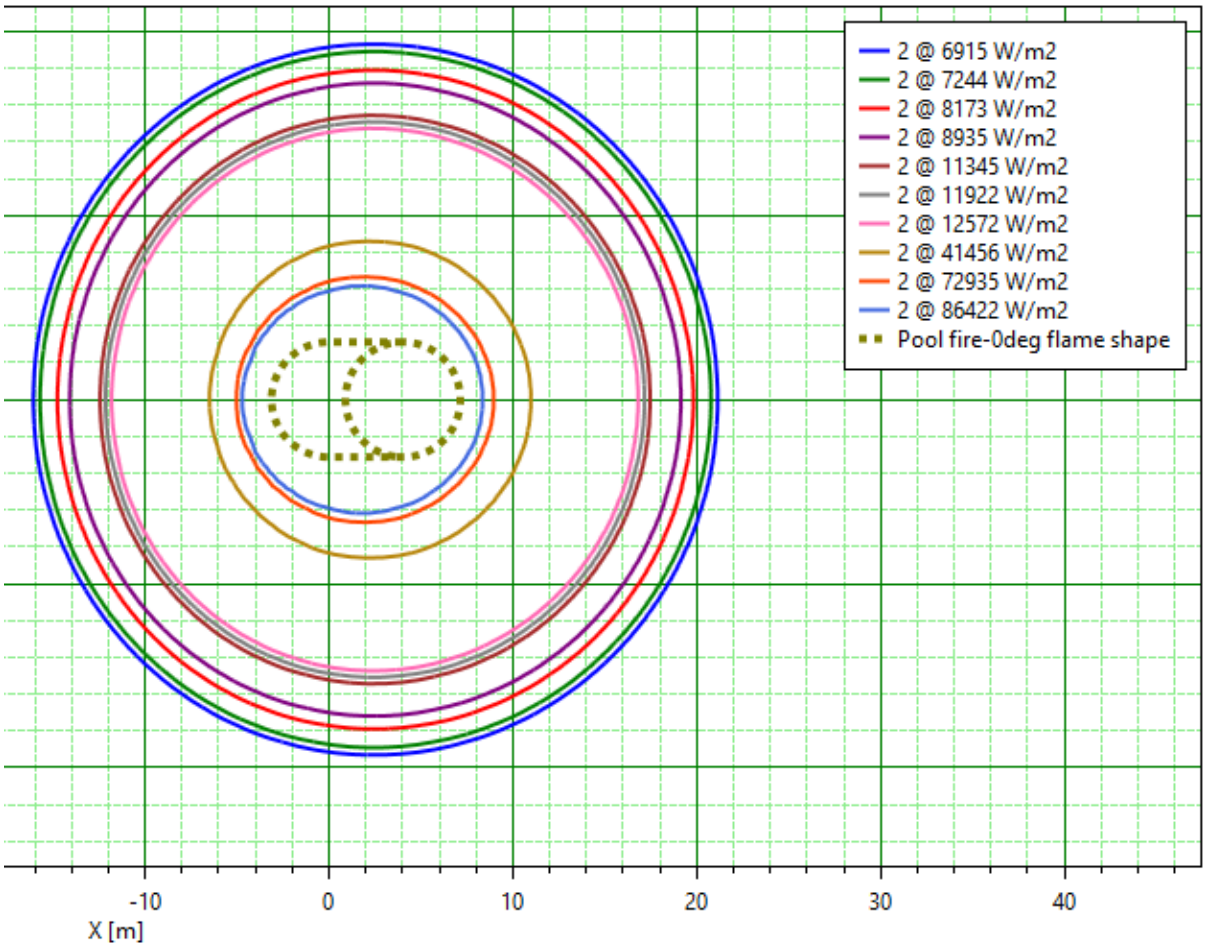

Figure 32 : Phast equivalent burn-rate pool fire radiation results with radiation levels corresponding to the 10 measured radiation values in Test 5 (averaged over time period 330 s to 350 s).

Plotting the radiation results vs distance from the release point does tend to emphasis the non-directional characteristic of the radiation.

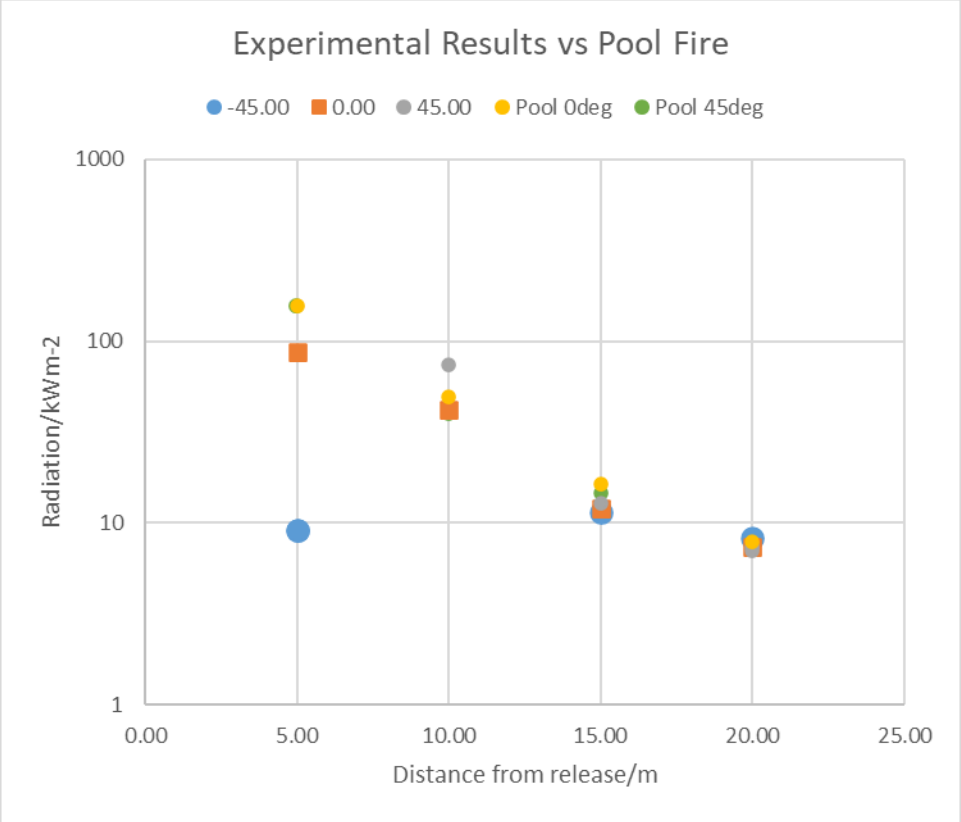

Figure 33 – Radiation vs distance from source using equivalent burn-rate pool fire model vs observations during Test 5.

The overprediction of the pool model might be accounted to the radiative fraction of 0.4 being applied. The jet fire models give a value with a magnitude of 0.3 but given all the uncertainties it does not seem justified. Overall though it does seem that this way of applying the pool fire model provides the most useful results for this type of impinging release. It would be useful also to have upwind radiation measurements in order to confirm that the radiation does indeed project in all directions.

3.3.3.3 Further work

For the ignited downward impinging release in Test 5, the use of the Phast pool fire model gave clearly improved results compared to predictions from the Cook jet fire model. However, this one experiment is too limited to propose a new approach based on the pool fire model for ignited downward impinging releases. We therefore recommend a literature survey and some CFD simulations before assessing how these releases can best be modelled in the future.

4 VALIDATION OF THE MILLER MODEL

4.1 List of experiments

The Miller[4] model has been validated against the same data as the Chamberlain, Johnson and Cook models. In addition, there are further tests involving hydrogen and syngas that have been used to develop the model. Table 17 summaries the test data used in this model validation. It has included published data and unpublished R&D work carried out by Air Products.

Data Source	Gas	Release Direction	Flare Diameter (mm)	Release Rate (kg/s)	Flame Length (m)	Data series in Figure 35 and Figure 36
Fishburne, 1979[19]	H2	Vertical	162–686	2–126	48–110	--
Chamberlain, 1987[1]	NG	Vertical	1070	21.1-55.6	--	--
Bennett et al 1991[3]	NG	Horizontal	20-152	2.6-8.8	18.6-32.9	--
Shirvill 2005[20]	H2	Horizontal	3–6	0.02–1	4–6	--
Miller et al 2014[21]	H2 and syngas	Vertical	685-914	1.3-13	25-33	APGaryville
Schefer 2006[22]	H2	Vertical	5–8	0.06–0.4	–	Schefer
Lowesmith 2008[23]	NG and NG/H2 mixtures	Horizontal	20-50	3–20	20–50	DNV
Willoughby, 2011[24]	H2	Vertical	19–50.8	0.04–0.4	3–7	Willoughby
Advantica 2009[25]	H2	Horizontal	20.9-50.2	1–7.5	17–49	AP&DNV
Kelly & Miller 2015[26]	NG, H2, mixtures with N2, CO2	Horizontal	25.4	0.02–0.07	3–5	APR&D

Table 17. Sources of data used to develop and validate the Miller model

4.2 Impact of extensions to the original Miller Model

As described in the companion theory manual, the Miller model implemented in Phast (labelled Miller/DNV in the figures) includes several extensions. The original Miller model (2017) is here labelled Miller AP Flame. The purpose of this section is to compare the model predictions of the two versions of the Miller model with experimental data for hydrogen and syngas in terms of radiation**.** Figure 34 compares results of the two versions of the Miller model. Impact of the individual extensions have been studied internally with the following conclusions:

- The two versions of the Miller model produced very similar results in general with a few exceptions.
- The inclusion of a small lift-off has improvements predictions near to the release point (i.e. the outliers with measured radiation at about 10 and 18kW/m2 as shown in Figure 34**)**
- The integration method in radiation calculation produces a small but consistent improvement in radiation predictions.
- Improved predictions are observed by including the effect of crosswind for test cases with strong crosswind, such as the tests of Air products/DNV 2009.
- The enhanced method to estimate natural gas flowrate for flame tilt of vertical releases of hydrogen and syngas has caused very small change of results.

In conclusion, the extensions to the original Miller model have produced minor improvements against the experimental data. Consequently, all the following Miller model predictions presented are based on the Miller/DNV model. Performance of this model is further analysed in the following sections.

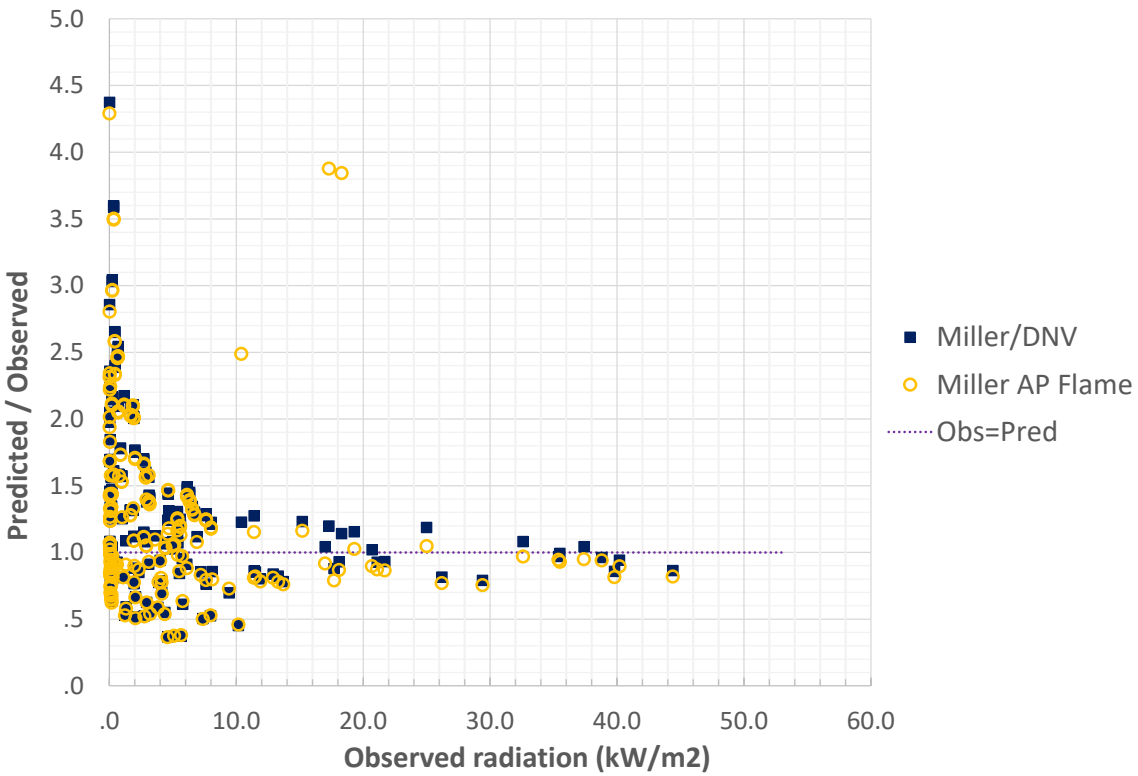

Figure 34 Comparing the prediction of Miller model in Phast and the AP Flame spreadsheet

4.3 Miller model for vertical and horizontal non-hydrocarbon flames

Figure 35 and Figure 36 compare predictions by the Miller model against test results of all non-hydrogen cases according to release direction, i.e. horizontal and vertical/angled releases. Please refer to Table 17 for data series in the figures. The observed values are measurements. Predictions by the Miller model are satisfactory. Predictions by the Miller model on horizontal releases spread in a narrow band around the measurements within a factor of 2 apart from some measurements of very low radiation. Predictions for vertical releases are also mainly good, the spread is a bit wider than the horizontal releases and a lot of the Willoughby experiments are underpredicted. This

underprediction diminishes if a higher wind speed is applied, implying that the tilt angle in the model is too low or the wind speed was under-reported.

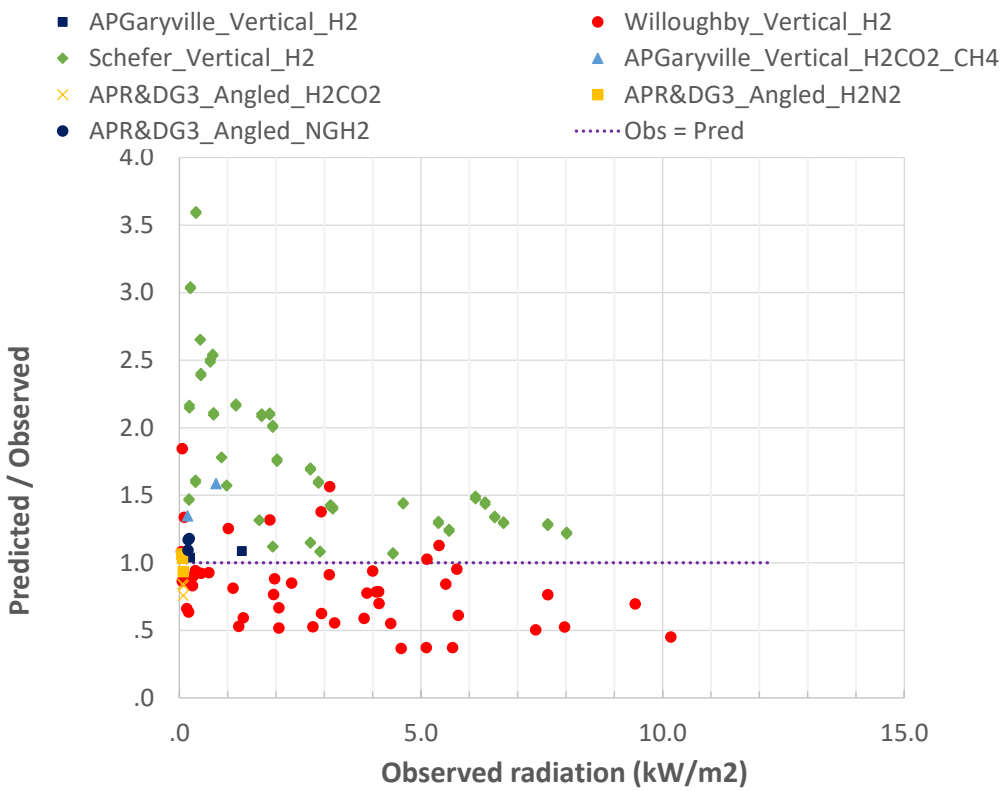

Figure 35 Predictions by the Miller model in Phast for vertical releases of hydrogen and hydrogen mixtures

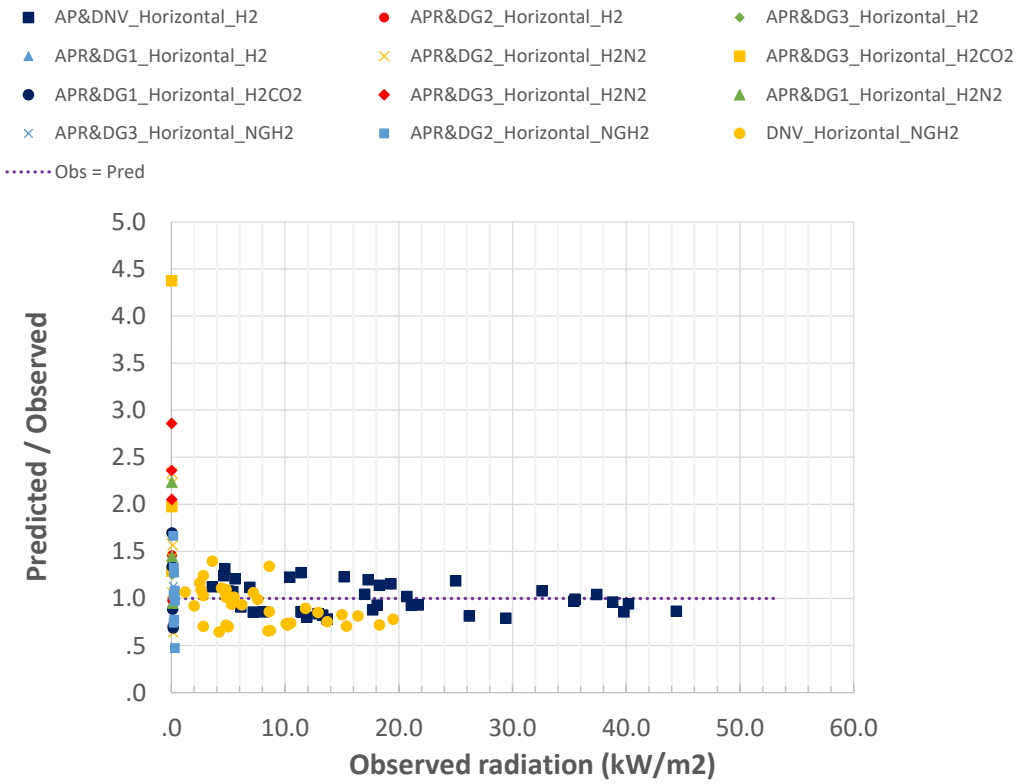

Figure 36 Predictions by the Miller model in Phast for horizontal releases of hydrogen and hydrogen mixtures

4.4 Miller vs Cone model for non-hydrocarbon jet fires

Current releases of Phast/Safeti have three jet fire models, i.e. the Chamberlain, Johnson and Cook models. These models assume a solid flame of a cone shape for jet fires; the geometry of the cone is estimated using correlations based on hydrocarbon jet fire tests. The Chamberlain model is usually applied for vertical and angled releases, the Johnson model for horizontal releases and the Cook model for liquid/two-phase releases. The three models are referred to as the Cone model in results given below. The Cone models have been validated and widely used for jet fires of hydrocarbon releases, but validity for jet fires of hydrogen and syngas can now be assessed. Figure 37 and Figure 40 compare the predictions by the Miller and the Cone models in Phast for non-hydrocarbon releases. Significant underpredictions by the Cone model are observed for horizontal hydrogen releases by a factor of 2. Underpredictions by the Cone model (i.e. the Johnson model) are mainly caused by two factors, namely underprediction of the fraction of radiated heat by the Johnson model and the flame shape for hydrogen releases. Figure 38 and Figure 39 illustrate the Cone model underpredictions of flame length and fraction of radiated heat for the Air Products/DNV tests (2009) of horizontal hydrogen jet fires.
Predictions by the Miller model for vertical releases is also better than the Cone model (i.e. the Chamberlain model) as shown in Figure 40. Predictions by both models are distributed around the perfect prediction line (i.e. observed value = predicted value), but spread of the predictions by the Miller model is narrower.

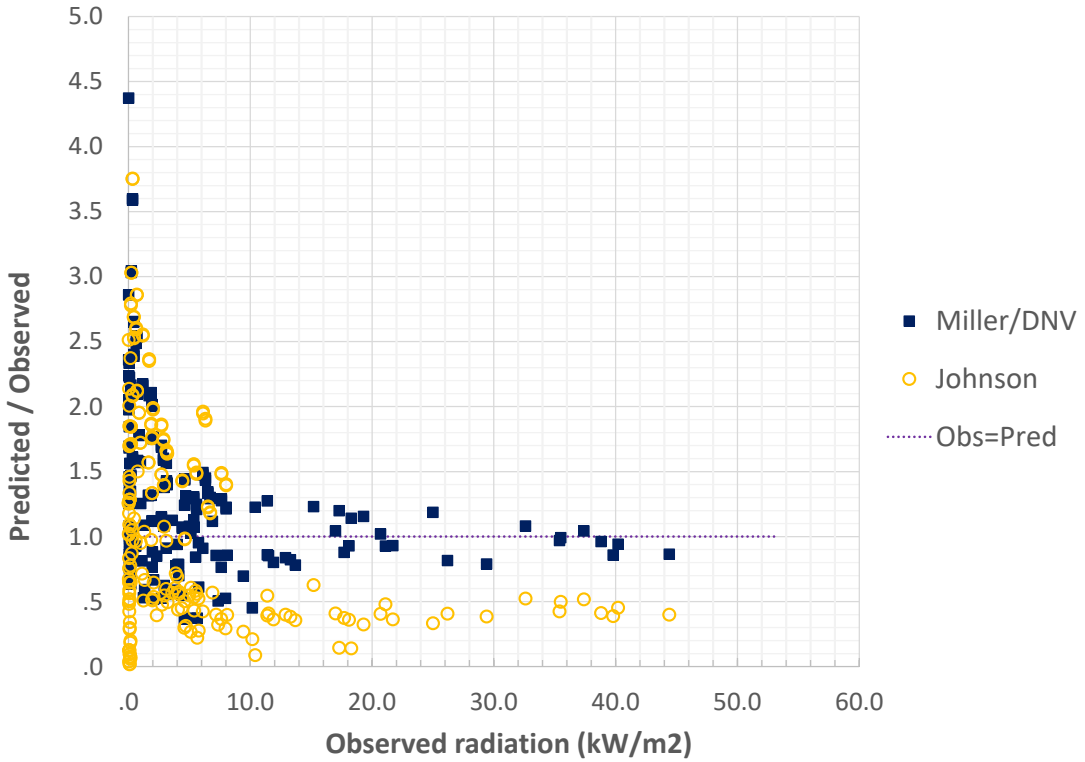

Figure 37 Comparing predictions by the Miller and the Cone model in Phast for horizontal releases of hydrogen and hydrogen mixtures

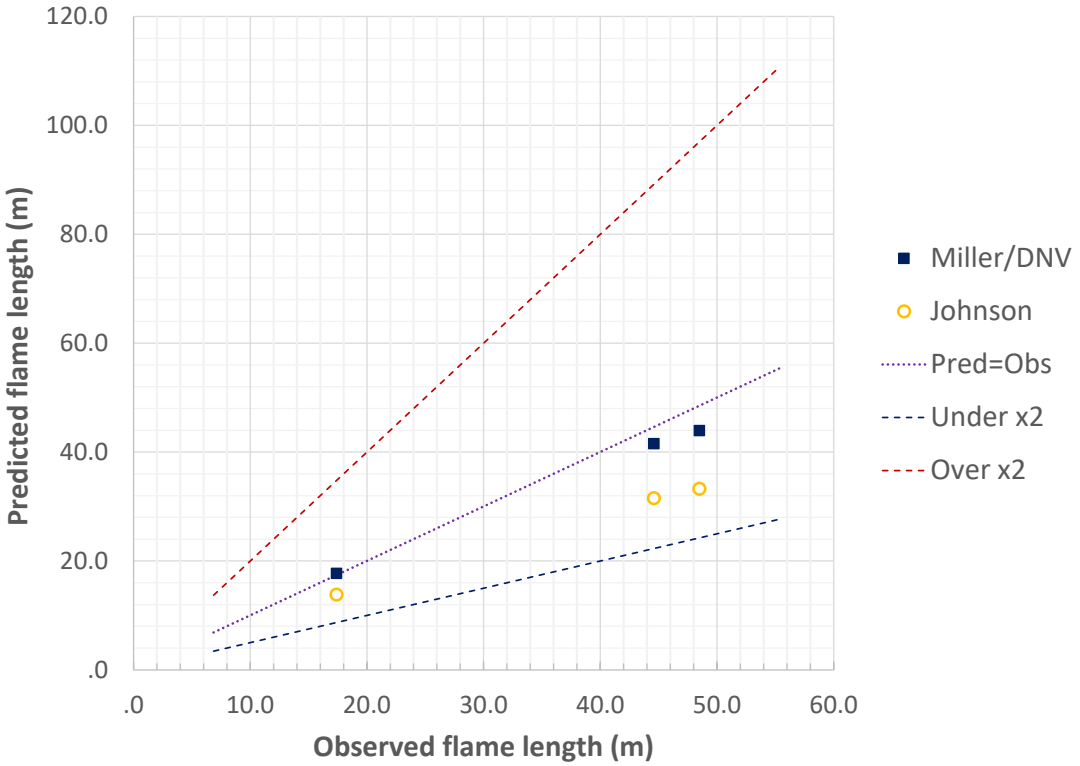

Figure 38 Comparing the predicted and measured flame length for Air Products/DNV tests of horizontal hydrogen jet fires

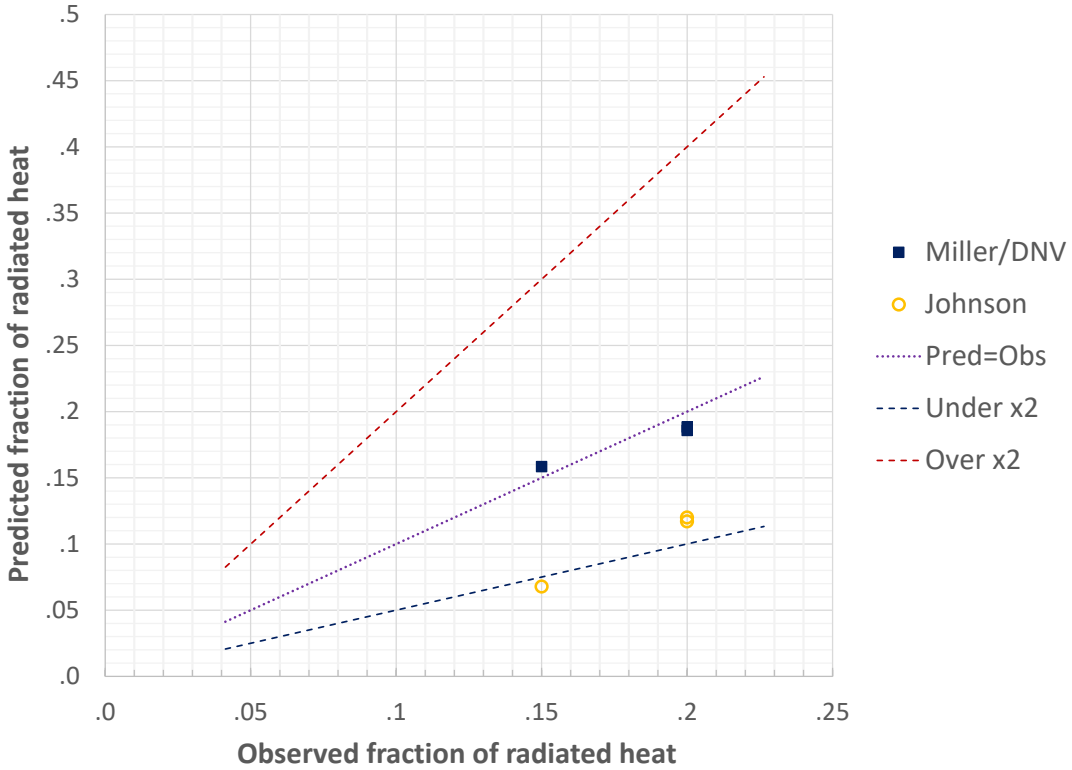

Figure 39 Comparing the predicted and measured fraction of radiated heat for Air Products/DNV tests of horizontal hydrogen jet fires

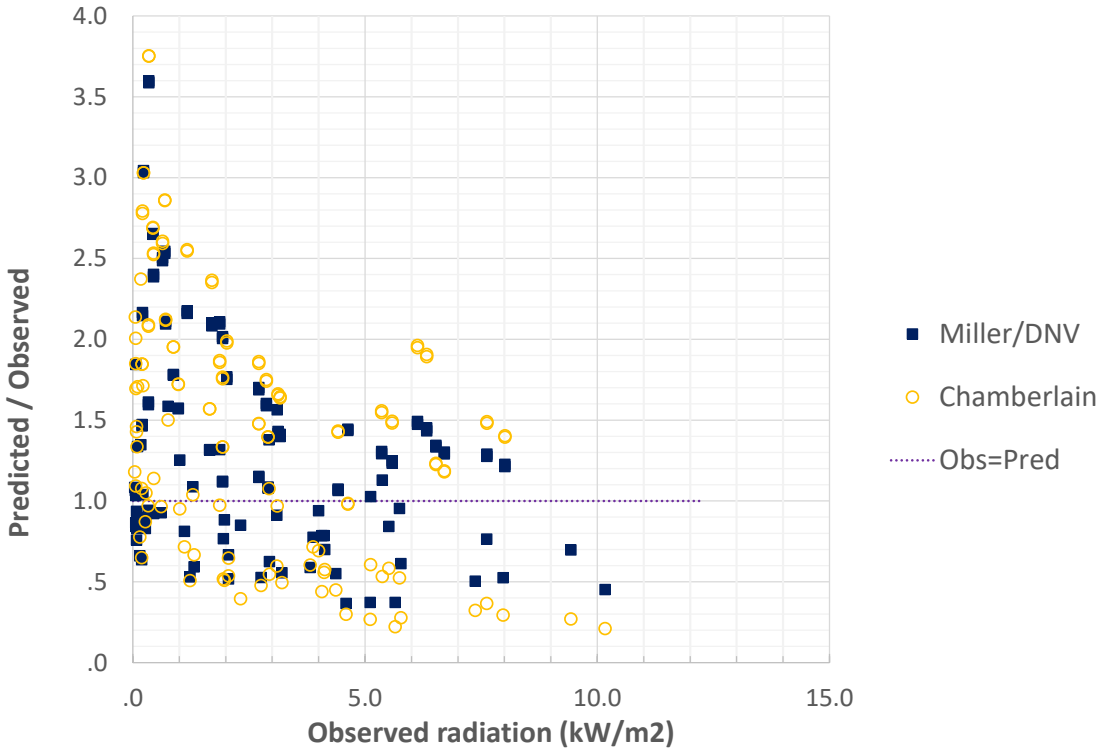

Figure 40 Comparing predictions by the Miller and the Cone model in Phast for vertical releases of hydrogen and hydrogen mixtures

4.5 Miller and Cone model for hydrocarbons and mixtures of hydrogen/Natural gas

Figure 41 shows results of applying the Miller and the Cone models for vapour releases of hydrocarbons and mixtures of hydrogen and natural gas listed in Table 17. On the whole, the Miller model gives good predictions for the vapor releases, even though the spread from measurements is a bit wider than that of the Cone model. On the other hand, there are groups of outliers both for the Miller model and the Cone model. These are indicated by the labels 'A' and 'B' on the graph. Points A correspond to measurements taken behind the flame closely aligned with the flame axis. We propose that the overprediction is a result of all the radiation from the flame reaching the radiometer whereas in reality there is significant shielding of the radiation from the furthest points of the flame by the flame shape itself. The view factor approach of the cone model overcomes this limitation. Group B shows significant underprediction by the cone model whilst the Miller model preforms well. These points correspond to the Air Products R&D tests and were part of the data set used to develop the model so it is not surprising that the Miller model performs well. Why the cone model underpredicts is likely a result of the Johnson model having a radiation fraction that reduces to much lower values, say than Chamberlain. It does suggest that there could be range of hydrocarbon tests where the Miller model will be preferable to the Cone model but there is not enough data to define such ranges with confidence.

The Miller model is not developed for liquid/two-phase releases and initial assessment of limited cases shows underpredictions for these scenarios. We don't recommend its use for this type of release and hence no data points are included in these graphs.

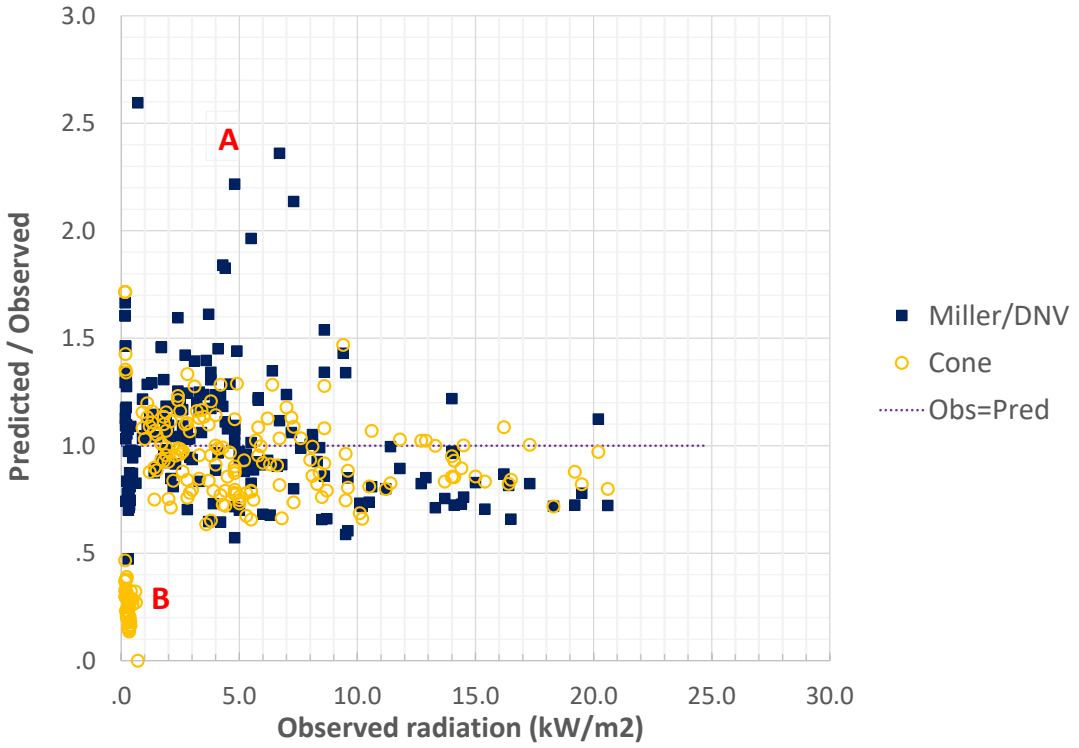

Figure 41 Comparing predictions between the Miller and the Cone models in Phast for hydrocarbon releases

4.6 Recommendations: choice of jet fire model

With the new Miller model and recent extensive validation of this and existing models, updated recommendations for selection of jet fire model can be given.

- The Cook model for non-vapour releases
- The Miller model for low luminosity gases (e.g. hydrogen and syngas)
- The Chamberlain model for all other releases except horizontal vapour releases where the Johnson model is recommended.

5 VALIDATION OF FLAME SHAPE ADJUSTMENT NEAR THE GROUND

The rotation of the jet fire was shown not to be required for the validation against the vapour jet fires. It was shown to improve the results for validation against two-phase jet fires. Figure 42 illustrates the effect of the jet-fire adjustment corresponding to the LPG jet-fire experiment B3029 (Bennett et al.[3]). The upper graph in the figure depicts the flame side-views with and without adjustments, while the lower graph shows that the adjustment has improved the predicted radiations. Please refer to the companion theory manual for details.

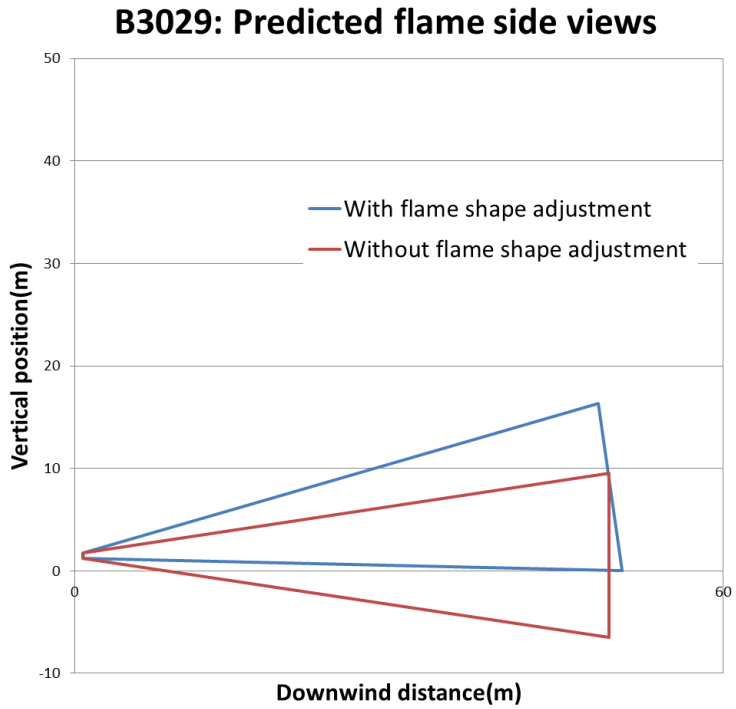

(a) Flame side views before and after flame shape adjustment

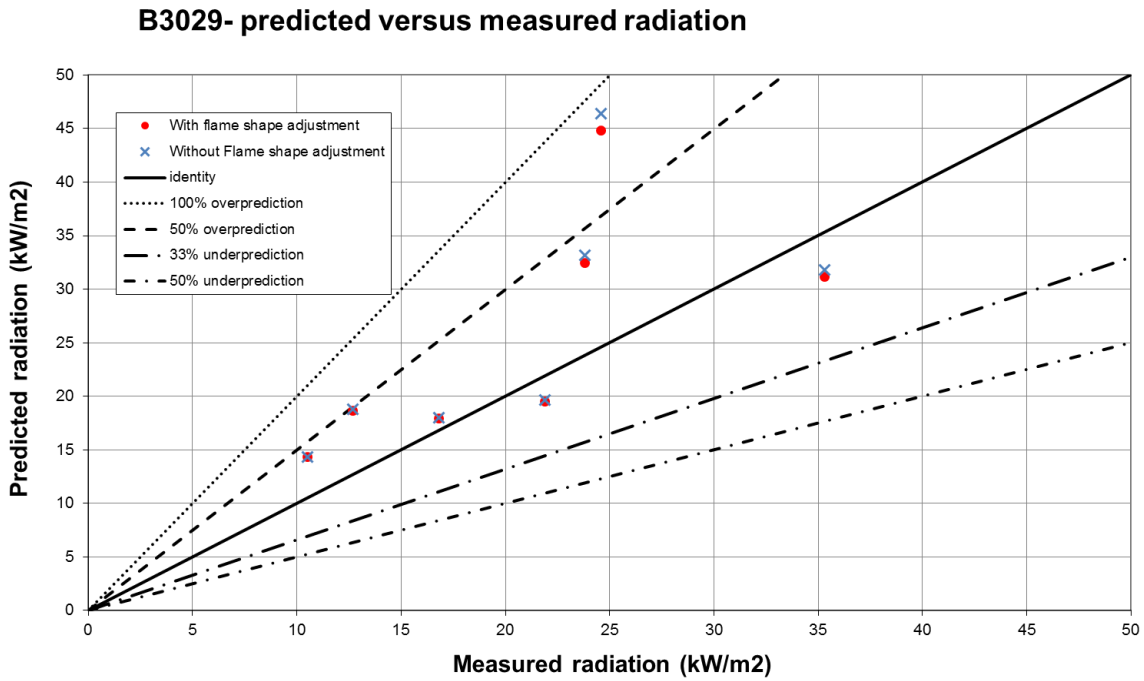

(b) Predicted (before and after flame adjustment) versus observed radiation

Figure 42 Effect of JFSH flame adjustment (Bennett LPG jet-fire experiment 3029)

6 SENSITIVITY ANALYSIS

The following summarises the observed trends following sensitivity analyses on the JFSH-Chamberlain/Cook and JFSH-Johnson models to model input parameters. Table 18 and Table 19 respectively list the default parameter value and their corresponding variation during sensitivity tests on the JFSH-Chamberlain/Cook and JFSH-Johnson models. The method employed in these sensitivity tests involves the variation of an input parameter while all other default parameter values are kept constant.

No	Parameter/Input Variable	JFSH-Chamberlain/Cook	
		Default	**Parameter Variation**
1	Mass discharge rate [kg/s]	20	5, 100, 500, 700, 900, 1000
2	Angle between release axis and the horizontal plane [º]	85,	67.5, 45, 22.5, 0, -22.5, -45, -67.5, -90
3	Angle between wind vector and the horizontal component of the release axis [º]	0	45, 90, 135, 180, -135, -90, -45, 0
4	Jet post-expansion temperature [K]	290	220, 250, 320, 350, 380
5	Two-phase liquid fraction [-]	0	1, 0.75, 0.5, 0.25
6	Jet post-expanded radius [m]	0.5	0.05, 0.1, 1, 5, 10
7	Jet post-expansion release velocity [m/s]	250	0.1, 5, 50, 100, 500, 1000, 5000, 10,000
8	Wind speed [m/s]	7.5	0, 2, 5, 10, 20, 30, 40, 50, 65
9	Atmospheric pressure [bara]	1.01	0.5, 0.7, .9, 1.1, 1.2
10	Atmospheric temperature [K]	290	250, 270, 300, 310, 325
11	Atmospheric %age humidity	50	0, 20, 40, 60, 80, 100

Table 18 Parameter variations employed in the sensitivity analyses of the JFSH-Chamberlain/Cook models

No	Parameter/Input Variable	JFSH-Johnson	
		Default	**Parameter Variation**
1	Mass discharge rate [kg/s]	20	5, 100, 500, 700, 900, 1000
2	Angle between wind vector and the horizontal component of the release axis [º]	0	45, 90, 135, 180, -135, -90, -45, 0
3	Jet post-expansion temperature [K]	290	220, 250, 320, 350, 380
4	Jet post-expanded radius [m]	0.5	0.05, 0.1, 1, 5, 10
5	Jet post-expansion release velocity [m/s]	250	0.1, 5, 50, 100, 500, 1000, 5000, 10,000
6	Wind speed [m/s]	7.5	0, 2, 5, 10, 20, 30, 40, 50, 65
7	Atmospheric pressure [bara]	1.01	0.5, 0.7, .9, 1.1, 1.2
8	Atmospheric temperature [K]	290	250, 270, 300, 310, 325
9	Atmospheric %age humidity	50	0, 20, 40, 60, 80, 100

Table 19 Parameter variations employed in the sensitivity analyses of the JFSH-Johnson model

The effect of varying (i.e., increasing) the above input variables (within the ranges specified in Table 18 and Table 19) on flame/Frustum length (L_B/R_L), angle between flame and discharge axis (α), frustum tip and base widths (W_2 and W_1), and flame SEP ($W_{surface}$) are summarised in tabular form below:

Flame characteristics	JFSH-Chamberlain/Cook	JFSH-Johnson
L_B and R_L	Increases	L_B increases while R_L increases to a maximum value and thereafter decreases
W_2	Increases	Increases
W_1	Increases to a maximum value at ca 700kg/s and begins to slightly decrease	Increases
α	Decreases	Increases
$W_{surface}$ (SEP)	Increases	Increases

Table 20 **Effect of increase in mass discharge rate on simulated data for L_B/R_L, α, W_2, W_1 and flame SEP ($W_{surface}$) based on JFSH-Chamberlain/Cook and JFSH-Johnson models**

Flame characteristics	JFSH-Chamberlain/Cook
L_B and R_L	Decreases from 0º to ±90º
W_2	Decreases from 0º to ±90º
W_1	Uninfluenced (constant)
α	Increases from 0º to ±90º
$W_{surface}$ (SEP)	Increases from 0º to ±90º

Table 21 **Effect of increase in angle between release axis and horizontal plane on simulated data for L_B/R_L, α, W_2, W_1 and flame SEP ($W_{surface}$) based on JFSH-Chamberlain/Cook models**

Flame characteristics	JFSH-Chamberlain/Cook	JFSH-Johnson
L_B and R_L	Decreases from 0º to ±180º	Increases from 0º to ±45º and thereafter decreases to ±180º
W_2	Decreases from 0º to ±180º	Increases from 0º to ±180º
W_1	Uninfluenced (constant)	Uninfluenced (constant)
α	Increases from 0º to ±180º	Increases from 0º to ±135º and thereafter decreases to ±180º
$W_{surface}$ (SEP)	Increases from 0º to ±180º	Decreases from 0º to ±180º

Table 22 **Effect of increase in angle between wind vector and horizontal component of release axis on simulated data for L_B/R_L, α, W_2, W_1 and flame SEP ($W_{surface}$) based on JFSH-Chamberlain/Cook and JFSH-Johnson models**

Flame characteristics	JFSH-Chamberlain/Cook	JFSH-Johnson
L_B and R_L	Decreases	Decreases
W_2	Increases to a maximum value at ca 330K and begins to decrease	Increases
W_1	Increases to a maximum value at ca 330K and begins to decrease	Increases
α	Decreases	Uninfluenced (constant)
$W_{surface}$ (SEP)	Decreases to a minimum value at ca 330K and begins to increase	Increases

Table 23 **Effect of increase in jet post-expansion temperature on simulated data for L_B/R_L, α, W_2, W_1 and flame SEP ($W_{surface}$) based on JFSH-Chamberlain/Cook and JFSH-Johnson models**

Flame characteristics	JFSH-Chamberlain/Cook
L_B and R_L	Increases
W_2	Increases
W_1	Increases
α	Constant
$W_{surface}$ (SEP)	Decreases

Table 24 **Effect of increase in two-phase liquid fraction on simulated data for L_B/R_L, α, W_2, W_1 and flame SEP ($W_{surface}$) based on JFSH-Cook liquid/two-phase model for horizontal releases**

Flame characteristics	JFSH-Chamberlain/Cook	JFSH-Johnson
L_B and R_L	Increases	Increases
W_2	Follows no particular trend (generally oscillates but will likely increase)	Follows no particular trend (generally oscillates but will likely decrease)
W_1	Follows no particular trend (generally oscillates but will likely increase)	Follows no particular trend (generally oscillates but will likely decrease)
α	Increases	Follows no particular trend (oscillates)
$W_{surface}$ (SEP)	Decreases	Follows no particular trend (oscillates)

Table 25 **Effect of increase in jet post-expanded radius on simulated data for L_B/R_L, α, W_2, W_1 and flame SEP ($W_{surface}$) based on JFSH-Chamberlain/Cook and JFSH-Johnson models**

Flame characteristics	JFSH-Chamberlain/Cook	JFSH-Johnson
L_B and R_L	Decreases	L_B decreases while R_L decreases to a minimum value at ca 5000m/s and thereafter increases
W_2	Decreases	Follows no particular trend (oscillates)
W_1	Decreases	Follows no particular trend (oscillates)
α	Decreases	Follows no particular trend (oscillates)
$W_{surface}$ (SEP)	Increases	Follows no particular trend (oscillates)

Table 26 Effect of increase in jet post-expansion velocity on simulated data for L_B/R_L, α, W_2, W_1 and flame SEP ($W_{surface}$) based on JFSH-Chamberlain/Cook and JFSH-Johnson models

Flame characteristics	JFSH-Chamberlain/Cook	JFSH-Johnson
L_B and R_L	Decreases to a minimum value after which R_L starts to slightly increase	Increases to a maximum value
W_2	Increases to a maximum value and begins to decrease	Decreases to a minimum value
W_1	Increases to a maximum value and begins to decrease	Uninfluenced (constant)
α	Increases	Decreases to a minimum value
$W_{surface}$ (SEP)	Increases	Increases to a peak value and thereafter decreases to a fixed value

Table 27 Effect of increase in wind speed on simulated data for L_B/R_L, α, W_2, W_1 and flame SEP ($W_{surface}$) based on JFSH-Chamberlain/Cook and JFSH-Johnson models

The trends reported above for the JFSH-Chamberlain/Cook models particularly agree with field data reported by Chamberlain for jet flames resulting from vertical releases.

Flame characteristics	JFSH-Chamberlain/Cook	JFSH-Johnson
L_B and R_L	Decreases	Decreases
W_2	Decreases	Increases
W_1	Decreases	Increases
α	Increases	Uninfluenced (constant)
$W_{surface}$ (SEP)	Increases	Increases

Table 28 Effect of increase in ambient pressure on simulated data for L_B/R_L, α, W_2, W_1 and flame SEP ($W_{surface}$) based on JFSH-Chamberlain/Cook and JFSH-Johnson models

Flame characteristics	JFSH-Chamberlain/Cook	JFSH-Johnson
L_B and R_L	Increases	Increases
W_2	Increases	Decreases
W_1	Increases	Decreases
α	Decreases	Uninfluenced (constant)
$W_{surface}$ (SEP)	Decreases	Decreases

Table 29 **Effect of increase in ambient temperature on simulated data for L_B/R_L, α, W_2, W_1 and flame SEP ($W_{surface}$) based on JFSH-Chamberlain/Cook and JFSH-Johnson models**

Flame characteristics	JFSH-Chamberlain/Cook	JFSH-Johnson
L_B and R_L	Slightly increases	Slightly increases
W_2	Slightly increases	Slightly decreases
W_1	Slightly increases	Slightly decreases
α	Slightly decreases	Uninfluenced (constant)
$W_{surface}$ (SEP)	Slightly decreases	Slightly decreases

Table 30 **Effect of increase in ambient percentage humidity on simulated data for L_B/R_L, α, W_2, W_1 and flame SEP ($W_{surface}$) based on JFSH-Chamberlain/Cook and JFSH-Johnson models**

7 FUTURE DEVELOPMENTS

This topic is discussed in the companion theory manual.

8 ACKNOWLEDGEMENT

Sincere thanks are due to Derek Miller for many fruitful discussions related to his new jet fire model and the authors gratefully acknowledge Air Products for supporting this work by sharing data from their jet fire experiments.

APPENDICES

Appendix A. Calculation of post-expansion JFSH input data

The following describes the procedure employed in back calculating the post-expansion temperature and velocity of a discharging fluid using the ideal gas isentropic discharge equations and secondary data reported by Chamberlain. The procedure requires the prior knowledge of the following variables:

- Discharge/orifice diameter (d_o) [m]
- Post-expansion mach number (M_j) [-]
- Ideal gas ratio of specific heats (γ_g) [-]
- Mass release rate of the fuel (m) [kg/s]
- Fluid's kilogram molecular weight ($M_{wkg} = M_W/1000$) [kg/mol]

For each test case, orifice diameter, mass release rate, and post-expansion Mach number were reported. The fuel's ideal gas ratio of specific heats (γ_g) was calculated by summing the product of each component's mole fraction and an average value of its ratio of specific heats (γ). The average value of each component's γ was calculated over a temperature range of 223K to 373K. Within this temperature range, the values of γ was observed to vary from 1.33 to 1.27 and 1.23 to 1.15 for methane and ethane respectively. Ideal gas specific heats for each component were calculated using the DIPPR correlation found in PHAST 6.4.

In general, the expressions for post-expansion temperature and velocity are given by[1]:

$$T_j = \frac{2T_s}{2 + (\gamma_g - 1)M_j^2} \quad (1)$$

$$v_j = M_j \sqrt{\frac{\gamma_g R_g T_j}{M_{Wkg}}} \quad (2)$$

Where:

R_g = Universal gas constant [J/mol/K]
T_s = Stagnation temperature [K]

The solution of equations (1) and (2) require the knowledge of T_s. The procedure for calculating T_s depends on whether the release at the discharge plane is choked ($\approx M_j \geqslant 1$) or unchoked ($M_j < 1$). The following presents the expressions employed in calculating T_s for choked and unchoked releases.

Unchoked Flow

From the expression for release mass flow rate, T_s can be obtained as[1]:

$$T_s = \left(\frac{F \times d_o^2}{3.6233 \times 10^{-5} \times m}\right)^2 \times \gamma_g \times M_{Wkg} \quad (3)$$

Where:

F = Mach number based on stagnation temperature at ambient pressure [-]

Assuming isentropic flow from stagnation conditions to the discharge plane, F can be calculated from the expression for jet Mach number (M_j) as[1]:

$$F = \left(\frac{\left(M_j^2(\gamma_g - 1) + 1\right)^2 - 1}{2(\gamma_g - 1)}\right)^{1/2} \quad (4)$$

Choked Flow

Assuming isentropic release, the stagnation temperature (T_s) is obtained from the expression for discharge/choked temperature (T_c) as:

$$\boldsymbol{T_s = \frac{T_c(1+\gamma_g)}{2}} \quad \textbf{(5)}$$

T_c is obtained from the expression for mass discharge rate based on flow conditions at the discharge plane as:

$$\boldsymbol{T_c = \left(\frac{P_c \times d_o^2}{3.6713 \times m}\right)^2 \times \gamma_g \times M_{Wkg}} \quad \textbf{(6)}$$

Where:

P_c = Static or choke pressure at the discharge plane [N/m^2]

From the expression relating post-expansion jet Mach number (M_j) to discharge pressure (P_c), P_c can be obtained as[1]:

$$P_c = \left(\frac{M_j^2(\gamma_g - 1) + 2}{(\gamma_g + 1)}\right)^{\left(\frac{\gamma_g}{\gamma_g - 1}\right)} \times P_o \quad (7)$$

Where

P_o = Ambient pressure [N/m^2]

Thus, for choked and unchoked releases, the calculation algorithms for T_j and v_j are summarised as:

Choked discharge:

- Determine $P_c = f(M_j, \gamma_g, P_o)$ from equation (7)
- Calculate $T_c = f(P_c, d_o, m, \gamma_g, M_{wkg})$ from equation (6)
- Obtain $T_s = f(T_c, \gamma_g)$ using equation (5)
- Calculate $T_j = f(T_s, \gamma_g, M_j)$ using equation (1)
- Determine $v_j = f(M_j, \gamma_g, T_j, R_g, M_{wkg})$ from equation (2)

Unchoked discharge:

- Calculate $F = f(M_j, \gamma_g)$ using equation (4)
- Obtain $T_s = f(F, d_o, m, \gamma_g, M_{wkg})$ from equation (3)
- Determine $T_j = f(T_s, \gamma_g, M_j)$ using equation (1)
- Calculate $v_j = f(M_j, \gamma_g, T_j, R_g, M_{wkg})$ from equation (2)

Appendix B. Effect of conservation-of-momentum assumption on JFSH results

Validation of the jet fires predicted with input from discharge results with the default Phast 6.7/7.2 assumption of minimum thermodynamic change from the orifice at discharge until the completion of atmospheric expansion (i.e. the range covered by ATEX, the atmospheric expansion model in Phast/Safet). However, conservation of momentum is considered a better alternative for dispersion. For the Johnson vapour jet fires it was found that the conservation-of-momentum assumption corresponds to the 'minimum-thermodynamic-change' option; see Table 5. Based on previous experiments with validation for high-pressure vapour releases (including hydrogen), it is expected that usually the 'conservation of momentum' option will be selected for vapour jet fires. However for two-phase releases, it was found that usually the 'isentropic option' corresponds with minimum thermodynamic change. Therefore this section compares jet-fire predictions for liquid/2-phase releases against experimental data based on the following different assumptions:

- JFSH results derived from DISC simulations based on minimum thermodynamic change
- JFSH results derived from DISC simulations based on conservation of momentum
- Predictions based on Lowesmith correlation

Figure 43 graphically compares the predicted versus measured flame length and SEP of liquid and 2-phase experiments (the measured results are given by tables 9 & 10). Flame lengths estimated by Lowesmith correlation are also included to assess the accuracy of the predictions by JFSH-Cook. The following conclusions can be drawn:

- When compared with the jet-fire predictions with minimum thermodynamic change at discharge, the assumption of conservation of momentum generally results larger jet flames, i.e. increased flame surface due to increased flame length and top & base widths of the frustum. Consequently, flame surface emissive power (SEP) is more under-predicted compared with the predictions with the assumption of minimum thermodynamic change.
- The overall over-prediction of flame length of all measurements is 34.6% for the assumptions of minimum thermodynamic change and 45.8% for the assumption of conservation of momentum.
- On the other hand, the overall under-prediction of SEP of all measurements is 2% and 12.8% for the assumptions of minimum thermodynamic exchange and conservation of momentum respectively.

Among the ten liquid/2-phase releases summarised in Table 9, conservation of momentum is equivalent to the assumption of minimum thermodynamic change for the Selby & Burgan cases (i.e. SB1 & SB2), so jet predictions of the two assumptions are the same for SB1 & SB2. All other eight test cases have shown differences in jet fire predictions between the two assumptions.

Figure 44 plots the flame length (m) as function of the flame power Q (MW). For each of the experiments, it compares the flame lengths predicted by JFSH-Cook (denoted by green triangular markers for minimum thermodynamic change and black cross for conservation of momentum) and estimations using the Lowesmith correlation (blue solid line) against the observed data (denoted by square markers). In general, the predictions by JFSH-Cook with the assumption of conservation of momentum are most conservative in the prediction of flame length.

Figure 45 graphically compares the predicted versus measured radiation. Figure 45a includes results for minimum thermodynamic change and Figure 45b includes radiation results with assumption of conservation of momentum. The corresponding measured and predicted radiations are given in Table 31 and Table 32. The overall over-prediction of all measurements is 91% and for minimum thermodynamic exchange and 113% for conservation of momentum respectively. So, the assumption of conservation of momentum has caused more conservative predictions in radiation.

Summary of the results

- Flame Length [LB]
  - Flame lengths predicted by the JFSH-Cook model with the assumption of conservation of momentum are generally more conservative (i.e. longer than the observed flame length), except a small under-prediction for the Selby & Burgan cases (i.e. SB1 & SB2).
  - On average, the percentage absolute deviation from measurements of simulated results by the JFSH-Cook model is 48.7% if conservation of momentum is maintained, compared with an overall deviation of 37.5% when minimum thermodynamic change is applied.
- Surface emissive power (SEP)

- On average, the percentage absolute deviation from measurements of simulated results by the JFSH-Cook model is 40.4% if conservation of momentum is maintained, compared with an overall deviation of 29.6% when minimum thermodynamic change is applied.

- Radiation
  - Radiation values are generally more over-predicted with the assumption of conservation of momentum compared with predictions with the assumption of minimum thermodynamic change for these test cases of liquid/2-phase releases.
  - On average, the percentage absolute deviation from measurements of simulated results is 113% if conservation of momentum is maintained compared with an overall deviation of 91% when minimum thermodynamic change is applied.

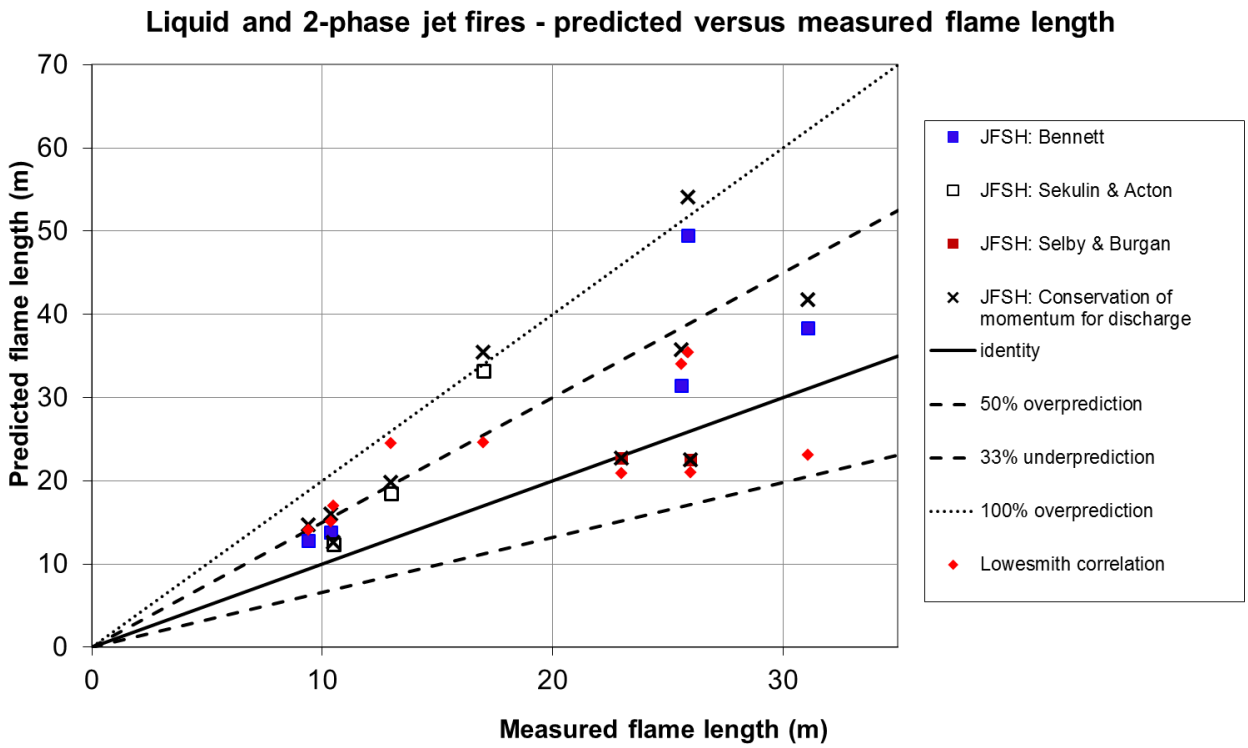

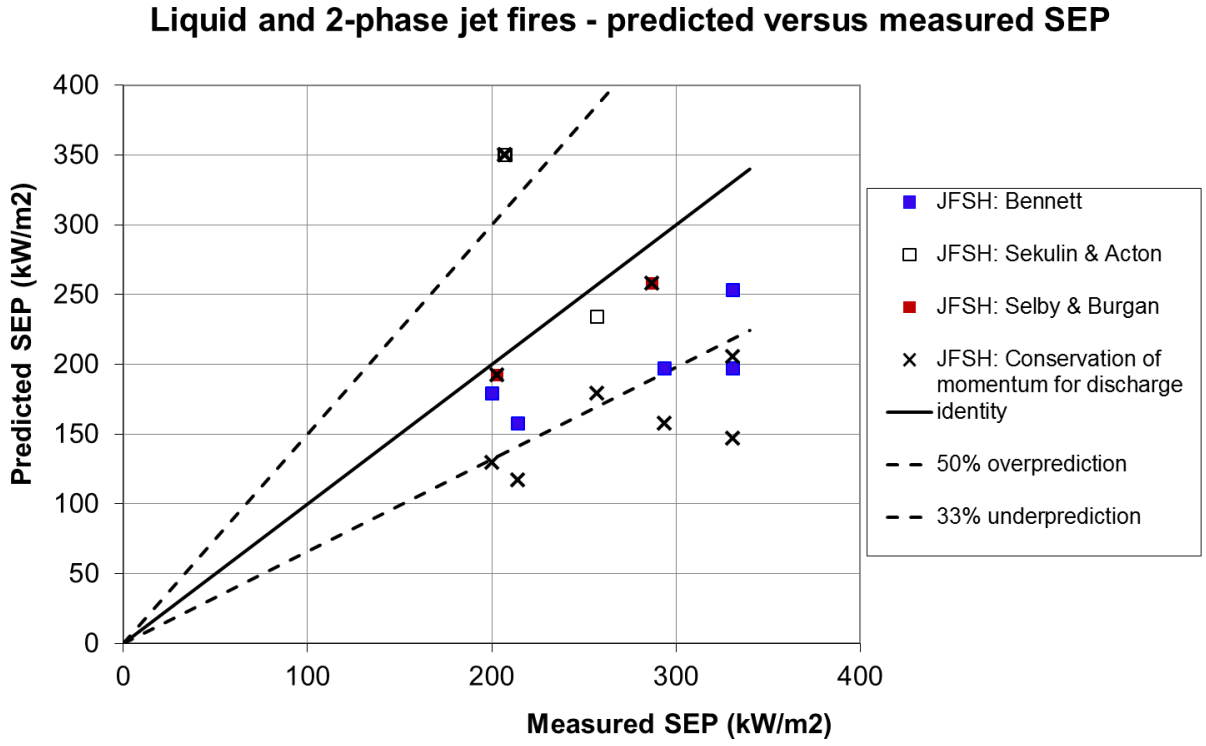

Figure 43. Two-phase fire tests - predicted versus measured flame length and SEP by JFSH with the input of the assumption of minimum thermodynamic change or conservation of momentum

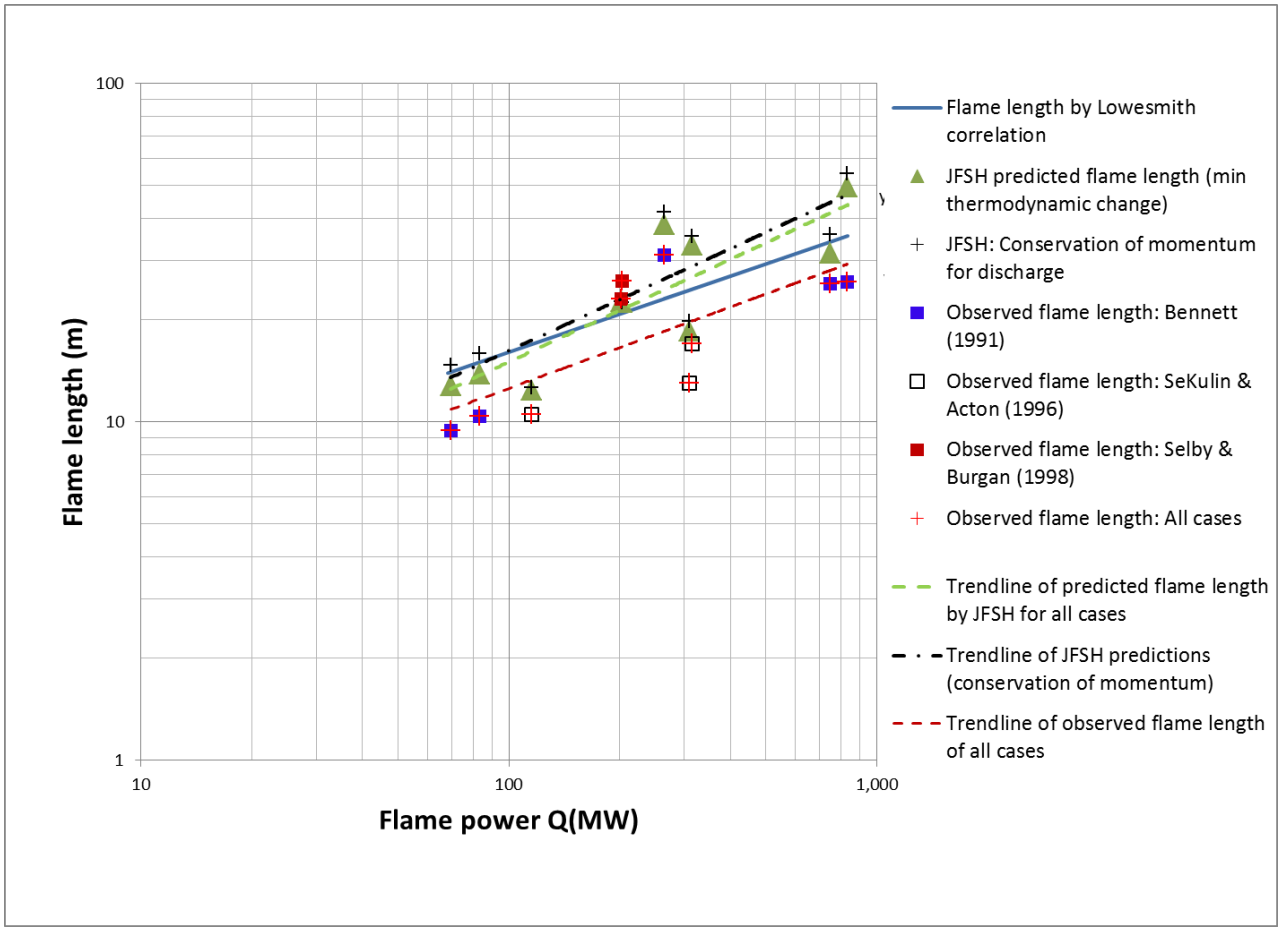

Figure 44 **JFSH predictions of flame length versus observed data and Lowesmith correlation**

Test	Radiometer	downstream X	crossstream Y	vertical Z	Observed	JFSH-Cook	JFSH-Cook	Average
		m	m	m	kW/m2	kW/m2	deviation	deviation
Bennett 3026	**3026-1**	15	10	1	48.7	59.6	22%	
Bennett	**3026-2**	15	14	1	45.2	43.5	-4%	
	3026-3	15	18	1	20	33.4	67%	
	3026-4	15	24	1	18.2	23.8	31%	
	3026-5	15	30	1	14.7	17.5	19%	
	3026-9	5	18	1	22.8	19.7	-14%	
	3026-10	10	18	1	29.5	26.5	-10%	
	3026-12	15	-14.6	1	27.8	41.7	50%	
	3026-13	15	-24.9	1	14.2	22.7	60%	25%
Bennett 3029	**3029-1**	15	10	1	24.6	43.6	77%	
	3029-2	15	14	1	23.8	31.8	34%	
	3029-4	15	24	1	12.7	18.7	47%	
	3029-5	15	30	1	10.5	14.6	39%	
	3029-10	10	18	1	21.9	19.5	-11%	
	3029-12	15	-14.6	1	35.3	30.6	-13%	
	3029-13	15	-24.9	1	16.8	18.0	7%	26%
Bennett 3006	**3006-1**	10	8.7	1	6	25.0	317%	
	3006-2	10	10.8	1	5.7	17.0	198%	
	3006-4	10	12.8	1	3.3	8.2	149%	
	3006-5	10	20.8	1	2.6	4.6	79%	
	3006-9	6	20.8	1	1.8	4.7	164%	
	3006-10	8	20.8	1	2.7	4.8	77%	
	3006-11	12	20.8	1	1.8	4.4	144%	
	3006-12	14	20.8	1	1.5	4.1	174%	
	3006-13	30	0	1	1.5	5.0	234%	
	3006-14	20	-15	1	4.4	5.8	32%	157%
Bennett 3007	**3007-2**	10	10.8	1	4.8	16.4	243%	
	3007-4	10	12.8	1	2.9	8.2	183%	
	3007-5	10	20.8	1	2.3	4.7	104%	
	3007-9	6	20.8	1	1.5	4.6	209%	
	3007-10	8	20.8	1	2.3	4.7	106%	
	3007-11	12	20.8	1	1.6	4.5	179%	
	3007-12	14	20.8	1	1.4	4.2	201%	
	3007-13	30	0	1	1.3	5.9	355%	
	3007-14	20	-15	1	3.6	6.0	67%	183%
Bennett 3028	**3028-1**	15	10	1	13.5	29.0	115%	
	3028-2	15	14	1	12.5	20.5	64%	
	3028-4	15	18	1	7.4	10.2	38%	
	3028-5	15	24	1	5.4	7.2	33%	
	3028-10	5	18	1	12.2	12.1	-1%	
	3028-12	15	-14.6	1	17.5	19.6	12%	
	3028-13	15	-24.9	1	8.7	9.7	11%	39%

Table 31. Two-phase fire tests –Phast radiation predictions versus observed data for Bennett Tests (i.e. B3006, B3008, B3026, B3028 & B3029)

Test	Radiometer	downstream X	crossstream Y	vertical Z	Observed	JFSH-Cook-Calc	JFSH-Cook	JFSH-Cook	Average
		m	m	m	kW/m2	W/m2	kW/m2	deviation	deviation
SA 8050	8050-1	14	10	1	10.29	17691.6909	17.7	72%	
Sekulin&Acton	8050-2	14	15	1	6.92	11863.34757	11.9	71%	
	8050-3	14	20	1	5.1	8496.759973	8.5	67%	
	8050-4	14	25	1	3.46	6286.623067	6.3	82%	
	8050-5	14	30	1	2.8	4799.278509	4.8	71%	
	8050-6	14	35	1	2.14	3765.381026	3.8	76%	
	8050-13	35	0	1	6.74	9520.59747	9.5	41%	
	8050-14	40	0	1	3.82	7046.340617	7.0	84%	
	8050-SH1	-10.2	-1.7	5.4	12.17	22014.45495	22.0	81%	
	8050-SH2	-10.2	28.3	2.3	2.63	2310.521676	2.3	-12%	
	8050-SH3	14	28.3	1	3.03	5243.376433	5.2	73%	
	8050-SH4	40	28.3	1	2.31	3623.3363	3.6	57%	
	8050-SH5	40	0.3	0.5	3.41	6982.493976	7.0	105%	
	8050-SH6	14	-27.7	1	8.24	32745.19046	32.7	297%	83%
SA 8051	8051-1	14	10	1	23.76	38832.81054	38.8	63%	
	8051-2	14	15	1	15.82	25495.30051	25.5	61%	
	8051-3	14	20	1	11.14	17936.84401	17.9	61%	
	8051-4	14	25	1	7.5	13126.24143	13.1	75%	
	8051-5	14	30	1	5.77	9893.404462	9.9	71%	
	8051-6	14	35	1	4.45	7646.062183	7.6	72%	
	8051-13	35	0	1	7.95	179170.7535	179.2	2154%	
	8051-14	40	0	1	4.74	61231.42291	61.2	1192%	
	8051-SH1	-10.2	-1.7	5.4	7.1	3991.094063	4.0	-44%	
	8051-SH2	-10.2	28.3	2.3	3.47	4199.545792	4.2	21%	
	8051-SH3	14	28.3	1	6.36	10859.09057	10.9	71%	
	8051-SH4	40	28.3	1	3.29	8213.444846	8.2	150%	
	8051-SH5	40	0.3	0.5	3.99	54038.04602	54.0	1254%	
	8051-SH6	14	-27.7	1	9.77	12744.21863	12.7	30%	374%
SA 8052	8052-1	14	10	1	5.91	10575.87605	10.6	79%	
Sekulin&Acton	8052-2	14	15	1	3.97	6558.448975	6.6	65%	
	8052-3	14	20	1	2.98	4516.847144	4.5	52%	
	8052-4	14	25	1	2.01	3243.346742	3.2	61%	
	8052-5	14	30	1	1.65	2417.912186	2.4	47%	
	8052-6	14	35	1	1.22	1860.607257	1.9	53%	
	8052-13	35	0	1	3	3734.477557	3.7	24%	
	8052-14	40	0	1	1.98	2775.091434	2.8	40%	
	8052-SH1	-10.2	-1.7	5.4	7.53	12296.10156	12.3	63%	
	8052-SH2	-10.2	28.3	2.3	1.51	1320.5913	1.3	-13%	
	8052-SH3	14	28.3	1	1.74	2661.444768	2.7	53%	
	8052-SH4	40	28.3	1	1.19	1490.122286	1.5	25%	
	8052-SH5	40	0.3	0.5	1.99	2761.789472	2.8	39%	
	8052-SH6	14	-27.7	1	4.53	6027.362421	6.0	33%	44%
SB1	SB1-1	14	10	1	35.9	55726.8055	55.7	55%	
Selby & Burgan	SB1-2	14	15	1	21.3	29544.93264	29.5	39%	
	SB1-3	14	20	1	13.7	17464.58124	17.5	27%	
	SB1-4	14	25	1	9.2	11295.69785	11.3	23%	
	SB1-5	14	30	1	6.8	7820.888376	7.8	15%	
	SB1-6	14	35	1	5.1	5700.608055	5.7	12%	
	SB1-7	14	40	1	3.7	4322.564776	4.3	17%	
	SB1-8	14	45	1	3.1	3380.978	3.4	9%	
	SB1-9	14	-10	1	30.8	55726.8055	55.7	81%	
	SB1-10	14	-20	1	12.8	17464.58124	17.5	36%	
	SB1-11	14	-30	1	6.4	7820.888376	7.8	22%	
	SB1-12	14	-40	1	3.7	4322.564776	4.3	17%	
	SB1-13	34	0	1	9.2	24560.52455	24.6	167%	
	SB1-14	39	0	1	3.8	13370.41933	13.4	252%	55%
SB2	SB2-1	14	10	1	39.8	44376.56662	44.4	11%	
	SB2-2	14	15	1	21.4	23806.01649	23.8	11%	
	SB2-3	14	20	1	12.7	14134.72899	14.1	11%	
	SB2-4	14	25	1	8	9155.70684	9.2	14%	
	SB2-5	14	30	1	5.5	6341.81558	6.3	15%	
	SB2-6	14	35	1	4	4622.532955	4.6	16%	
	SB2-7	14	40	1	2.8	3504.559149	3.5	25%	
	SB2-8	14	45	1	2.3	2740.645818	2.7	19%	
	SB2-9	14	-10	1	19.5	44376.56662	44.4	128%	
	SB2-10	14	-20	1	7.9	14134.72899	14.1	79%	
	SB2-11	14	-30	1	4.1	6341.81558	6.3	55%	
	SB2-12	14	-40	1	2.4	3504.559149	3.5	46%	
	SB2-13	34	0	1	6.5	20423.70962	20.4	214%	
	SB2-14	39	0	1	2.5	11239.57611	11.2	350%	
	SB2-15	0	0	1	12.4	24880.50881	24.9	101%	73%

Table 32 **Two-phase fire tests –Phast radiation predictions versus observed data for Sekulin & Acton and Selby & Burgan**

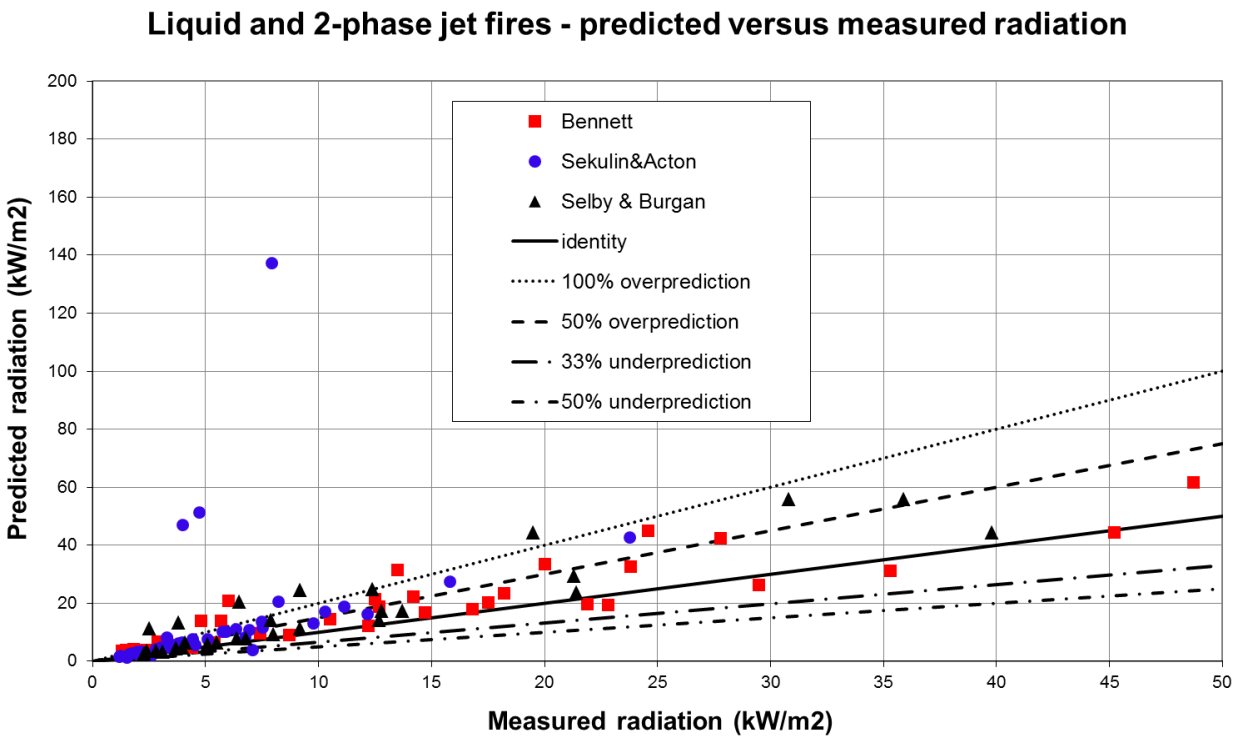

(c) Minimum thermodynamic change

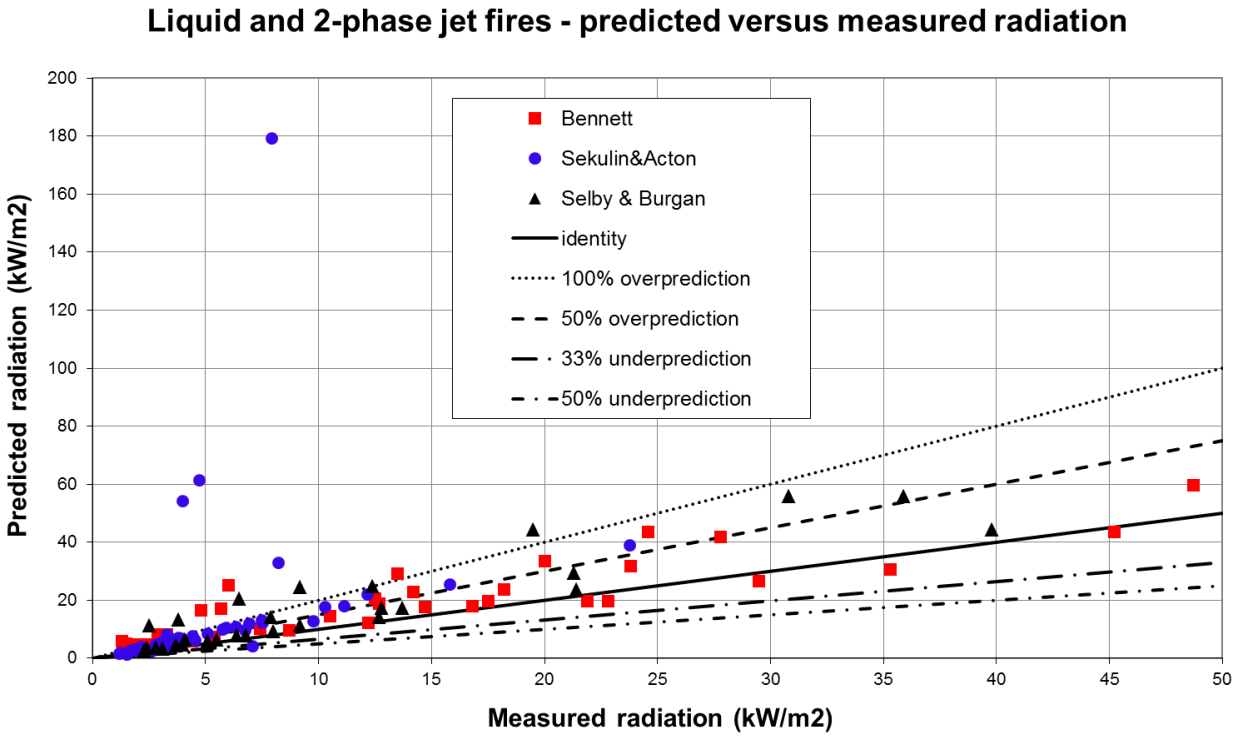

Conservation of momentum

Figure 45. Two-phase fire tests - predicted versus measured incident radiations

NOMENCLATURE

A	total surface area of the flame (conical frustum) [m^2]
B	frustum lift-off height/distance [m]
B_M	momentum dominated flame length [m]
d_o	orifice or discharge diameter [m]
D_s	combustion or effective source diameter [m]
F	Mach number of non-choked discharging fluid at stagnation temperature and ambient pressure [-]
F_{AP}	Flame radiant heat fraction along the flame centreline [-]
F_s	fraction of heat radiated from the surface of the flame [-]
g	gravitational acceleration [m/s^2]
H_{COMB}	heat of combustion of the fuel mixture [J/kg]
L_B	flame length measured from tip of flame to centre of exit plane [m]
L_{B0}	flame length in still air [m]
L_f	flame centreline length [m]
m	mass flow rate [kg/s]
M_d	mass release rates from discharge calculation [kg/s]
M_j	Mach number of the expanded jet [-]
M_W	fluid's molecular weight [g/mol]
M_{Wkg}	fluid's kilogram molecular weight [kg/mol]
P_c	static or choke pressure at the discharge plane [N/m^2]
P_o	atmospheric pressure [N/m^2]
Q_{rad}	total heat radiating (flame emissive power) from the flame along the flame centreline [W]
r_j	expanded radius of the escaping fluid [m]
$r_{jetmass}$	mass modification factor for jet fire calculation
R	ratio of wind speed to post-expansion jet velocity [-]
R_g	gas constant [8.314 J/mol/K]
R_L	flame frustum length [m]
t_j	durations of the release rate [s]
t_{jet}	jet fire average time (set under jet fire parameters) [s]
T_{Air}	atmospheric temperature [K]

T_c	temperature at discharge plane during choked discharge [K]
T_j	post-expansion discharge temperature [K]
T_s	stagnation temperature [K]
T_1	adiabatic combustion temperature [K]
U_w	wind speed [m/s]
v_j	post-expansion velocity of fluid [m/s]
W_{st}	Mass fraction of fuel in a stoichiometric mixture with air [-]
W_{Air}	Molecular weight of air [g/mol]
W_p	Mean product molecular weight [g/mol]
$W_{surface}$	Surface emissive power of flame [W/m^2]
W_1	width of frustum base [m]
W_2	width of frustum tip [m]
x_1	horizontal distance of the frustum base from the virtual origin along the vertical plane cutting the flame into symmetrical halves [m]
x_2	horizontal distance of the frustum tip from the virtual origin along the vertical plane cutting the flame into symmetrical halves [m]
z_{Elev}	elevation of the release point (e.g., flare tip) from the horizontal plane [m]
z_1	vertical distance of the frustum base from the virtual origin along the vertical plane cutting the flame into symmetrical halves [m]
z_2	vertical distance of the frustum tip from the virtual origin along the vertical plane cutting the flame into symmetrical halves [m]

Greek letters

α	angle between hole axis and flame axis [degrees]
β	constant in Becker and Liang's flame length correlation
ϕ	angle between the wind vector and the projection of the release axis on the horizontal plane [degrees]
ϕ_{flame}	angle between the vertical planes cutting the release source and jet flame respectively into symmetrical halves [degrees]
γ_g	ratio of specific heats [-]
$\eta_{rainout}^{i}$	rainout mass fraction for segment i (kg/kg)
ϑ	inclination of the frustum base to the horizontal plane [degrees]
θ_j	angle between hole axis and the horizontal in the vertical plane [degrees]
θ_{jv}	angle between hole axis and wind vector in the plane containing the hole axis, flame axis, and wind vector [degrees]
ρ_{amb}	density of air at ambient conditions [kg/m^3]

ρ_j	density of expanded fluid jet [kg/m^3]
$\rho_{T_{SatVap}}$	Fuel's saturated vapour density at ambient pressure [kg/m^3]
$\xi(D_s)$	Richardson number based on D_s (i.e., source diameter) [-]
$\xi(L_{B0})$	Richardson number based on flame length in still air [-]

REFERENCES

[1] Chamberlain, G. A., “Developments in design methods for predicting thermal radiation from flares”, Chem. Eng. Res. Des., Vol. 65, pp 299-309, (July 1987)

[2] Johnson, A. D., Brightwell, H. M., and Carsley, A. J., “A model for predicting the thermal radiation hazard from large scale horizontally released natural gas jet fires,” Trans. IChemE., Vol. 72, Part B, pp 157-166, (1994)

[3] Bennett, J. F., Cowley, L. T., Davenport, J. N., and Rowson, J. J., “Large scale natural gas and LPG jet fires final report to the CEC”, TNER 91.022, (1991)

[4] Miller, D. (2017), “New model for predicting thermal radiation from flares and high pressure jet fires for hydrogen and syngas”. Proc. Safety Prog., 36: 237-251. https://doi.org/10.1002/prs.11867

[5] Selby, C. A., and Burgan, B. A., “Blast and fire engineering for topside structures- phase 2, final summary report,” The Steel Construction Institute, Silwood Park, pp I-A7 - I-A18, (1998)

[6] Harper, M., “Continuous and Instantaneous Discharge Models (DISC)”, DNV (July 2002)

[7] Holt, A., Topalis, P., Witlox, H. W. M., Clements, F., and Harper, M., “Atmospheric Expansion Model (ATEX),” DNV (July 2002).

[8] Kooi, E.S. and Uijt de Haag, P.A.M., “A comparison of three jet-fire models”, National Institute for Public Health and the Environment, RIVM Report 620550005/2011 (2011)

[9] Davenport, J. N., Bennett, J. F., Cowley, L. T., , and Rowson, J. J., “Large scale natural gas and LPG jet fires – Data report for test 3006”, TNER 91.059, Shell Research Ltd., Thornton Research Centre (1991)

[10] Davenport, J. N., Bennett, J. F., Cowley, L. T., , and Rowson, J. J., “Large scale natural gas and LPG jet fires – Data report for test 3007”, TNER 91.058, Shell Research Ltd., Thornton Research Centre (1991)

[11] Davenport, J. N., Bennett, J. F., Cowley, L. T., , and Rowson, J. J., “Large scale natural gas and LPG jet fires – Data report for test 3028”, TNER 91.060, Shell Research Ltd., Thornton Research Centre (1991)

[12] Davenport, J. N., Bennett, J. F., Cowley, L. T., , and Rowson, J. J., “Large scale natural gas and LPG jet fires – Data report for test 3026”, TNER 91.062, Shell Research Ltd., Thornton Research Centre (1991)

[13] Davenport, J. N., Bennett, J. F., Cowley, L. T., , and Rowson, J. J., “Large scale natural gas and LPG jet fires – Data report for test 3029”, TNER 91.063, Shell Research Ltd., Thornton Research Centre (1991)

[14] Sekulin, A.J. and Action, M.R., “Large Scale Experiments to Study Horizontal Jet Fires of Mixtures of Natural Gas and Butane – Data Report For Test 8051”, GRC report R0367 (8051), (1995)

[15] Acton, M.R., Evans, J.A., and Sekulin, A.J., “Blast and fire engineering project Phase 2 – Horizontal jet fires of oil and gas: data report for jet fire test 1”, Contract number GRC/2190/105, GRC Report 1019 (1), British Gas, Gas Research Centre, Loughborough (1996)

[16] Acton, M.R., Evans, J.A., and Sekulin, A.J., “Blast and fire engineering project Phase 2 – Horizontal jet fires of oil and gas: data report for jet fire test 2”, Contract number GRC/2190/105, GRC Report 1019 (2), British Gas, Gas Research Centre, Loughborough (1996)

[17] Lowesmith, B.J., Henkinson, G., Acton R. & Chamberlain, G., “An overview of the nature of hydrocarbon jet fire hazard in the oil and gas industry and a simplified approach to assessing the hazards”, Trans IChemE, Part B, Process Safety and Environmental Protection, 85(B3), 2007

[18] Medina, C.H., Halford, A., Stene, J. & Allason, D. “LIQUID HYDROGEN SAFETY Data Report: Outdoor leakage studies”, Report No.: 853182, Rev. 1, Date: 2020-06-29, DNVGL

[19] E.S. Fishburne and H.S. Pergament, “The dynamics and radiant intensity of large hydrogen flames,” Colloquium on Fire and Explosion, 1979.

[20] L.C. Shirvill, P. Roberts, C.J. Butler, T.A. Roberts, and M. Royle, Characterisation of the Hazards from Jet Releases of Hydrogen, Health and Safety Laboratory, UK, 2005.

[21] D. Miller, and J. Bedenbaugh, “Hydrogen and syngas flares – Comparison between experimental data and model predictions,” AFPRC Industrial Combustion Sym¬posium, Houston TX, 2014.

[22] R.W. Schefer, W.G. Houf, B. Bourne, and J. Colton, Spa¬tial and radiative properties of an open-flame hydrogen plume, Int J Hydrogen Energy 31 (2006), 1332–1340.

[23] B.J. Lowesmith, An experimental programme to study high pressure jet fires following releases of natural gas/ hydrogen mixtures, R0051-WP2-R-0 (Part of Deliverable D37), 2008.

[24] D.B. Willoughby, M. Royle, S. Nilsen, and T. Gautier, Hydrogen Venting under Variable Flow Conditions, Health and Safety Laboratory, UK, 2011.

[25] Advantica, Report on Hydrogen Jet Fires Carried Out On Behalf of Air Products & Chemicals Inc., Private Report, 2009.

[26] Miller, D. and Kelly, T.G., Development of Correlations for the Radiant Fraction from Hydrogen Flares: Testing at the Clean Energy Lab, Air Products Internal Report, 2015

About DNV

We are the independent expert in risk management and quality assurance. Driven by our purpose, to safeguard life, property and the environment, we empower our customers and their stakeholders with facts and reliable insights so that critical decisions can be made with confidence. As a trusted voice for many of the world's most successful organizations, we use our knowledge to advance safety and performance, set industry benchmarks, and inspire and invent solutions to tackle global transformations.

Digital Solutions

DNV is a world-leading provider of digital solutions and software applications with focus on the energy, maritime and healthcare markets. Our solutions are used worldwide to manage risk and performance for wind turbines, electric grids, pipelines, processing plants, offshore structures, ships, and more. Supported by our domain knowledge and Veracity assurance platform, we enable companies to digitize and manage business critical activities in a sustainable, cost-efficient, safe and secure way.